

# Lawrence Berkeley National Laboratory

## Recent Work

### Title

THE EFFECT OF HYDRODYNAMIC FLOW ON THE MORPHOLOGY OF ELECTRODEPOSITED ZINC

### Permalink

<https://escholarship.org/uc/item/0dx567zh>

### Authors

Faltemier, J.L.

Tobias, C. W.

### Publication Date

1983-08-01



# Lawrence Berkeley Laboratory

UNIVERSITY OF CALIFORNIA

RECEIVED  
LAWRENCE  
BERKELEY LABORATORY

NOV 1 1983

LIBRARY AND  
DOCUMENTS SECTION

## Materials & Molecular Research Division

THE EFFECT OF HYDRODYNAMIC FLOW ON THE MORPHOLOGY  
OF ELECTRODEPOSITED ZINC

J.L. Faltemier\* and C.W. Tobias  
(\*Ph.D. Thesis)

August 1983

**For Reference**

Not to be taken from this room



LBL-16485  
c.1



## **DISCLAIMER**

This document was prepared as an account of work sponsored by the United States Government. While this document is believed to contain correct information, neither the United States Government nor any agency thereof, nor the Regents of the University of California, nor any of their employees, makes any warranty, express or implied, or assumes any legal responsibility for the accuracy, completeness, or usefulness of any information, apparatus, product, or process disclosed, or represents that its use would not infringe privately owned rights. Reference herein to any specific commercial product, process, or service by its trade name, trademark, manufacturer, or otherwise, does not necessarily constitute or imply its endorsement, recommendation, or favoring by the United States Government or any agency thereof, or the Regents of the University of California. The views and opinions of authors expressed herein do not necessarily state or reflect those of the United States Government or any agency thereof or the Regents of the University of California.

THE EFFECT OF HYDRODYNAMIC FLOW  
ON THE MORPHOLOGY OF ELECTRODEPOSITED ZINC

James L. Faltemier

(Ph.D. Thesis)

with Charles W. Tobias

August 1983

Materials and Molecular Research Division  
Lawrence Berkeley Laboratory

and

Department of Chemical Engineering  
University of California, Berkeley  
Berkeley, California 94720

The United States Department of Energy has the right to use  
this thesis for any purpose whatsoever including the right  
to reproduce all or any part thereof.

This work was supported by the Assistant Secretary for Conservation and  
Renewable Energy, Office of Energy Systems Research, Energy Storage  
Division of the U. S. Department of Energy under Contract No. DE-AC03-  
76SF00098.

The Effect of Hydrodynamic Flow  
on the Morphology of Electrodeposited Zinc

Copyright © 1983

by

James L. Faltemier

## TABLE OF CONTENTS

	PAGE
ABSTRACT .....	iii
DEDICATION .....	v
1. INTRODUCTION .....	1
1.1 Zinc - Properties and Applications .....	1
1.2 Zinc Batteries .....	3
1.3 Purpose of Study .....	6
2. LITERATURE REVIEW .....	7
2.1 Striated Deposition and Dissolution .....	7
2.2 Aspects of Zinc Electrochemistry .....	18
2.3 Current Distribution and Convective-Mass Transport along a Planar Electrode .....	20
2.4 Zinc Batteries .....	23
3. EXPERIMENTAL .....	25
3.1 Experimental Apparatus .....	25
3.1.1 Experimental Cells .....	25
3.1.1a Rotating Disk Electrode System	
3.1.1b Channel Flow Cells	
3.1.2 Electrodes .....	36
3.1.2a Electrode Construction	
3.1.2b Cathodes	
3.1.2c Anodes	
3.1.3 Electrolytes .....	39
3.1.3a Different Solutions	
3.1.3b Purity	
3.1.4 Equipment .....	42
3.1.4a Rotating Disk Electrode Equipment	
3.1.4b Channel Flow Cell Equipment	
3.1.4c Photographic Equipment	
3.1.4d Accessory Instruments	
3.2 Experimental Procedures .....	45
3.2.1 Electrode Preparation .....	45
3.2.1a Carbide Sanding	
3.2.1b Diamond Paste Polishing	
3.2.1c Solvent Cleaning	
3.2.1d Preelectrolysis	
3.2.2 Details of Operation .....	46
3.2.2a RDE	
3.2.2b Channel	
3.2.2c In-situ Apparatus	
3.2.2d Limiting Current Experiments	
3.2.3 Examination of Deposits .....	48

4.	RESULTS AND DISCUSSION .....	50
4.1	Overview .....	50
4.1.1	Striations: Definition, Characteristics, and Development .....	50
4.1.2	Range of Striation Appearance .....	53
4.2	Influence of Parameters & Variables .....	54
4.2.1	Effect of Hydrodynamic Flow .....	54
4.2.2	Effect of Current Density .....	56
4.2.3	Variable Current Techniques .....	64
4.2.4	Effect of Zinc Concentration .....	65
4.2.5	Effect of Substrates .....	68
4.2.6	Effect of pH .....	70
4.2.7	Effect of Impurities, Surfactants, and Electrolyte Purity .....	73
4.2.8	Effect of Anions .....	76
4.2.9	Effect of Electrode Size .....	76
4.3	Limiting Current Studies .....	80
4.4	In situ Time-Lapse Photographic Studies .....	80
4.5	Discussion of Causes for the Development of Striated Deposits .....	86
4.5.1	Proposed Hypotheses .....	86
4.5.2	Development of Striations .....	92
	4.5.2a Initiation	
	4.5.2b Propagation	
5.	SUMMARY AND CONCLUDING REMARKS .....	106
	REFERENCES .....	110
	ACKNOWLEDGMENTS .....	122
APPENDIX A	Remarks on the Background of This Investigation .....	124
APPENDIX B	Detailed Descriptions of All Experimental Systems .....	127
APPENDIX C	Chemical Analysis of Solutions .....	134
APPENDIX D	Motion Pictures in In Situ Cell .....	137
APPENDIX E	Calculation of Reynolds Number for Cells and RDE .....	139
APPENDIX F	Experimental Conditions .....	141
APPENDIX G	Physical Data on Zinc Electrolytes .....	144
APPENDIX H	Experimental Data .....	147

THE EFFECT OF HYDRODYNAMIC FLOW  
ON THE MORPHOLOGY OF ELECTRODEPOSITED ZINC

James L. Faltemier  
with Charles W. Tobias

Materials and Molecular Research Division  
Lawrence Berkeley Laboratory

and

Department of Chemical Engineering  
University of California, Berkeley  
Berkeley, California 94720

ABSTRACT

The influence of hydrodynamic flow and other process variables on the macromorphology of electrodeposited zinc have been investigated under galvanostatic control at a rotating disk electrode (RDE) and in three channel flow cells by using photomacrography, SEM, and in situ time-lapse motion photography. In addition, variable-current step techniques were employed, and mass transfer limiting currents of zinc were determined using an RDE. Unlike other metals, zinc deposited from acidic halide and sulfate solutions at rates far below the mass transfer controlled region show remarkable impressions of the hydrodynamic flow.

Up to approximately  $80 \text{ mA/cm}^2$  in  $1 \text{ M ZnCl}_2$ , zinc forms a striated deposit within 3 - 15 minutes. Grooves develop parallel to the flow direction; straight in channel cells, spiral-shaped on RDE. Increasing flowrate or rpm causes more rapid development of more sharply contoured striations in the flow direction. Macroscopically smooth deposits are always obtained in both laminar and turbulent flow above  $100 \text{ mA/cm}^2$  or when the current is pulsed. Although they develop sooner near the lead-

ing edge, striations form along the entire length of the electrode, up to 30 cm in this study. Time-lapse motion photography reveals detailed morphological sequences without interruption of the electrolysis and without any external handling. Zinc deposits first smoothly on the substrate surface, then after several minutes, protrusions appear randomly on the smooth surface, grow laterally in the flow direction, and join with other protrusions downstream, producing ridges. Substrate material, surface roughness, and variations in pH (in the 2 - 5 range) are of only secondary importance.

The experimental evidence supports the idea that a sharp dependence of nucleation rate, as against rate of crystal growth, on overpotential (or current density) is the principal cause for the development of striations. The nucleation rate of crystals progressively increases as the current density level is raised, dominating any preferential, outward growth of crystallites and producing a smooth surface. At the lower current density levels (far below transport limiting conditions), wakes forming behind the largest crystallites cause improved mass transport because of small decreases in the mass transfer overpotential; as a consequence, current density increases locally in the wakes. Better mass transport and smaller ohmic resistance to the developing ridges support their continued preferential growth, resulting eventually in fully striated deposits.

DEDICATED TO SHARON, TO MY MOTHER,

AND TO THE MEMORY OF MY DEAR FATHER

His spirit will remain with me for as long as I live.



## 1. INTRODUCTION

### 1.1 Zinc - Properties and Applications

Zinc is a very common and important metal to mankind because of its availability and low cost, low molecular weight, relatively low toxicity, and most of all, its moderately negative standard potential,  $V_0 = -0.76$  volt. These qualities help make zinc the ideal metal for many applications including diecasting, manufacture of brass, galvanizing, corrosion protection, and the production of coins.

Zinc is produced almost entirely by electrowinning processes from sulfide ores [1]. On a tonnage basis, it is the second most important metal, next to aluminum, industrially claimed today by electrowinning processes. Zinc electroplating from various sulfate, zincate, or cyanide plating baths is also widely used for decorative coating or corrosion protection. In the electrolytic field, zinc is the most widely used negative electrode in both acidic and alkaline batteries. Its use in cells and batteries dates back to 1800 when zinc and silver were combined to form Volta piles, essentially crude primary batteries.

Zinc consumption in the United States has improved slightly over the past decade even with continuing weakness in the auto and steel industries. Fig. 1.1 gives a breakdown of the world zinc production and consumption rates by geographical area and a breakdown of the U.S. zinc consumption rate [2]. Galvanizing and zinc diecasting account for approximately 79% of the zinc market. Zinc in batteries comprises only a small portion (5%) of the zinc market; consequently, this use could expand considerably without significant economic impact.

1981 WORLD ZINC SLAB  
PRODUCTION & CONSUMPTION

(000 SHORT TONS)

	PROD. -----	CONS. -----
UNITED STATES	410	910
CANADA	660	150
OTHER W. HEMISPHERE	410	390
AFRICA	210	180
WESTERN EUROPE	2020	1850
ASIA	940	1240
OCEANIA	330	130
EASTERN BLOC	1870	1880
	-----	-----
TOTAL	6850	6730

1981 U.S. CONSUMPTION OF  
SLAB ZINC

(000 SHORT TONS)

DIECASTING	285
GALVANIZING	435
BRASS	110
ROLLED ZINC	24
ZINC OXIDE	30
OTHER USES	26
	-----
TOTAL	910

-2-

Figure 1.1

XBL 834-9320A

## 1.2 Zinc Batteries

Several candidate battery systems are being targeted today for electric vehicle and utility load-leveling energy storage. These systems are shown in the following table.

Table 1.1

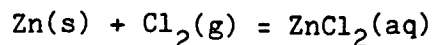
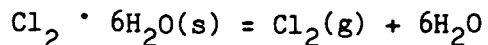
### Candidate Systems for Major Energy Storage

<u>Ambient Temperature</u>	<u>Elevated Temperature</u>
Pb/Acid	Li/FeS <sub>2</sub>
Zn/NiOOH	Li/FeS
Fe/NiOOH	Na/S
H <sub>2</sub> /NiOOH	
Zn/Air	
Fe/Air	
Al/Air	
Zn/Cl <sub>2</sub>	
Zn/Br <sub>2</sub>	

Zinc is an active component in a significant portion of the secondary batteries currently being considered for these applications by the Department of Energy.

In the last decade, the two acidic battery systems, ZnCl<sub>2</sub> and ZnBr<sub>2</sub>, have been receiving increasing amounts of attention. These two are becoming very attractive among the various candidate batteries for a number of reasons: materials are cheap and available, theoretical energy densities are moderately high, cell voltages are high, and the reactions are relatively fast at ambient temperatures.

The ZnCl<sub>2</sub> battery involves a flow system, with the following cell reaction:



It has a cell voltage of 2.1 volts, and a theoretical specific energy of 436 watt-hour/kilogram. The flow diagram [3] is shown in Fig. 1.2. On charging, zinc deposits at the graphite cathode and the chloride ions react at the graphite anode evolving  $\text{Cl}_2$  gas, which is chilled and stored as solid  $\text{Cl}_2\text{-}6\text{H}_2\text{O}$  hydrate. In the discharge mode, the hydrate releases  $\text{Cl}_2$  upon heating and the  $\text{Cl}_2$  in solution is pumped through the porous carbon electrodes where it reacts cathodically, and the zinc is dissolved anodically to form the  $\text{ZnCl}_2$  electrolyte again. This battery can be charged during the night and discharged during the day when needed for utility peak power or for daily commuting in a vehicle.

The  $\text{ZnBr}_2$  battery also involves a flow system. The differences between the two acidic zinc systems arise in that the bromine is complexed with a quaternary-ammonium compound instead of being chilled and stored as a solid hydrate, and that a separator between the cathodic and anodic processes must be used to prevent the bromide ion from attacking and corroding the zinc deposit.

These two zinc systems have problems that, hopefully, will be solved or at least minimized with additional research. They have scaling-up complexities, low energy efficiencies (60%), which are caused mainly by  $\text{Cl}_2$  or  $\text{Br}_2$  transport across the cell to the zinc electrode, and low demonstrated cycle lives (100X-300X), which are caused partly by rough and dendritic zinc deposition. This nonsmooth deposition, which surprisingly occurs in current density ranges far below mass transport

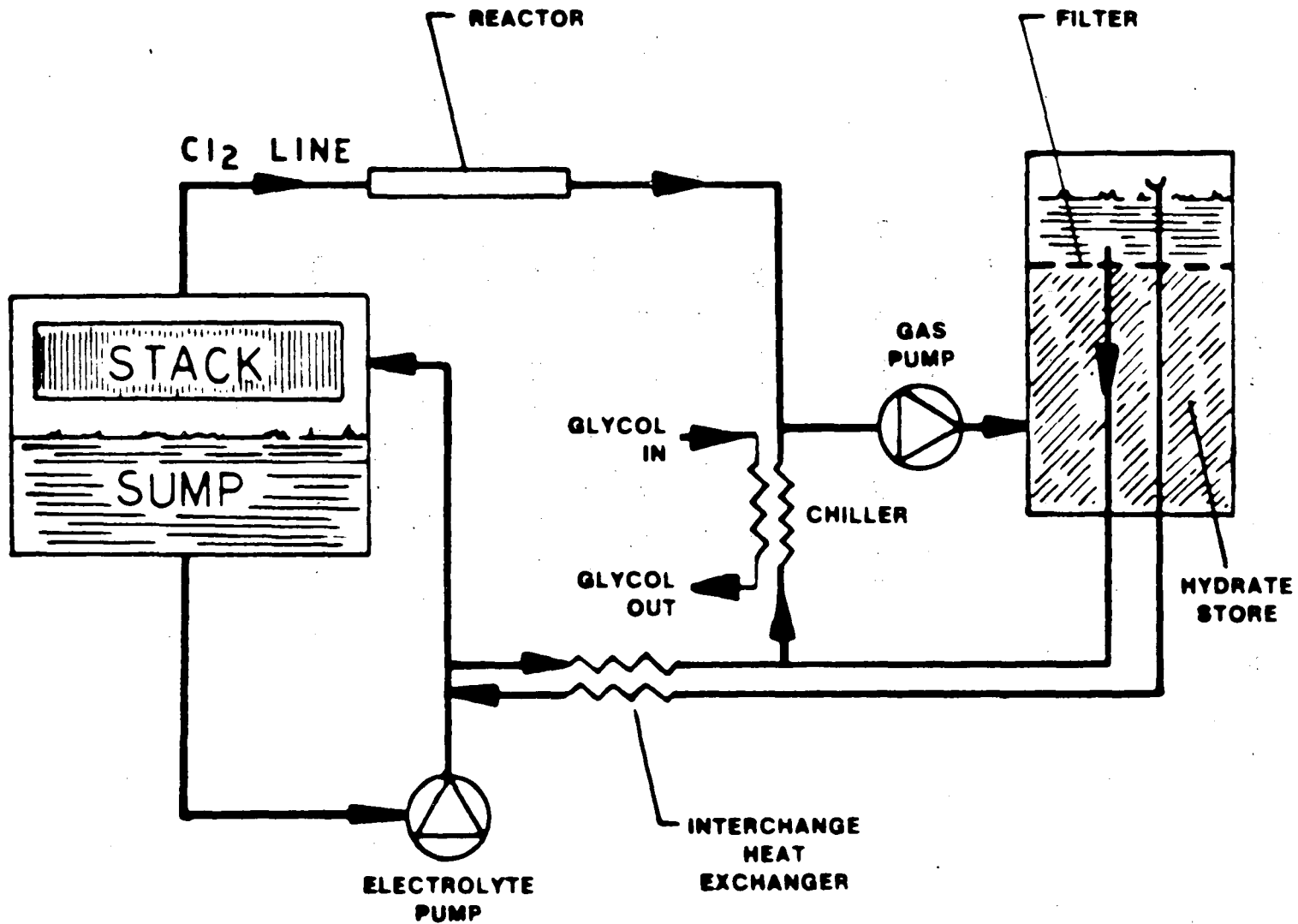


Figure 1.2 Zn/Cl<sub>2</sub> Battery Flow Diagram [3]

limiting conditions, eventually causes reduced loading of the battery because of zinc material loss or reshaping and possibly battery failure because of electrical shorting across the cell gap.

### 1.3 Purpose of Study

The morphology of electrodeposited zinc is one major problem which is preventing these cells from being economical and having sufficient cycle life. The prospects of these zinc batteries ever becoming feasible depends largely upon the optimization of the quality of the zinc deposit.

Research efforts in this laboratory have involved over several decades many facets of the interaction between deposit morphology and hydrodynamic flow. A chronological history of the zinc project since 1976 is provided in Appendix A. The objectives of this research are to investigate the influence of hydrodynamic flow on the morphology of electrodeposited zinc and to elucidate the roles of the other system variables in the electrodeposition process in acid media. By understanding the mechanisms involved and the effects that system parameters have on the electrodeposition process, development of acidic zinc batteries will hopefully be enhanced.

## 2. LITERATURE REVIEW

### 2.1 Striated Deposition and Dissolution

The formation of striated surfaces from metal electrodeposition or metal dissolution has been reported by many authors since the early 1940's. It is likely that observations of striated patterns in metal dissolution were actually made before the turn of the century, since the dissolution of metals in acids was being studied already in the 1800's [4].

These striated surfaces form in the shape of spiral patterns on rotating disk and hemispherical electrodes and as straight grooves, parallel to the hydrodynamic flow, on planar electrodes in channel flow cells. These phenomena have been observed under a wide variety of conditions and in a number of metal systems, including nickel, iron, copper, iron-nickel alloy, manganese, magnesium, and zinc systems.

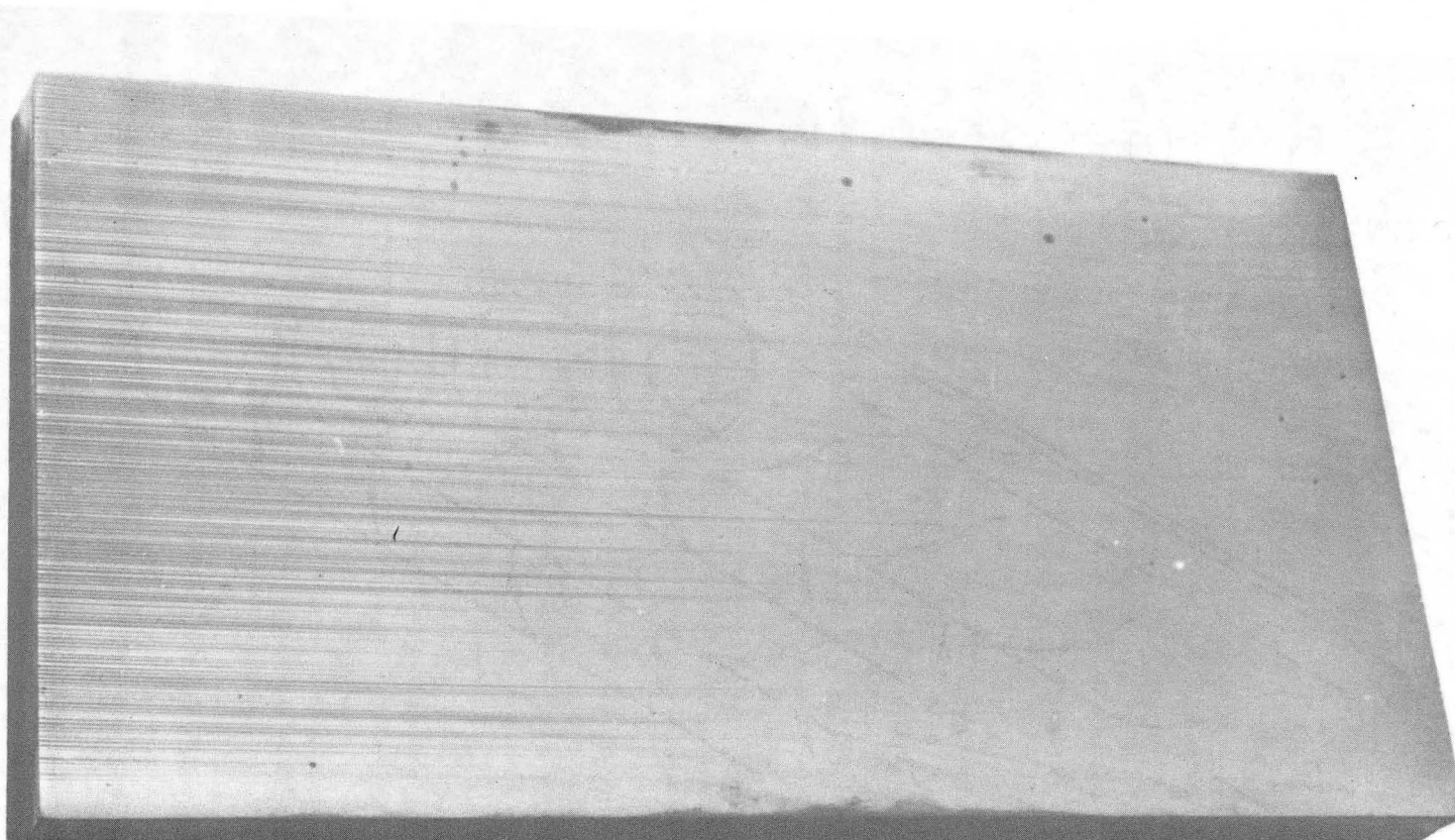
The literature principally concerned with the morphological structure of a striated surface is reviewed in chronological order, followed by references in which researchers report observation of striated surfaces while studying other electrochemical aspects or in which the mechanism of development of rough or dendritic surfaces was the principal subject of investigation.

Hickman and Tobias [5,6] investigated the effects of buoyancy forces on mass transfer in channel-type cells in both laminar and turbulent flow. They deposited copper at limiting current from an acidified copper sulfate electrolyte onto horizontal planar cathodes, and observed striated growth in the copper in the downstream region under

certain conditions. The authors noted that buoyancy forces had negligible effects on the mass transfer under turbulent conditions, but that under laminar conditions buoyancy forces induced secondary flows near the electrode interface. This free convection secondary effect resulted from instabilities which are caused by local density gradients across the mass transfer boundary layer in the transverse direction. A typical deposit is shown in Fig. 2.1. The direction of fluid flow in this Figure is from right to left, parallel to the surface of the electrode. Hickman and Tobias suggested that this secondary flow effect was in the form of "roll cells" with flow profiles across the electrode similar to that shown in Fig. 2.2. The distance from the leading edge at which striations started depended on solution composition and flow rate, and could be predicted from the Rayleigh stability criterion.

Rogers and Taylor [7] and Hill, Rogers, and Taylor [8] found spirals on nickel, silver, and copper electrodeposits. Uniform electrodeposits should have resulted from all their rotating disk electrode experiments. The authors examined the effects that several organic additives had on the deposits; specifically, they noted that submicroscopic protrusions or depressions in the substrate surface were present whenever spirals tended to form. No protrusions large enough to produce wakes were present in these experiments. They observed no spiral angle dependence on the rotation speed, in agreement with theory worked out by White, et.al. [9] according to which, spiral shape is independent of the rotation speed in the limit of protrusions of atomic height. According

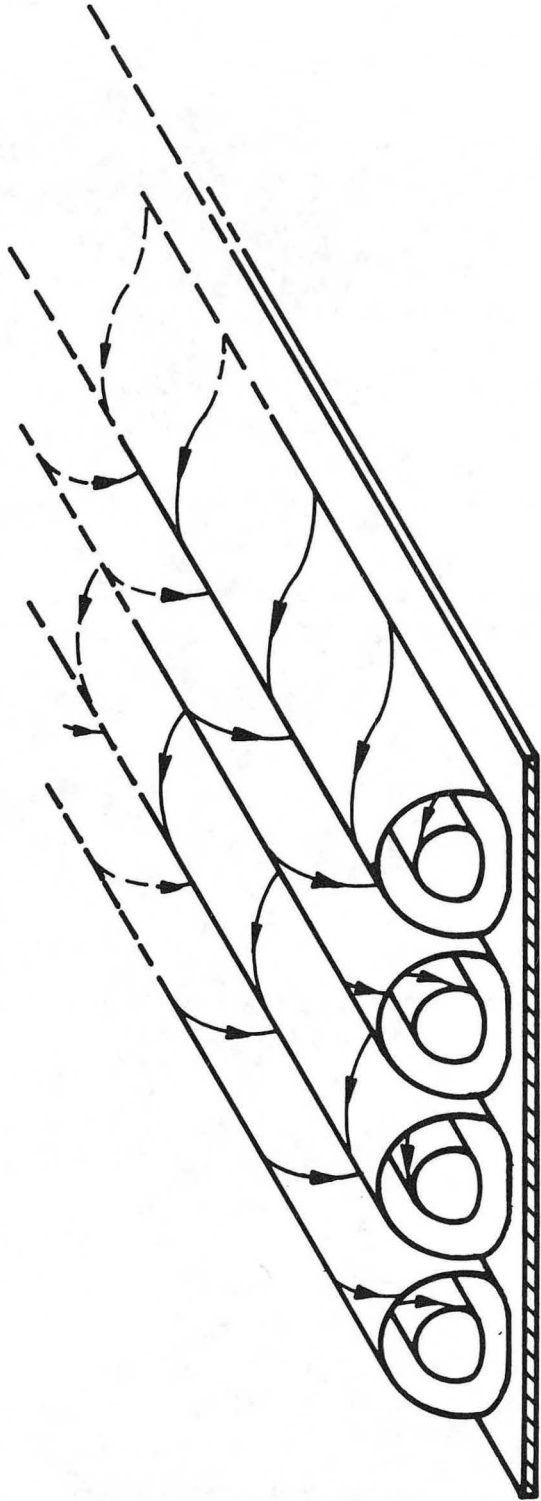




-9-

Chem 3121

Figure 2.1 Striated Copper Deposit on a 10 X 20 cm Electrode, Flow Direction is Right to Left [6]



MU 31511

Figure 2.2 "Roll Cell" Cellular Flow Pattern [6]

to these authors, protrusions with heights comparable to the hydrodynamic boundary layer cause logarithmic spiral wakes described by the equation

$$\theta = (1-G)/F \ln r/r_0$$

where  $\theta$  is the angle that a spiral covers between radial distances  $r$  and  $r_0$  from the disk center and the factor  $(1-G)/F$  is a complex function of the protrusion's height, the disk angular velocity, and the electrolyte kinematic viscosity [9]. As the protrusion height becomes microscopic, the factor  $(1-G)/F$  becomes a constant and theoretically, a logarithmic spiral which is independent of rotation speed is formed. The authors deduced the height of a protrusion from the curvature of the spiral, and showed that in each case this height was too small to cause local turbulence. They explained that submicroscopic protrusions or depressions on the surface caused spirals to appear on electrodeposits that are plated at the "low current density end of sections of current density versus potential curves that have very large negative gradients", which would essentially indicate the presence of a strongly potential dependent, electrode reaction inhibiting adsorbed film is present on the surface. Tsuda [10] discusses further the physical interpretation of this spiral independence with rotation speed in his Master's thesis.

Carlson and Tobias [11] studied the deposition of copper around small protrusions on a planar surface in turbulent flow as a function of the protrusion height and diameter and of the related process parameters. They noted a distinctive wake region which was caused by flow

fluctuations induced by the protrusions, as shown in Figs. 2.3 and 2.4. They found an enhanced rate of deposition (approximately double) inside the wake, and that no wake was reflected in the deposit when the protrusion height was below 0.1 mm and when the fraction of limiting current was below 90%. They explained these observations in terms of mass transport control of the process. The interference of the hydrodynamic flow with the protrusion causes the diffusion boundary layer to decrease which causes an increase in limiting current density and total current in the wake region. Below the limiting current range, surface overpotential dominated and no rate enhancement occurred.

Parallel to these studies on various aspects of the morphology of copper electrodeposits [5,6,11,12,13], extensive experimental efforts in this laboratory have been devoted to the nature of zinc deposits obtained in acidic solutions. Milan Jaksic [14] conducted detailed studies involving rotating disk electrodes, and on small electrodes in flow channels, devoting attention to effects of flow rate (or rpm), current density, time of deposition, pH, and presence of surfactants and metallic impurities. Jaksic also examined the microstructural appearance of zinc deposits by using the scanning electron microscope (SEM). The record of this work so far is primarily in form of macro- and microphotographs of striated surfaces under various magnifications. Preliminary attempts at the interpretation of the mechanism responsible for the generation of grooved deposits has been presented [15,16,17,18]. Detailed reports are still not available, but currently are in preparation.

Tsuda and Tobias [10] investigated the development of macromorphology of zinc electrodeposits using rotating disk electrodes in this

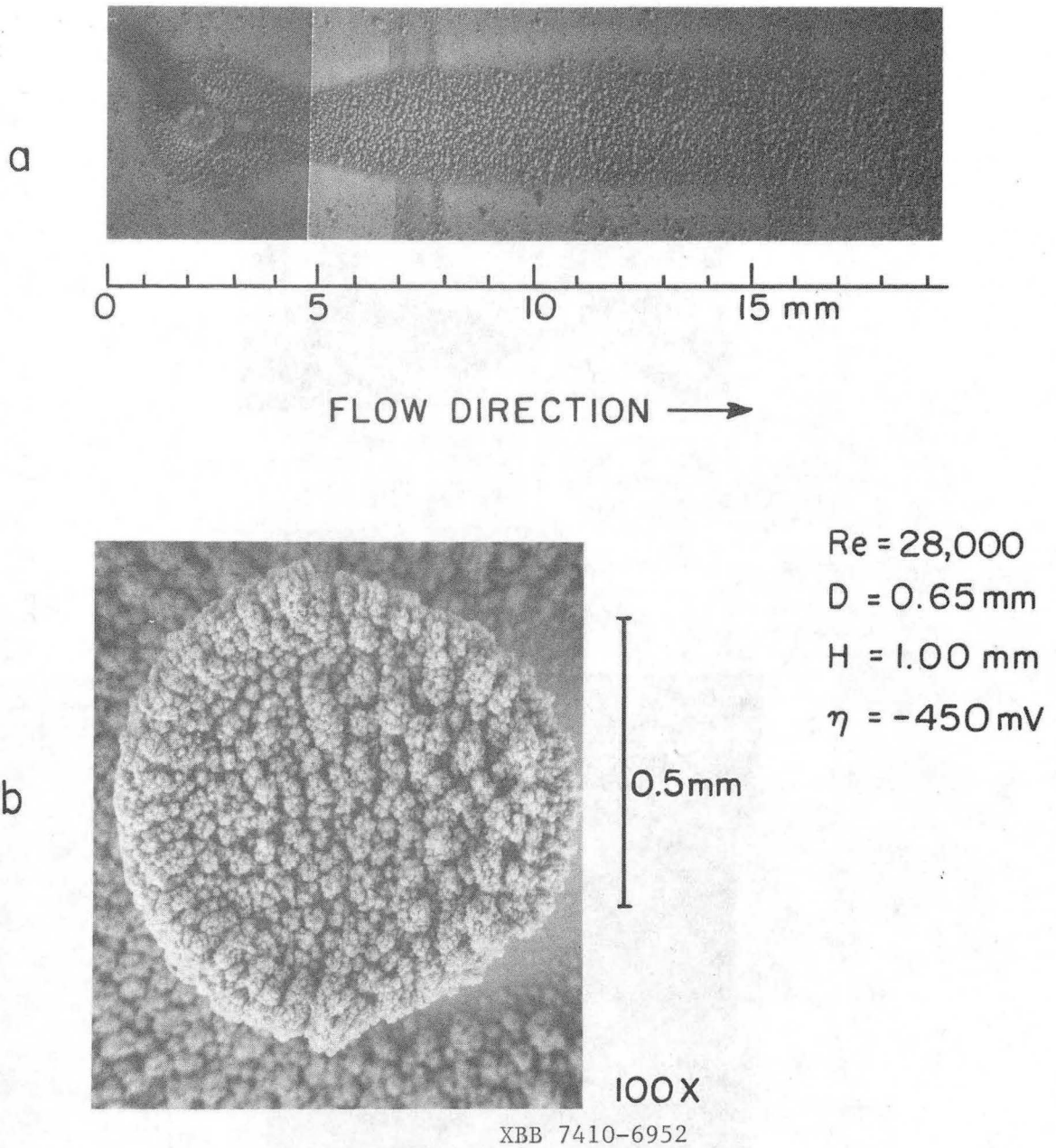
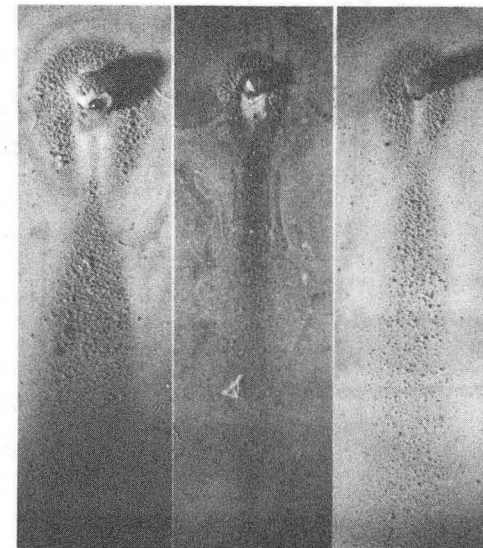
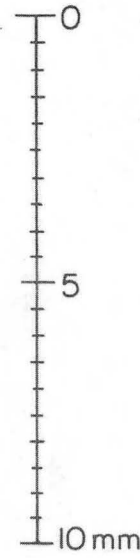
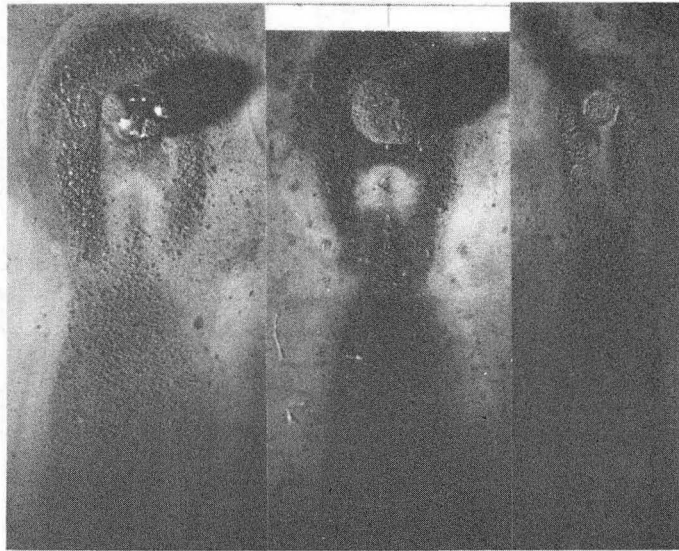


Figure 2.3 A. Composite Photograph Showing Wake Downstream of 0.65 mm Diameter, 1.0 mm High Cylindrical Obstruction in  $\text{CuSO}_4 + \text{H}_2\text{SO}_4$  Solution  
B. SEM Micrograph of Top of Obstruction [11]



	a	b	c
D(mm)	1.30	1.30	0.65
H(mm)	—	—	1.00

	a	b	c
D(mm)	0.62	0.31	0.31
H(mm)	—	0.50	1.00

$Re = 23,000; i/i_L = 1.0$

XBB 7410-6951

Figure 2.4 Wake Formations Downstream of Obstructions [11]

laboratory. They noted a strong dependence of crystallite formation (nucleation) frequency on current density and found only minor influence of small concentrations of lead ions in solution on the overall appearance of spirals. Their results agreed with Jaksic and Tobias's earlier hypothesis that secondary flows in the diffusion boundary layer due to the evolving surface roughness was a major cause for striated zinc deposits. Tsuda, Kommenic, Faltemier and Tobias [19,20] present more preliminary results about the electrocrystallization and striation formation of zinc from acidic electrolytes.

Durdin and Dukhnyakova [21] dissolved manganese and magnesium from RDE's in 0.1 N HCl solution in a study of corrosion rates and observed attacked contours on the disks that accurately followed the fluid streamlines. The number of spiral markings across the surface was in the range of 20, and the spiral shape and angle were highly dependent on the rotation speed.

Gregory and Riddiford [22] investigated the dissolution of a rotating copper disk in 1 M sulfuric acid solutions. They noticed the appearance of spiral markings which followed the fluid flow lines at the surface, and attributed the markings to an onset of localized turbulence around surface obstructions.

Johnson and Turner [23] investigated the effect of organic additives on the kinetics of copper electrodeposition from a sulfate plating solution. They employed a rotating disk electrode system, and deposited copper from 1 M  $\text{CuSO}_4$  + 1 M  $\text{H}_2\text{SO}_4$  solutions which contained small concentrations of addition agents, such as thiourea and gelatin. Their plating conditions and use of addition agents produced deposits with



striation ridges outlining the solution path over the rotating surface. Two interesting observations resulted from this study: the spirals were displaced from the disk center almost proportionally to the angular displacement, and the spiral pattern was not dependent on the rotational speed.

Kim and Jorne [24] studied the mass transport rates of dissolved  $\text{Cl}_2$  to a Zn rotating hemispherical electrode. Spiral shape patterns of dissolution were evident on the corroding hemispherical surfaces at the higher rotation rates. The authors noted that earlier literature [8,25] had shown that the spiral markings were caused by the formation of hydrodynamic wakes around and behind small protrusions and that this initiates secondary flows into the three dimensional boundary layer on the rotating disk or hemisphere.

McBreen [26] investigated the deposition of zinc from zincate solutions using chronopotentiometry, cyclic voltammetry, and electron microscopy. Although his efforts were focused on the morphology changes under random cycling conditions and additive and substrate effects on improving the zinc morphology, in certain regimes of variables he did observe spiral formation in the zinc deposits. He found that by superimposing a small alternating voltage, the morphology of the deposits was greatly improved.

Horkans [27] deposited a nickel-iron alloy galvanostatically from acidic  $\text{Cl}^-$  solutions and  $\text{SO}_4^{2-}$  solutions with no additives present, and observed spirals that "appeared to originate from small macroscopic protrusions on the surface". The appearance of the protrusions could not be fully explained. She also saw evidence of hydrogen evolution



blocking random sites on the electrode.

Oren and Landau [28] investigated the physical characteristics of zinc dendrites deposited from concentrated, acidic  $ZnCl_2$  solutions. They noted that initiation of dendritic growth occurred at an overpotential which was independent of concentration, that dendrite height increased linearly with time at a constant overpotential, and that dendrite growth increased with an increase in concentration or overpotential or with a decrease in pH. They discussed dendrite tip propagation rates in terms of an extended Barton-Bockris model.

A massive, critical report of theoretical and experimental work has been compiled by U. Landau, B.D. Cahan, and J.R. Selman [29] on zinc deposition from acidic chloride and bromide electrolytes. These authors studied many aspects of zinc electrochemistry including the actual measurement of physical-chemical properties of zinc halide electrolytes, modelling of the various stages of dendritic growth, and characterization of zinc morphology under simulated flow cell conditions. The authors' goals were very practical and immediate--to compile and compare theoretical models of dendritic growth and any existing empirical information in order to gain a better understanding of zinc deposition and zinc dendrite growth, and to define conditions for obtaining improved zinc deposits. They quantitatively modeled various stages of zinc dendritic growth including a microscopic analysis of the initiation and propagation stages and a macroscopic analysis of the operation (steady-state and unsteady-state) of a zinc flow cell. A large number of conclusions are listed concerning modelling of electrodeposition, and dendritic growth in zinc batteries, and possible directions for further

investigation of the mechanism and inhibition of dendritic zinc deposition are suggested.

Striated markings in deposition and dissolution have also been observed by a number of other investigators [30,31,32,33].

## 2.2 Aspects of Zinc Electrochemistry

The electrochemistry of zinc, in spite of the long standing technological significance of the metal, is not very well understood. In part responsible for this state of affairs is the tendency of zinc ions to form complexes in solution, and the fast kinetics of the charge transfer reaction. The solution-side transport of zinc ions, which are partially present in the form of complexes is still not clarified [29,34-42]. The negative transference numbers observed in concentrated halide solutions are responsible for rather adverse mass transport conditions, namely various zinc ionic species migrate in the unfavourable direction with respect to both electrodes. Perhaps the most weakly understood aspect of zinc deposition is the mechanism of nucleation and crystal growth.

Several authors who dealt with relevant aspects of zinc electrochemistry and observed striated surfaces were listed in the previous section. Bard [34] gives a general, comprehensive review of the electrochemical behavior of zinc. Other relevant investigations are reviewed in the following.

Despic and Popov deposited zinc under a pulsating potential, and then analyzed the surface roughness of the deposit [43]. Their results showed no increase in surface roughness with time under certain alternating potential conditions, resulting in smoother deposits.

Selman and Tobias [44] describe in an extensive review the theory and experimental methods involved in measurement of mass transport coefficients by the limiting current technique. Selman and Tobias [45] and Andricacos and Ross [46] also investigated the unsteady-state effects associated with potentiodynamic and galvanodynamic limiting current measurements.

Several authors have measured zinc diffusion coefficients in zinc electrolytes using both the limiting current technique [47,48] on a RDE and an interferometric technique [49,50]. Rajhenbah, Faltemier, and Tobias [47] obtained diffusion limiting currents for zinc on a RDE in several acidic zinc chloride and sulfate solutions. They compared their diffusion coefficient values with other experimental zinc diffusion coefficients found in the literature.

McBreen and Gannon [51] have investigated zinc deposition in ultra-pure acidic electrolytes. Their work examined several different methods of controlling the initial stages of morphology including variable charging techniques, substrates, and organic and inorganic additives. McBreen and Gannon found that by superposition of square wave potential pulses, the zinc nucleation rate increased and the deposit orientation was modified. They suggested that deposition of zinc occurs with nucleation of three dimensional centers and simultaneous two dimensional layer growth.

Several investigators have examined the effects of addition of other metallic ions or additives on zinc morphology. MacKinnon, et. al. [52] observed a relationship between the amount of lead contamination on the zinc deposit morphology and orientation and the polarization

required for zinc on zinc deposit structures. They noted no significant effects in deposit orientation, however, they did observe a refinement of the crystal grain size upon cadmium addition to the electrolyte. Gay and Bergsma [54] studied the effect of nitrate ions on the morphology of zinc electrodeposits. Spongy zinc deposits were always obtained, independent of the current density and flow conditions, due to the oxidizing nitrate ion. Thomas and Fray [55] investigated the morphology of zinc electrodeposited at high current densities from a zinc chloride solution with proteinous additives. They noted that at  $200 \text{ mA/cm}^2$  with use of the proteinous additives, the metal deposited in the form of zinc platelets inclined (at an angle) to the original cathode surface rather than in platelets which are parallel with it. The current efficiencies were also higher (up to 85%) in solutions containing the additives. The effects of dissolved oxygen, antimony, glue, and other organic additives on the morphology of zinc have also been investigated [88-92].

### 2.3 Current Distribution and Convective-Mass Transport along a Planar Electrode

The current distribution on the rotating disk electrode below the limiting current has been evaluated by Newman and his coworkers [56,57,58]. Due to the geometry of the cell involving disk electrodes, the disk is nonuniformly accessible to ions and hence, the primary distribution of current is nonuniform. Current density is infinite along the edge, and low in the center. However, at the limiting current, mass transport controls the distribution of the overall electrode reaction, and since the boundary layer is uniform over the disk, the limiting current density distribution is also uniform.

The case of current distribution on plane parallel electrodes embedded in a channel flow cell in the presence of charge transfer overpotential and mass transfer in laminar flow has also been solved by Newman and his coworkers [56,59]. Wagner [60] solved the case of the primary current distribution, which assumes an equipotential electrode surface and no concentration effects. The primary current distribution is symmetric about the electrode center in the direction of flow, and exhibits infinite current densities at both the leading and trailing edges. Secondary current distribution, depending on the magnitude of the Wagner number, may be quite uniform, if the current density is a strong function of overpotential. In the case of limiting mass transport, the current distribution exhibits infinite current density at the leading edge and decays inversely proportionally to the  $1/3$  power of the electrode length in the downstream direction.

Current distribution in channel flow was measured with high precision by Landau [12] on a 40 cm long segmented electrode. His results are in full agreement with the predicted values from the Norris and Stried equation. Landau, et.al. [29] show calculated current distributions for the channel flow cell used in their zinc deposition model study. They noted fairly uniform current distribution along the electrode in their zinc-bromine flowcells for current values below approximately 50% of the mass transfer limiting current because of compensating effects of mass transfer resistance and the potential drop within the electrodes (terminal effect).

The convective-mass transport equations of the rotating disk electrode were first successfully solved in 1942 by Levich [61]. The rotat-

ing disk electrode has since been aggressively used for studying various electrochemical phenomena. A. C. Riddiford [25] has reviewed the fundamentals and applications of the rotating disk electrode, and Pleskov and Filinovskii [62] have extensively covered the theory and experimental techniques of the rotating disk electrode. Newman and his coworkers [56,63,64,65] have refined Levich's original solution and examined other mass transport effects on the disk electrode.

The fluid flow along the rotating disk electrode is in the radial direction due to the inertial effect of rotating the disk, and in the angular direction due to frictional forces between the fluid and disk surface. In order to replace the fluid flowing out in the radial direction near the disk, fluid from far away flows perpendicularly toward the rotating disk. The path that a fluid element would take along the surface when the disk rotates is as follows: the fluid element would travel perpendicularly toward the rotating disk from far away; when near the electrode surface, it would feel both a radial force due to the disk rotation and a frictional angular force, and it would travel parallel to the disk surface in a spiral motion toward the disk edge, as reflected in the spiral shaped surfaces discussed earlier.

The current distribution around perturbations on a flat surface has been investigated by several researchers. Landau [12] and Carlson [11], as mentioned previously, investigated copper deposition around small protrusions on planar electrodes. They showed an enhanced rate of deposition in the wake regions of these protrusions. Hickman [5,6] showed that in the presence of roll cells, in the limiting current region, grooves appear in the copper deposit. Landau, et. al. [29] modeled den-

drite growth inside a diffusion layer taking into account the varying concentration inside the diffusion layer, effects of flow velocity, and perturbations of the current distribution caused by the dendrite. They listed several major conclusions, including that convective mass transfer affects dendrite growth both through the flow velocity in the vicinity of the dendrite tip and by perturbations in the concentration and current distribution caused by the convection.

#### 2.4 Zinc Batteries

Zinc is a major, active component in several secondary batteries that are currently being examined for utility load-leveling or electric vehicle applications. All the zinc secondary batteries have low demonstrated cycle lives, partly due to rough and dendritic zinc deposition which leads to accelerated zinc material loss, densification, and reshaping, and electrical shorting failures. Striated deposits have been observed in prototype zinc bromide and chloride batteries, and these nonsmooth surfaces help to cause short cycle lives. These zinc batteries may become viable as alternative storage devices only when the deposit quality has been greatly improved. Other problems such as current efficiency levels and scaling-up complexities in zinc batteries must be investigated in assembled prototype batteries. Several publications address these efforts that are more closely related to batteries [66-73].

McBreen and Cairns [66] present an interesting, competent review on the zinc electrode in both acidic and alkaline cells. They discuss the many complexities associated with the zinc species in chloride and bromide solutions, as well as in KOH solutions, and the major problems

concerning the zinc electrode still unsolved for several battery systems.

Jorne, Kim and Kralik [67] have studied the overall efficiency and voltaic behavior of the zinc-chlorine battery. Energy efficiencies in the range of 65% have been achieved for a full cycle. Jorne [68] has also modeled the fluid and gaseous flow distribution in an actual zinc-chlorine battery.

A number of Department of Energy (DOE) and Electric Power Research Institute (EPRI) proceedings and reports on different aspects of zinc batteries as well as other advanced batteries are available in the literature [69,70,71,72,73].



### 3. EXPERIMENTAL

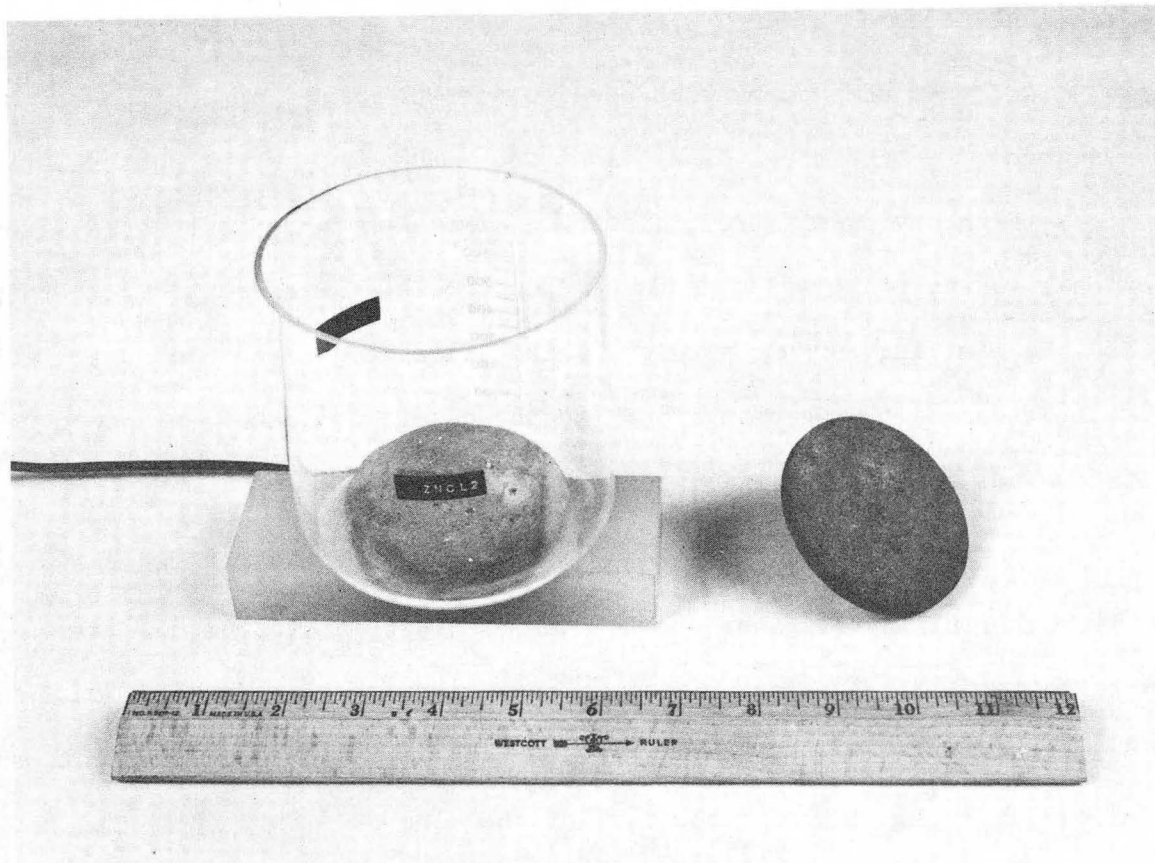
#### 3.1 Experimental Apparatus

##### 3.1.1 Experimental Cells

Two types of systems were used to accomplish the objectives of this research: a rotating disk electrode (RDE) and several channel flow cells, each having different electrode dimensions and flow cross-sectional areas. All experiments were controlled galvanostatically except for the limiting current studies, which were conducted potentiostatically. Periodic upgrading and turnover of equipment also occurred throughout the span of this project.

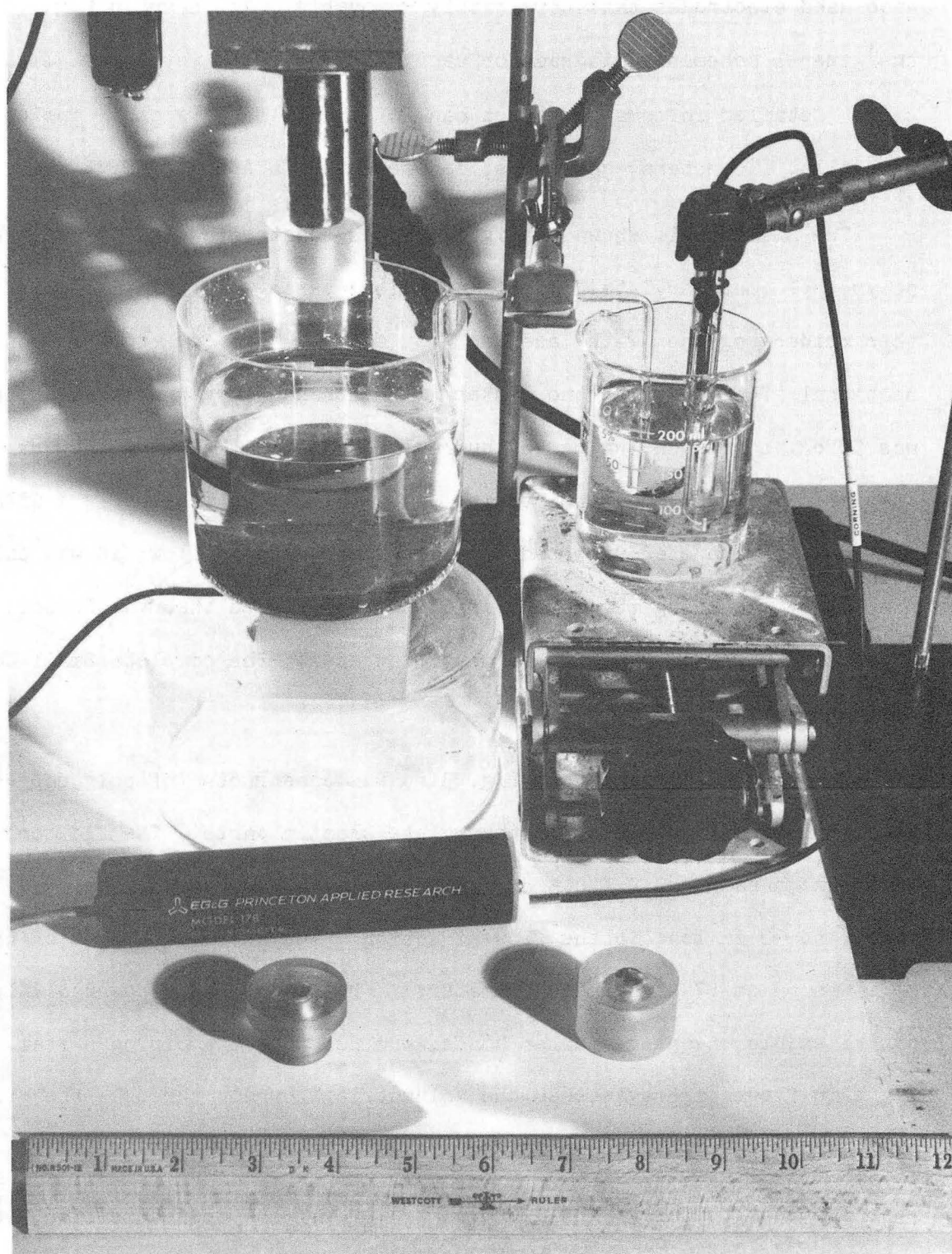
For the rotating disk electrode (RDE) experiments, a shortened 1-liter borosilicate glass beaker was used with a 0.64 cm hole blown in the center of the bottom so that a large circular zinc anode could be positioned at the bottom facing upward, sealed solution-tight, and electrically connected to the rest of the circuit. This cell is shown in Fig. 3.1. In limiting-current studies, a Luggin capillary leading to a calomel reference electrode was also inserted into this beaker, as shown in Fig. 3.2.

All three channel-flow cells used in this study had rectangular cross-sectional flow areas and planar electrodes of different dimensions. The three cells consisted of a small cell with a long entrance length (hereafter, denoted Small Cell), a large cell (Large Cell), and a cell specially-built for the in situ studies (In situ Cell). The Small Cell was originally designed and used by Dr. Milan Jaksic in 1976-1978. Each of the cells was constructed out of different types of plastic, and



CBB 833-2341

Figure 3.1 RDE Electrolysis Cell and Zinc Anode



CBB 823-2854

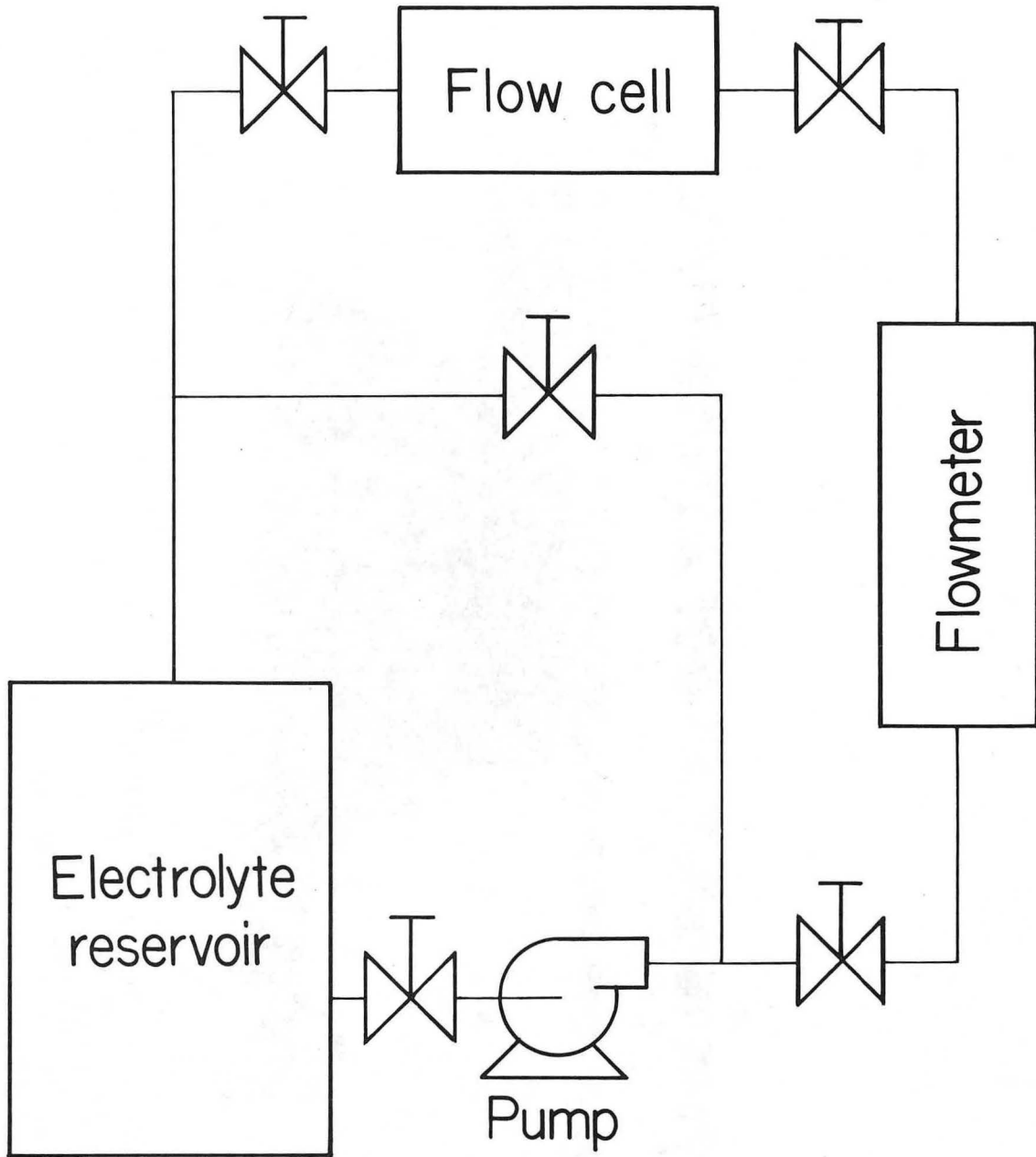
Figure 3.2 RDE Electrolysis Cell and Reference Electrode Compartment Connected by Luggin Capillary

each used electrodes that were easily removable. As shown in Fig. 3.3, the general schematic diagram for each of these cells is essentially the same. Detailed information about each of the flow systems, including the cells, flowmeters, and pumps, is presented in Appendix B.

The Small Cell, shown in Fig. 3.4, was constructed of transparent polymethyl methacrylate plastic (Lucite) parts that were machined and then melded together with acetone to form a 0.5 cm square cross-sectional flow area at the center. The entrance length of this channel was 50 cm, corresponding to 100 hydraulic diameters. The piping system consisted of polyethylene tubing and teflon connectors. A Gilman Instruments rotameter was used to measure the rate of flow; it was calibrated by measuring the amount of fluid that flowed through the cell in a certain amount of time for various flowrates. The complete Small Cell system is shown in Fig. 3.5.

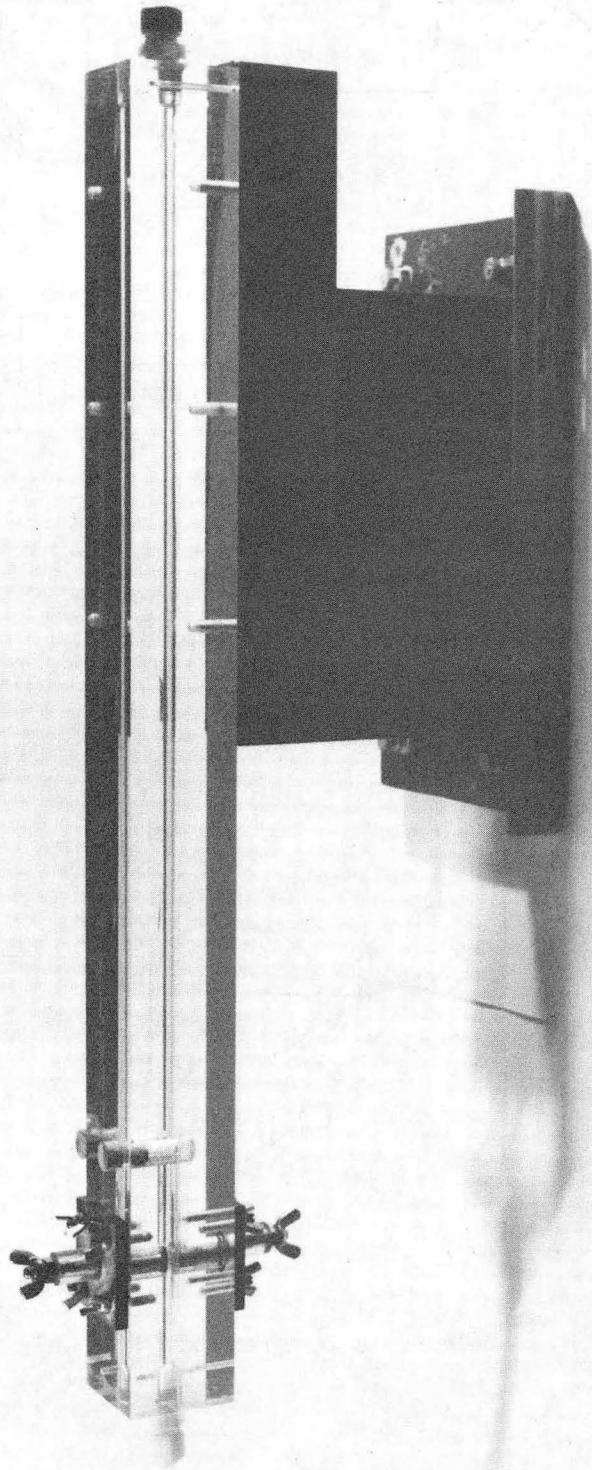
The Large Cell, shown in Fig. 3.6, was constructed of polypropylene and transparent polymethyl methacrylate plastic parts. The flow cross-sectional area was 3.0 x 0.5 cm; and the planar electrodes were 3.0 cm wide and 30 cm long in the flow direction. The entrance length of this cell was 63 cm (74 hydraulic diameters). Polypropylene pipes and valves and flexible neoprene rubber hoses were used for the piping system. A magnetic flowmeter registered the volumetric flowrate through the flow cell. This system is shown in Fig. 3.7.

The In situ Cell, with a 0.6 cm x 1.0 cm flow cross section, was constructed of polypropylene and transparent polymethyl methacrylate plastic through which the cathode could be photographed. The flow system and cell are shown in Figs. 3.8 and 3.9. The piping system



XBL 835-9572

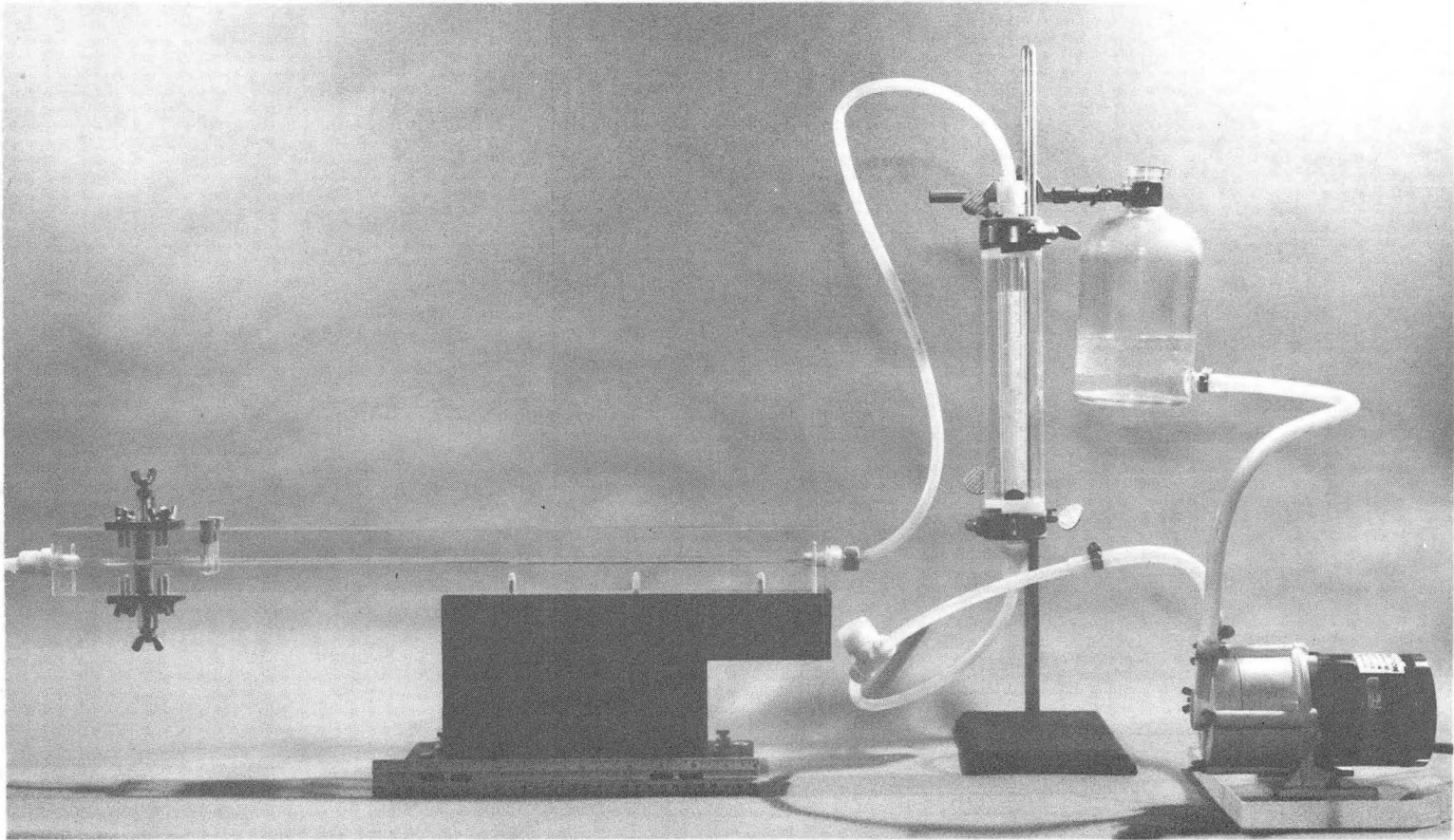
Figure 3.3 Schematic Diagram of Flow Cell Systems



CBB 780-15940

Figure 3.4 Small Channel Flowcell





CBB 780-15938

Figure 3.5 Small Channel Flowcell System

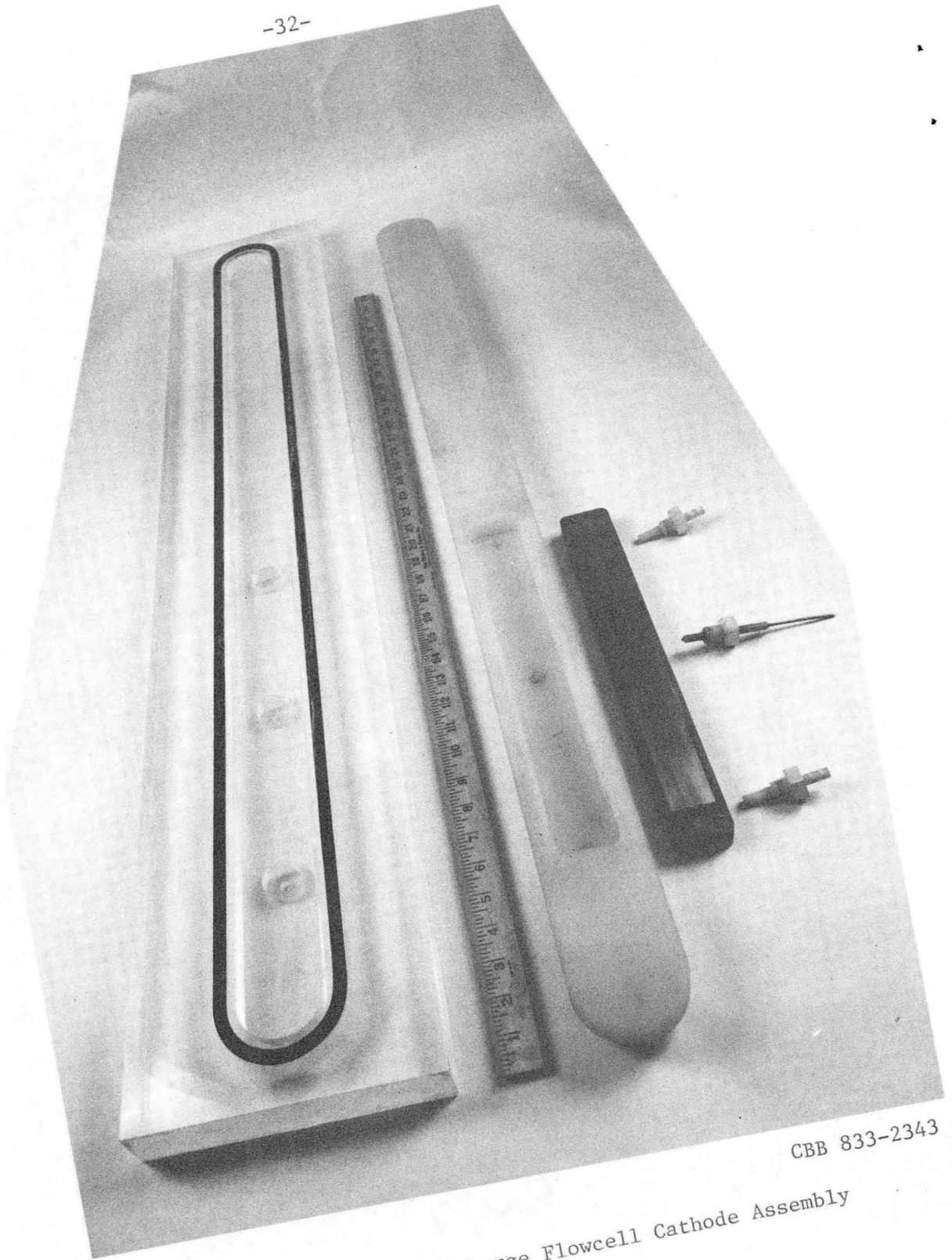
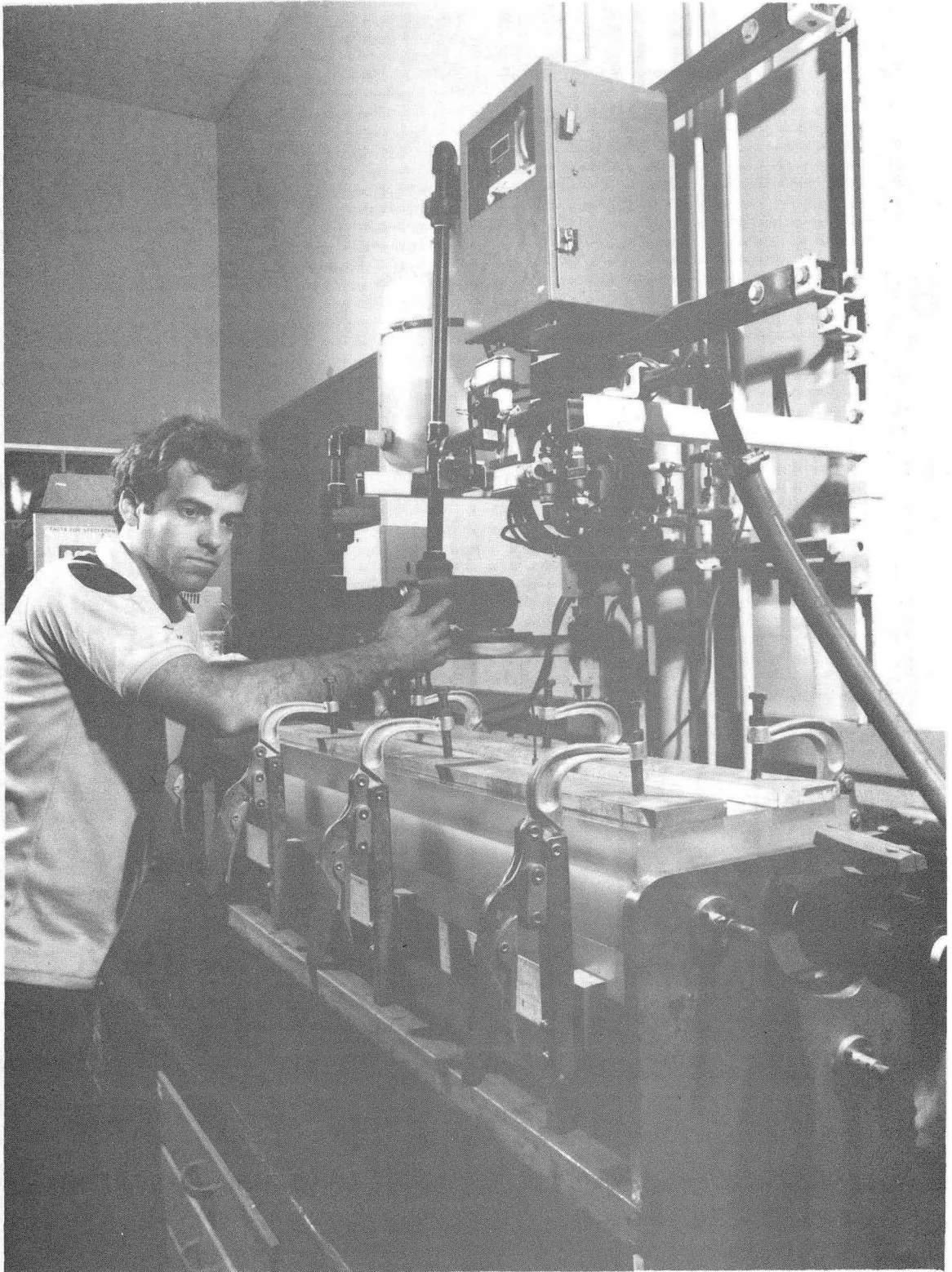


Figure 3.6 Exploded View of Large Flowcell Cathode Assembly

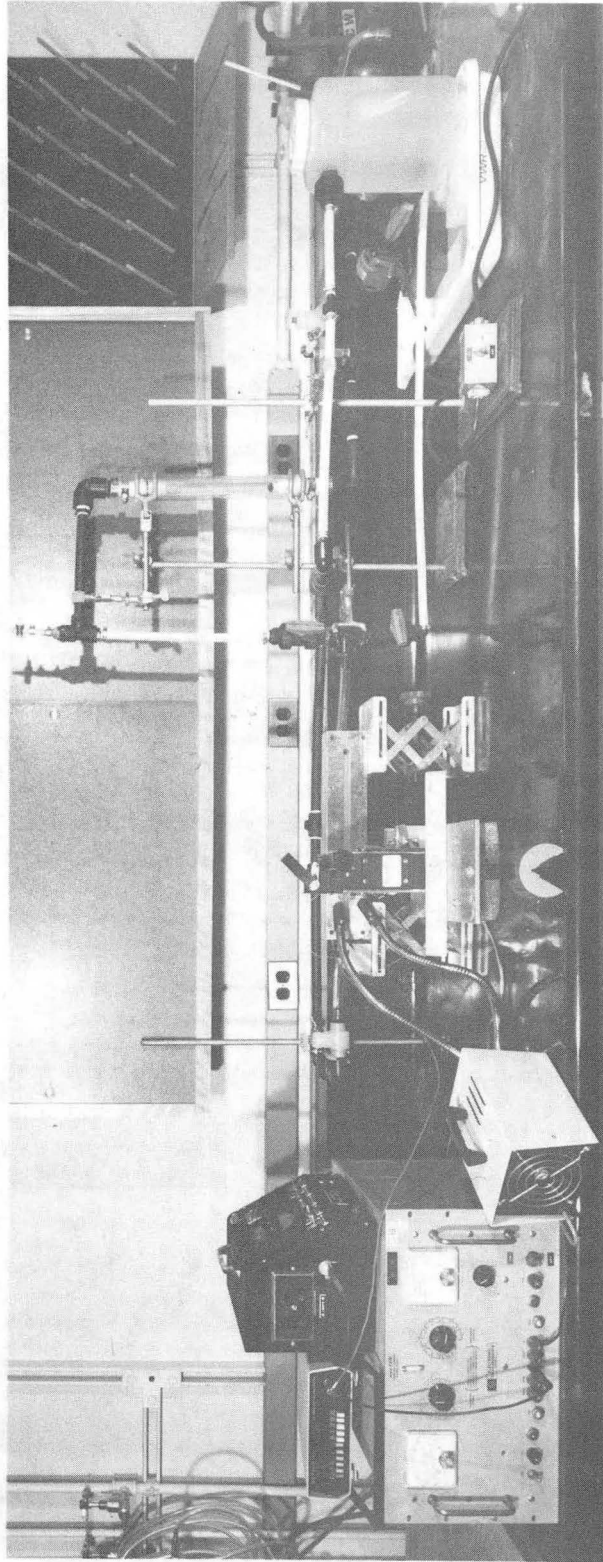
CBB 833-2343





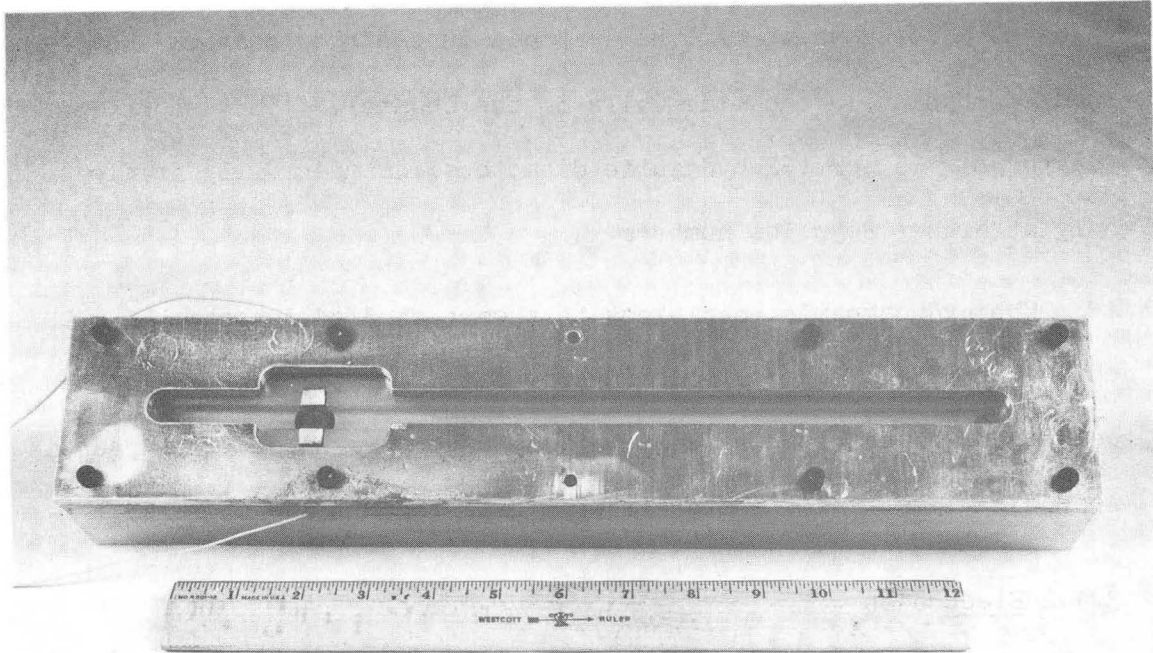
CBB 833-2351

Figure 3.7 Large Flowcell System



CBB 820-10761

Figure 3.8 In Situ Flowcell Experimental Apparatus



CBB 833-2347

Figure 3.9 Top View of In Situ Flowcell

consisted of polyethylene pipes and valves and Tygon hoses. Fig. 3.10 gives a close view of the cathode in the flow channel and the zinc anodes embedded in the side walls of the channel. The short entrance length of 25 cm (52 hydraulic diameters) assures fully developed flow only at higher Reynolds numbers.

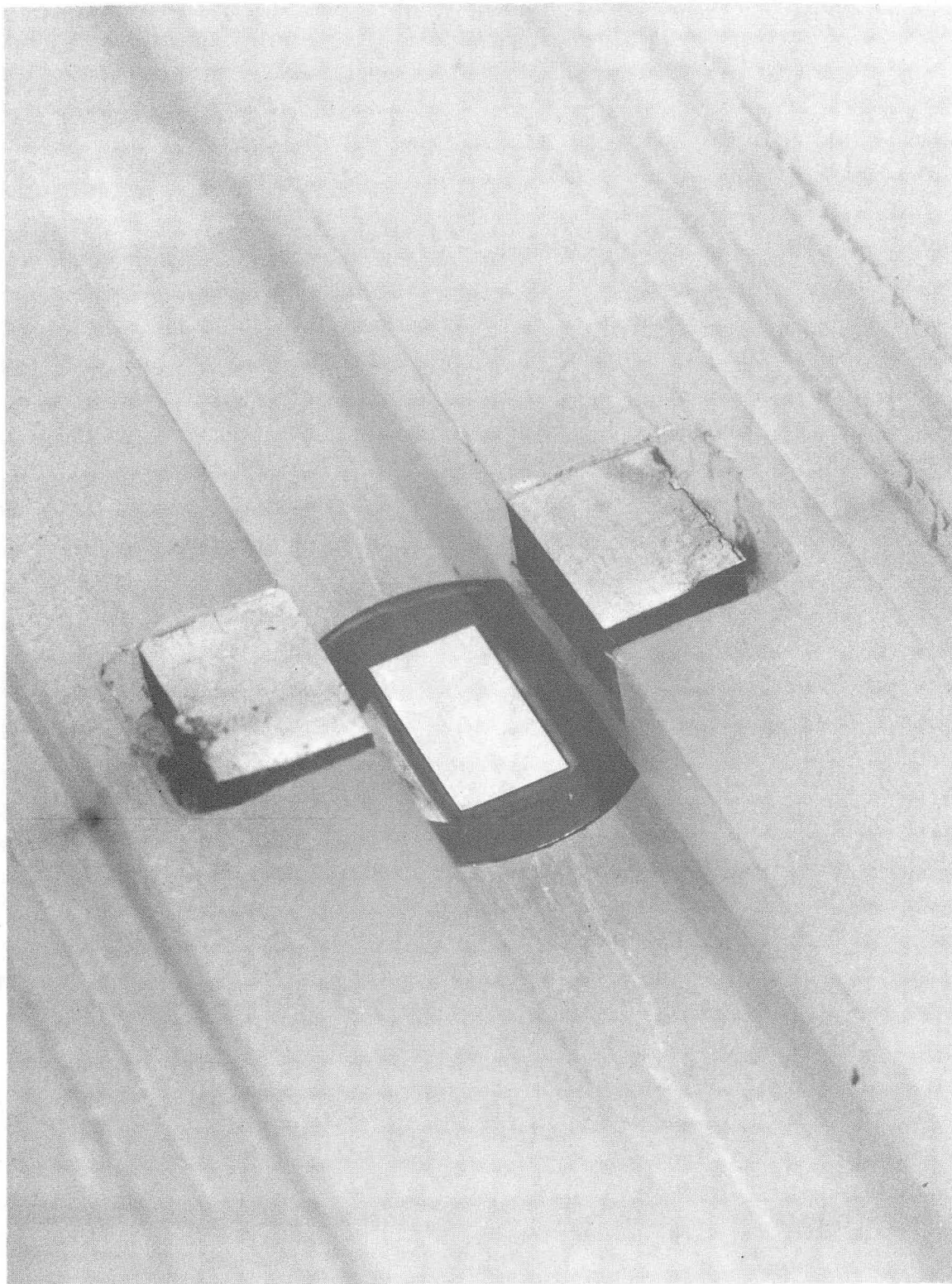
The hydrodynamic conditions that were studied in both the RDE and channel systems are listed in Appendix F. The definition of the Reynolds number and sample calculations are presented in Appendix E. Appendix H contains the experimental data for all the systems.

### 3.1.2 Electrodes

The electrodes used in both the RDE and the three flow cells were very similar in construction and design. The RDE cathodes are shown in Fig. 3.11. An electrode disk was attached to a brass core using silver epoxy-resin. The brass core was threaded so it could be attached to the rotating shaft of the rotating disk assembly. Nonconductive epoxy-resin was poured around this core and electrode, and then the entire assembly was oven-cured, and machined to produce the cylindrical shapes. The platinum disks were of two sizes, 1.13 cm and 1.45 cm in diameter. The zinc disks used for the limiting current studies were 1.0 cm in diameter.

The zinc anode used in the RDE studies was a large 99.99% zinc disk, 7.5 cm in diameter and 0.7 cm thick. A 0.64 cm steel bolt was attached to the back using silver epoxy-resin and then coated with nonconductive epoxy-resin to prevent corrosion. This anode is also shown in Fig. 3.1.





CBB 820-10747

Figure 3.10 Close View of In Situ Flowcell Showing Cathode and 2 Anodes

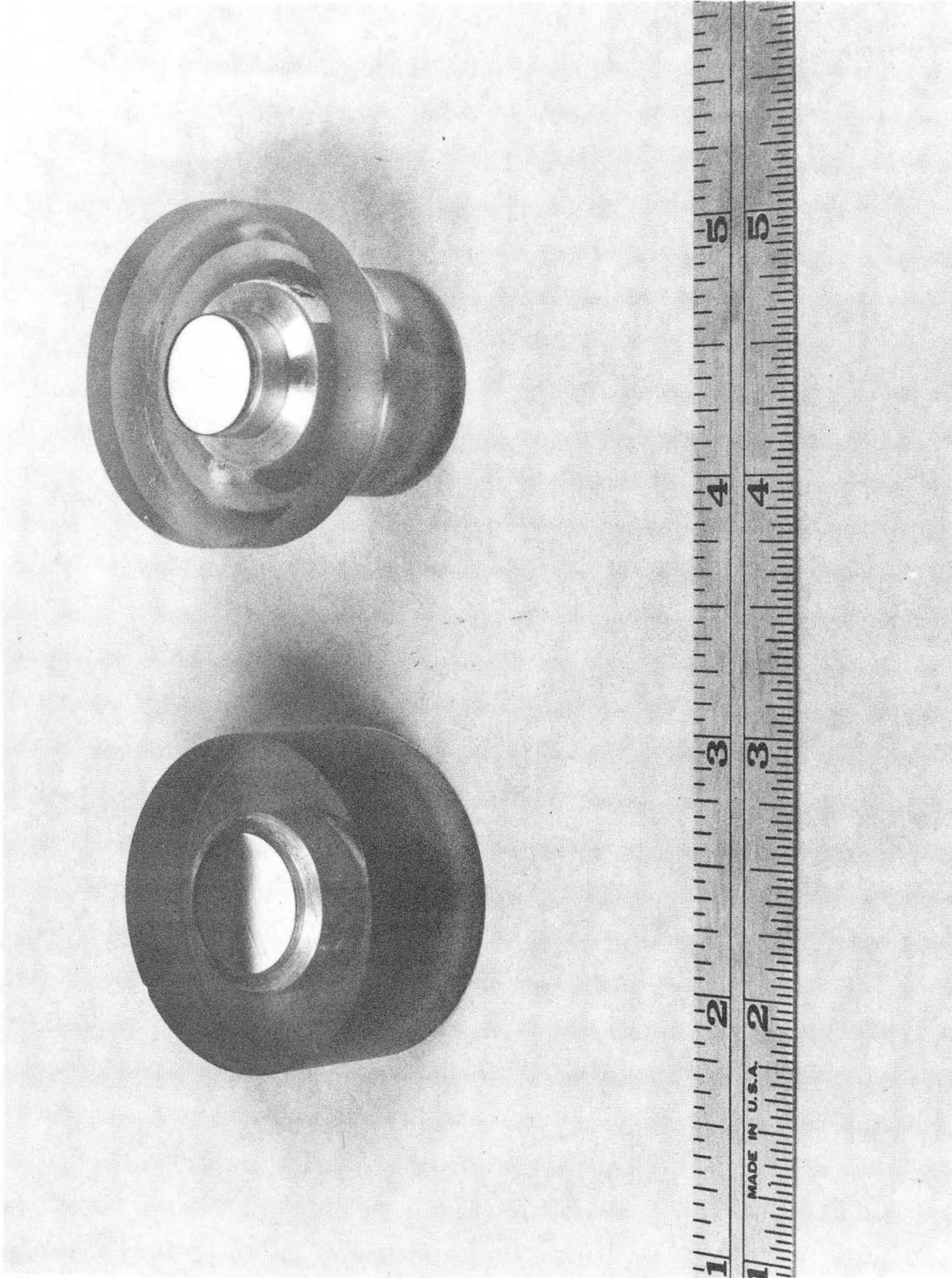


Figure 3.11 RDE Cathodes

CBB 820-10749

The cathodes and anodes in the Small Cell\* were constructed in a similar fashion to the RDE cathodes. Rectangular substrates of either platinum, pyrolytic carbon, zinc, or copper were attached to a brass core with silver epoxy-resin, and then cast in nonconductive epoxy-resin and machined to 1.3 cm diameter. These electrodes, shown in Fig. 3.12, have rectangular surface dimensions of 0.95 cm X 0.50 cm. Circular zinc anodes of 0.95 cm diameter were also constructed and used in the Small Cell.

The In situ Cell accomodates the same cathodes as the Small Cell, but requires different zinc anodes, shown in Fig. 3.12. The two 0.4 cm X 0.9 cm anodes fit into two machined cavities in opposing walls of the polypropylene channel. A 24 gauge (0.12 cm diameter insulated wire) silver wire was attached to the back of the zinc, and then all sides except the face that was in the channel were coated with nonconductive epoxy-resin to insulate them from the electrolyte.

The Large Cell uses large rectangular cathodes and anodes, which are shown in Fig. 3.13. The cathode, a platinum bar of dimensions 30 cm X 3 cm X 0.63 cm thick was cast into a nonconductive epoxy-resin mold. The zinc anodes of similar dimensions were also embedded in epoxy. Electrical connection to the electrodes was made through threaded holes on the back side of the molds.

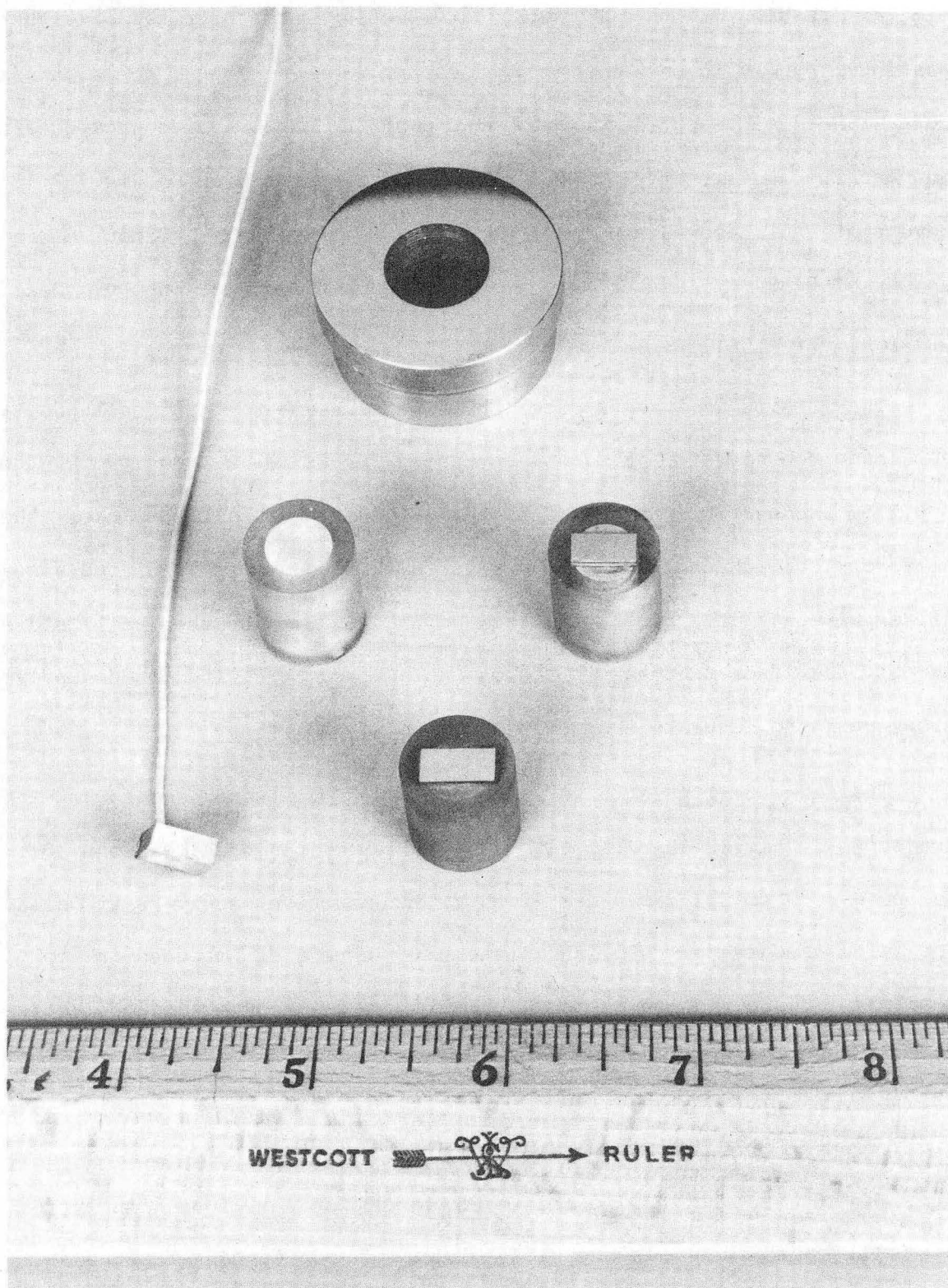
### 3.1.3 Electrolytes

All of the solutions in this study were prepared from "Analytical Reagent grade" chemicals and water distilled in a Corning Water Distil-

---

\*designed by Milan Jaksic and Larry Galovich



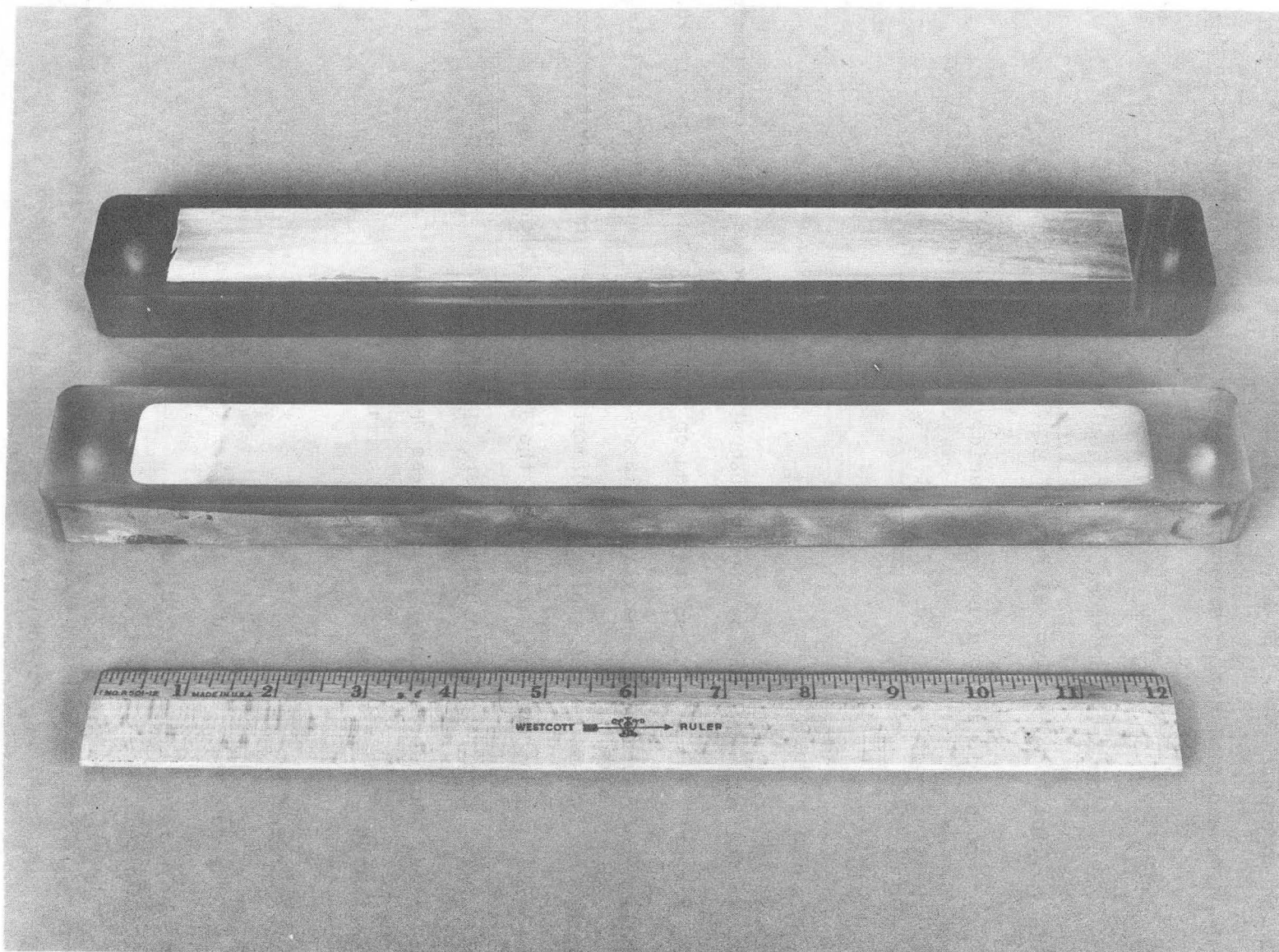


CBB 820-10755

Figure 3.12 Small Flowcell and In Situ Flowcell Electrodes

(Top to Bottom, Left to Right), Polishing Jig, Circular Zinc Anode, Platinum Cathode, Copper Cathode, In Situ Flowcell Zinc Anode with Silver Wire





CBB 820-10751

Figure 3.13 Large Flowcell Platinum Cathode (Top) and Zinc Anode

lation Apparatus (Model AG-2). The majority of the experimental data were obtained in 1 M zinc solutions of various pH's; a few other concentrations of zinc solutions were sampled.

- (1) Zinc chloride, zinc bromide, zinc sulfate  
Mallinckrodt, Analytical Reagent grade
- (2) Hydrochloric acid, hydrobromic acid, sulfuric acid  
Mallinckrodt, Analytical Reagent grade
- (3) Zonyl FSB  
duPont Corp.

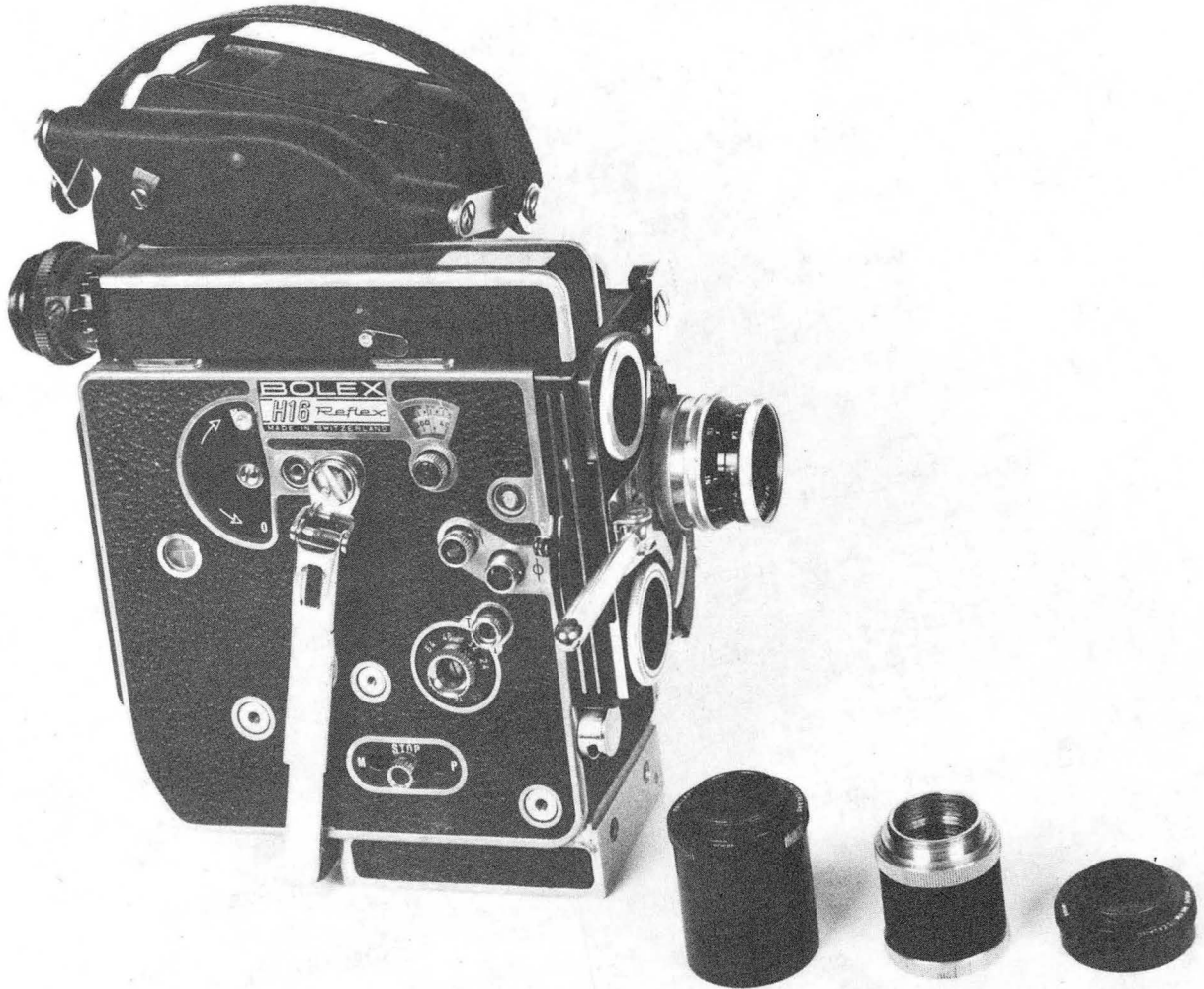
A chemical analysis by atomic absorption spectroscopy was performed on several 1 M  $ZnCl_2$  solutions and on distilled water samples by the College of Chemistry analytical laboratory. The results of this analysis, shown in Appendix C, demonstrate that no impurities are present in the distilled water above the limits of detection and that no seemingly significant impurities are present in the "AR" grade  $ZnCl_2$  solution. Further explanation of these data are given in the "Results and Discussion" chapter.

#### 3.1.4 Equipment

The equipment items used in the various stages of this research are listed below in four categories:

- (1) Rotating disk electrode experiments
  - (a) Wenking Potentiostat, superseded by PAR Model 371  
Potentiostat-Galvanostat with Model 178 Electrometer probe

- (b) PAR Model 175 Universal Programmer
  - (c) Keithley Model 173A Digital Multimeter
  - (d) Hewlett-Packard Model 7001A XY Recorder, superceded by Gould Model 7056 XY Recorder
  - (e) A disk rotator, constructed in house, using a Servo-Tek Products Model STE-231T-1C variable speed motor and Type ST-556 Controller, replaced in 1980 with Pines Instruments Model ASR2 Analytical Rotator
- (2) Channel Flow Cell experiments
- (a) Electronic Measurements Model C618 Constant Current Power Supply or a Sorenson Model SRL 10-50 Power Supply
  - (b) Keithley Model 179TRMS Digital Multimeter
  - (c) Clampitron Magnetic Flowmeter Model 241R (in Large Cell)
  - (d) Gilmont Instruments Rotameter Model F-1500 (in Small Cell)
  - (e) Gilmont Instruments Rotameter Model F-1560A (in In situ Cell)
- (3) Photographic equipment
- (a) Polaroid MP-3 Land Camera with Polaroid Type 55 4x5 Land Film
  - (b) Paillard-Bolex 16 mm Camera Model H16 Rex with Kodak 7276 Plus-X Reversal Film (Figure 3.14)
  - (c) Samenco Movie Control Model No. MC-5E50
  - (d) AMR Model 1000 Scanning Electron Microscope
  - (e) L-W International Photo-optical Data Analyzer Mark V Model 224A



CBB 820-10753

Figure 3.14 Bolex 16 mm Camera with Extension Tubes

(4) Accessory Instruments

- (a) Gould-Clevite Corporation Surfanalyzer Model 21-1330-20
- (b) Casio Chronograph Model 79QS-39
- (c) Mettler Balance Type K7T
- (d) Power Designs Inc. Power Source Model 2005 (preelectrolysis).

3.2 Experimental Procedure

3.2.1 Electrode Preparation

The general purpose in the polishing procedure was to give reproducible and well-defined substrate surfaces upon which zinc could be electrodeposited. The aim was not to give perfect, scratch-free surfaces, which would have been virtually impossible, but rather to get highly polished, clean, reproducible surfaces. The standard technique, consisting of sanding with silicon carbide paper and then polishing with diamond paste, was used for all the platinum, zinc, carbon, and copper substrates.

All of the electrodes were sanded with silicon carbide sanding papers, beginning with the coarse (grit 250) and finishing with the very fine paper (grit 600). The electrodes were cleaned with a dilute soap solution and rinsed thoroughly with water, and then rotated 90 degrees before continuing with the next finer grade of sanding paper.

After this procedure, the electrodes were polished on a standard 10 inch canvas polishing wheel. Diamond paste (1 micron size) was coated on the canvas, and kerosene was used to lubricate the polishing surface. After polishing to a mirror-like finish, the electrodes were washed in

soap and water and scrubbed with cotton applicators, then rinsed in water, acetone, and ethanol, and finally dried with compressed air. The polished and cleaned electrodes were then stored in dust-free plastic containers until they were needed for experiments.

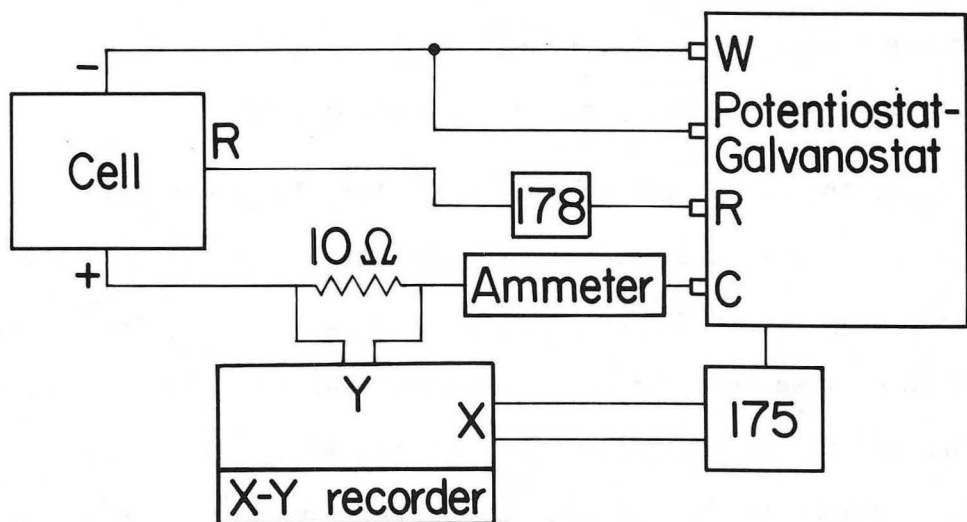
Just before the electrodeposition experiments, some of the substrate materials were pretreated. The platinum and graphite electrode surfaces were subjected first to cathodic polarization for approximately 15 minutes and then to anodic polarization for the same length of time, in a solution of 1 M KOH and either 0.5 M  $K_2HPO_4$  or 0.5 M NaCl, at approximately 300 mA/cm<sup>2</sup>. The zinc electrodes were dipped in concentrated  $HNO_3$  for 1 second. The copper electrodes had no special pretreatment. Each electrode was then rinsed thoroughly with distilled water and immediately placed in the cell.

### 3.2.2 Details of Operation

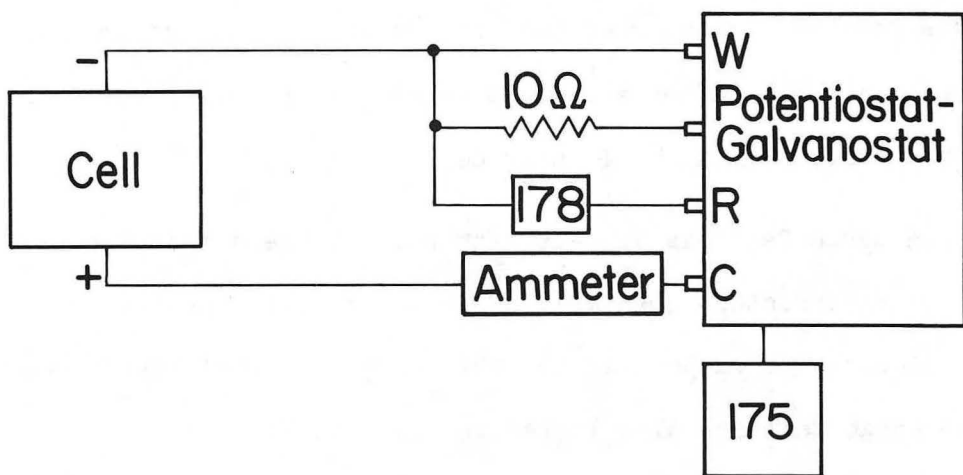
The general experimental procedure adopted was exactly the same for both the RDE and channel systems. First, the cell was electrically connected to the instrumentation, the electrolyte flow was started and allowed to develop to steady state, and then the electrodeposition was begun. Electrical circuit diagrams for the galvanostatically and potentiostatically controlled experiments are shown in Fig. 3.15.

Zinc was electrodeposited at room temperature (20° - 25° C) in experiments of various current densities and hydrodynamic conditions (flowrates or rpms). The experiments were periodically interrupted every few minutes to allow recording of the development of the deposit by macrophotography. During the interruptions, the electrical current

### POTENTIOSTATIC OPERATION



### GALVANOSTATIC OPERATION



XBL 835-9573

Figure 3.15 Electrical Circuit Diagrams



and electrolyte flow was turned off, and the electrode immediately removed and washed thoroughly with distilled water. After the photograph was taken, the same electrode was returned to the cell and the experiment continued until the next interruption.

After the experiment was finished, the electrode was removed and washed with distilled water, then delicately dried with compressed air, and stored in the dust-free container for possible later examination. Appendix F gives the major experimental conditions that were examined in the RDE and the channel flow cells. Detailed descriptions and photograph numbers of the various experiments are listed in Appendix H and are also included in an LBL Report LBL-16601 [14].

For the Insitu Cell, in addition to the above instructions, the fiberoptic light was turned on, and the camera shutter mechanism engaged before the experiment was started. The Bolex Model H16 camera was set for 1 frame per second for the first 10 minutes and then 1 frame per 4 seconds for the remainder of the experiment. The camera had to be rewound manually after every 650 frames. Appendix F gives the various conditions studied in the In situ Cell.

The Large Cell was operated for the full length of the experiments without interruption because of the difficulty involved with removing and replacing the cathode in the cell. Experimental conditions employed in the Large Cell are also listed in Appendix F.

### 3.2.3 Examination of Deposits

The zinc deposits were examined by several photo-imaging techniques. In the RDE and the Small Cell, the deposit was photographed



periodically during the experiment with the Polaroid Industrial Land Camera. This macrophotographic camera gave low magnification images (approximately 10X). A full history of the deposit development could be seen by arranging these photos sequentially. Some of the deposits were also examined at higher magnification (< 10,000X) by scanning electron microscopy. The motion picture resulting from the In situ Cell experiments was developed by Leo Diner Laboratories in San Francisco and then analyzed in this laboratory. Appendix D gives an expanded explanation of the motion photography experiments and of the film.

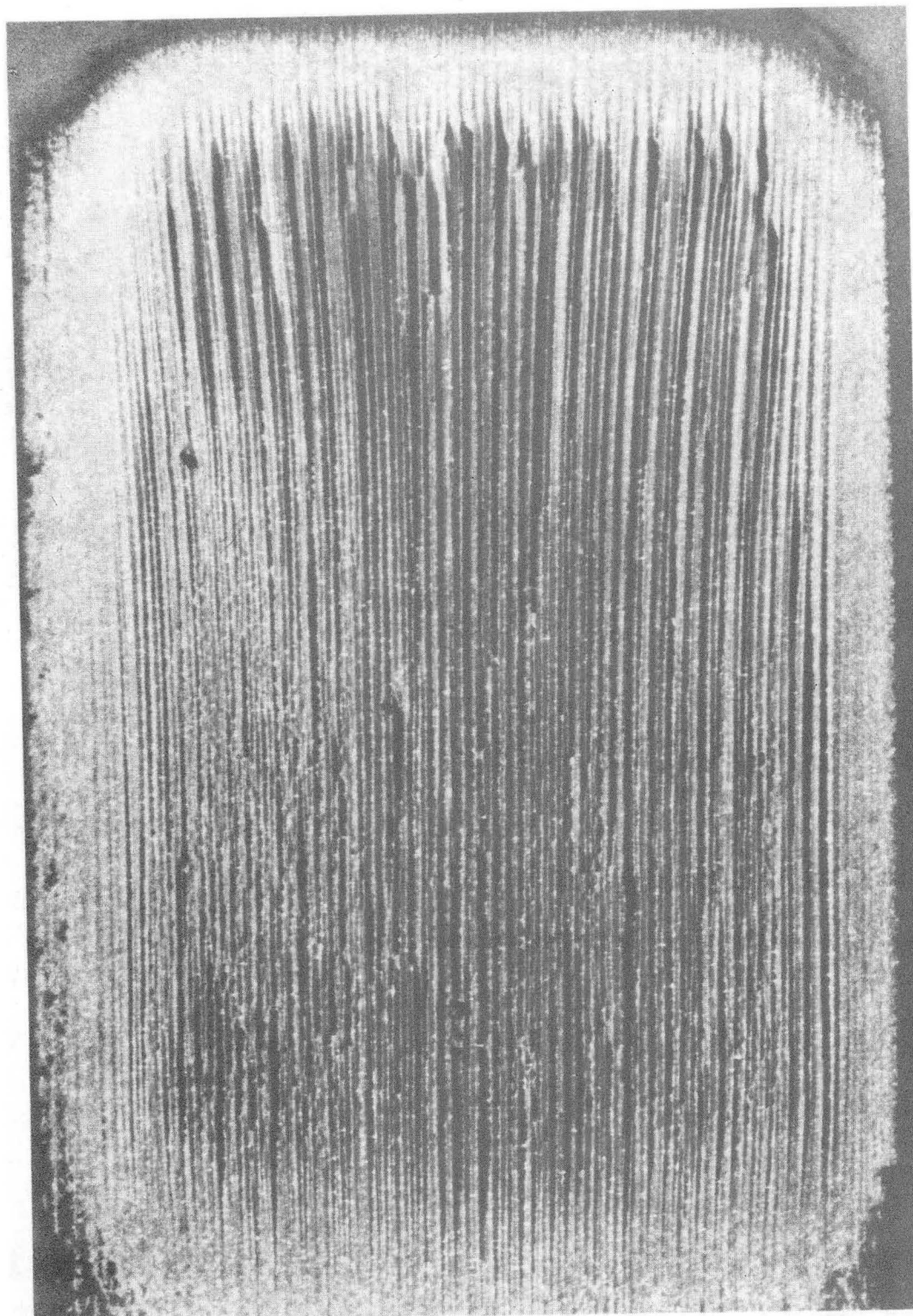
## 4. RESULTS AND DISCUSSION

### 4.1 Overview

#### 4.1.1 Striations: Definition, Characteristics, and Development

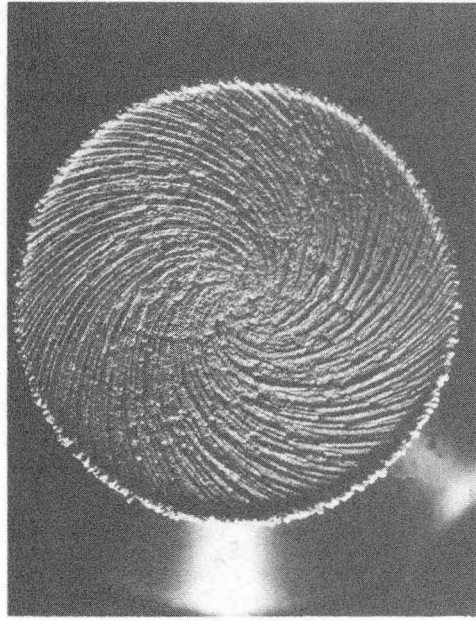
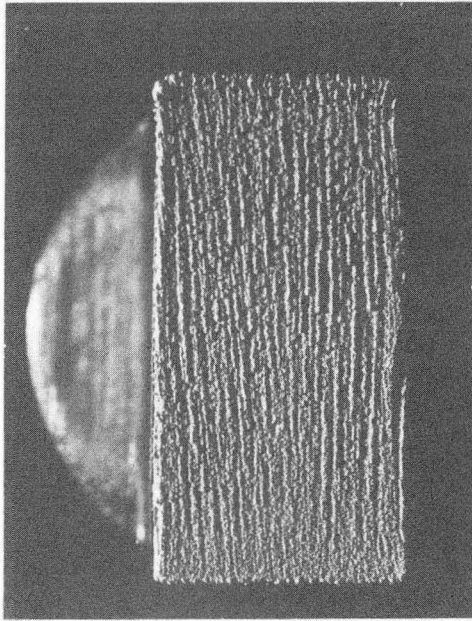
A striation is defined by Webster's dictionary [74] as "a minute groove or channel". This same definition fits accurately the phenomena addressed in this research effort. Striations are groove-shaped areas of deposited zinc that are parallel to the flow direction, typically fractions of millimeters wide and fractions of millimeters apart on the surface in the time frame of most of these experiments. The time needed for striations to appear on the depositing surface in "AR" grade 1 M  $\text{ZnCl}_2$  solutions depends primarily upon the current density and is in the range of 3 - 15 minutes. An example of developed striations is shown in Fig. 4.1. This Figure was generously donated by Ronald Putt from Gould Corporate Research Center, Rolling Meadows, Illinois. It shows a typical zinc deposit that their zinc research staff obtained by using a channel flow cell similar in design to the flow cells in this research. The process conditions under which this deposit was obtained were the following: 1.9 M  $\text{ZnCl}_2$ , pH 2.4, 20° C, 40 mA/cm<sup>2</sup>, 300 minutes, geometrical area 10 cm<sup>2</sup>, hydraulic diameter 0.29 cm, Re 100.

Striated deposits on the planar channel electrodes are parallel to the direction of flow. Striations on rotating disk electrodes are of spiral shape because of the more complex fluid motion associated with a rotating disk. The shape of spirals is relatively independent of the rotation speed, and in appearance is quite similar for different process conditions. Two examples of striated deposits, from work done in collaboration with Jaksic, are shown in Fig. 4.2.



XBB 835-4459

Figure 4.1 Striated Zinc Deposit Courtesy of Ronald Putt, Gould, Inc., Rolling Meadows, IL  
1.9 M  $\text{ZnCl}_2$ , pH 2.4,  $20^\circ\text{C}$ ,  $40 \text{ mA/cm}^2$ , 300 minutes,  
Geometrical Area  $10 \text{ cm}^2$ ,  $D_H$  0.29 cm, RE 100



XBB 784-11239A

RE 5300, 45 MIN

400 RPM, 40 MIN

1 M  $\text{ZnCl}_2$ , PH 2.4, 30 MA/CM<sup>2</sup>

Figure 4.2 Typical Striated Deposits  
(M. Jaksic with J. Faltemier, Experiment Nos.  
P-183, P-237 [14])

Striations on the channel electrodes start near the leading edge and eventually reach the downstream edge; spirals typically start nearer to the disk edge rather than the center. The reason for this difference is the nature of the current distribution in the two systems. On the channel electrode, the current is highest at the leading edge, so this area of deposit develops faster, while on a RDE electrode, the current density is highest near the disk edge, the downstream edge for the fluid flow.

As a deposition experiment progresses, the number of striations across the channel width or on the disk tends to diminish. As the average deposit thickness increases, the striations grow in size and meld together to form fewer, but larger striations in the flow direction. As this event progresses, the electrode surface becomes more rough and granular, and the probability of dendritic growth occurring on the surface increases enormously.

#### 4.1.2 Range of Striation Appearance

Striations have been observed under a large range of conditions of hydrodynamic flow, current density, electrolyte concentration, pH, and substrate material. Within the ranges studied, current density is the only variable which causes a major difference in deposit structure and appearance. The striated zinc deposits do not appear above a moderate value of current density; the zinc surface above this value is macroscopically smooth, without the appearance of striations.

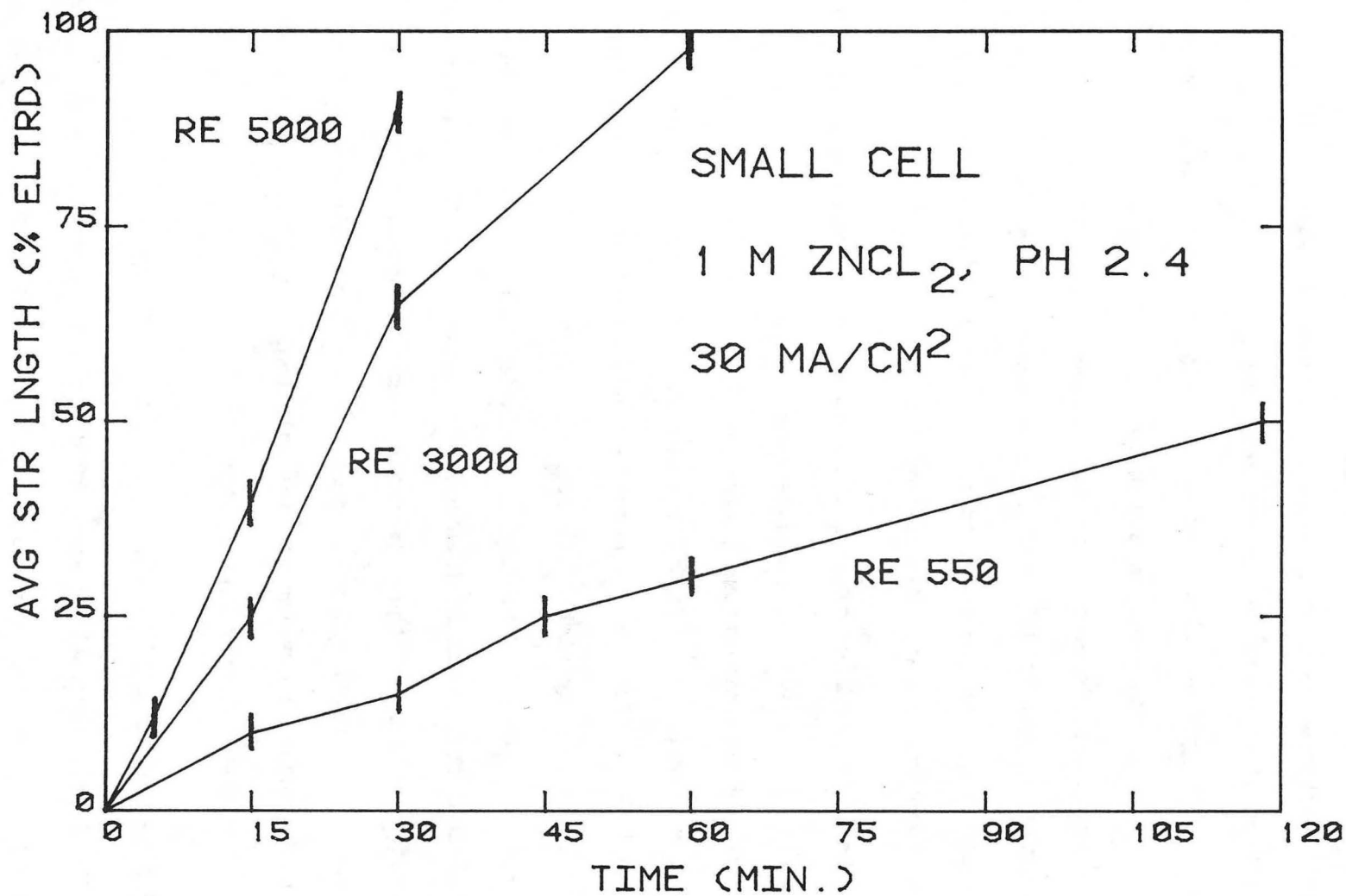
In the 1 M zinc halide solutions, the upper limit where striations were observed was  $80 \pm 10 \text{ mA/cm}^2$ . The upper current density limit in 1

M ZnSO<sub>4</sub> solutions was  $15 \pm 2$  mA/cm<sup>2</sup>. Above these limits, macroscopically smooth deposits were always obtained for all flow conditions included in this study. No lower current density limits were noted; striations appeared after very long deposition times even for 1 - 2 mA/cm<sup>2</sup>. Striations have been consistently observed in both laminar and turbulent flow in the channels, but only the laminar regime was a subject of investigation on the RDE. The pH has been varied in the acidic range 1.9 - 5.0, and different substrate materials have been employed with no major resulting differences in the striation phenomenon.

#### 4.2 Influence of Process Variables

##### 4.2.1 Effect of Hydrodynamic Flow

Hydrodynamic flow is one of the most influential variables on the morphology of zinc. In the current density range where striations appear, the hydrodynamic flow determines the speed with which the striations propagate downstream. By increasing the rate of fluid flow past an electrode surface, the striated deposit develops much faster, especially in the turbulent regime. The striated deposit is also more sharply delineated in the flow direction as the flow rate is increased. Fig. 4.3, obtained in the Small Cell, shows how the average length of fully developed striations (shown as percent of Small Cell electrode length) depends on time for three different Re numbers. In turbulent flow, deposits in the Small Cell were completely striated in less than an hour at 30 mA/cm<sup>2</sup>, while in laminar conditions at the same current density, the average time needed to fully develop grooves over the



-55-

XBL 837-10748

Figure 4.3 Change in Lengths of Striations in the Small Cell



entire electrode was in the range of 4 hours. Figs. 4.4 and 4.5\*, show the effect of flowrate in the channel flow cell and RDE system, respectively. At higher flowrates, especially in the turbulent regime, the striations are much more sharply drawn in the flow direction, and they appear and propagate downstream much faster. Fig. 4.6\*, shows no appearance of striations at  $100 \text{ mA/cm}^2$  for two different flowrates. The resulting deposits in these cases are macroscopically smooth, and look almost identical for the two different flowrates.

The average number of striations appearing across the planar electrode in  $1 \text{ M ZnCl}_2$  solutions decreases with time after becoming fully developed because striations begin to meld together as the deposit thickness increases. Fig. 4.7 shows this effect for turbulent flow in the Small Cell. The average number of striations observed across the Small Cell in turbulent flow decreased from approximately 22 to 13 in the first two hours. Variation of striation number with Reynolds number was minimal for turbulent flow or for laminar flow. The average number of striations across the electrode remains approximately the same throughout the first 120 minutes of laminar flow because the striations take much longer to develop and are only beginning to meld into fewer, larger striations at the 2 hour mark.

#### 4.2.2 Effect of Current Density

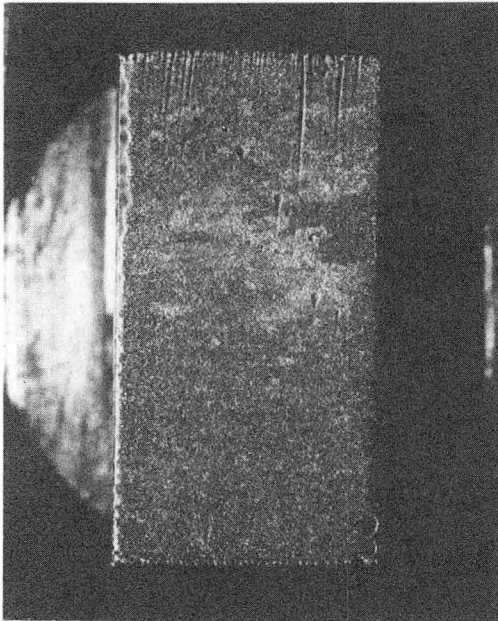
The deposit morphology strongly depends on current density. The influence of current density on the deposit morphology can be seen

---

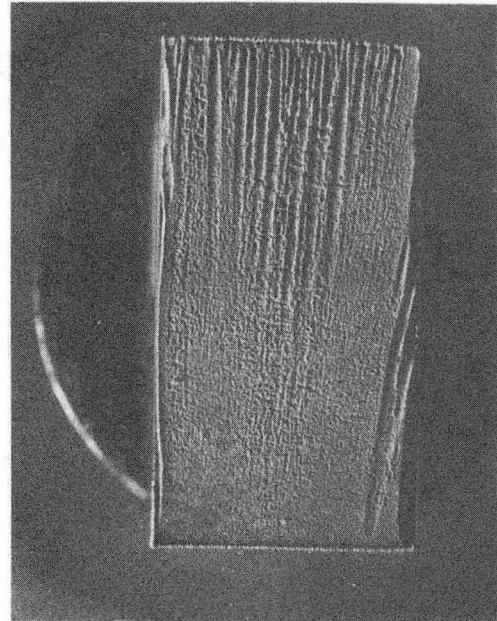
\*from work done in collaboration with Milan Jaksic



# EFFECT OF FLOW AT 30 MA/CM<sup>2</sup>



RE 350



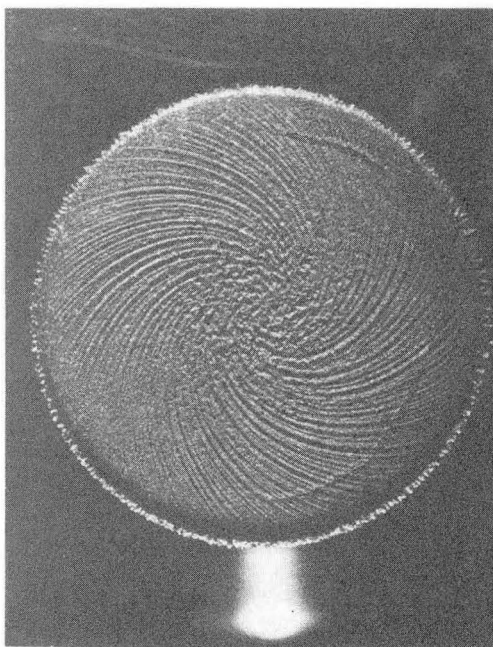
XBB 784-11693A

RE 5300

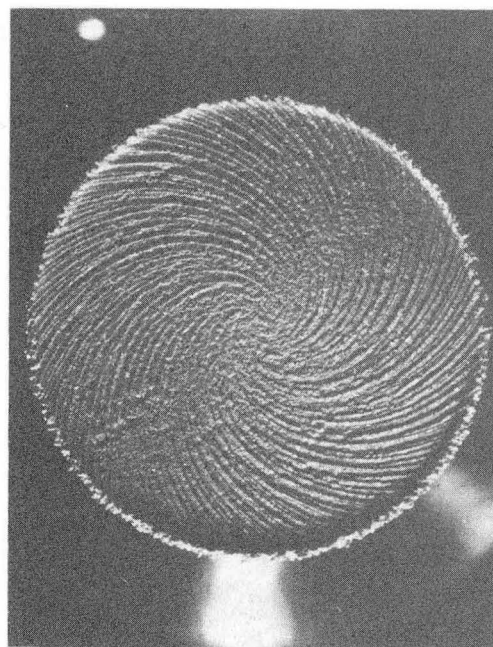
1 M ZNCL<sub>2</sub>, PH 2.4, 15 MIN

Figure 4.4 (M. Jaksic with J. Faltemier, Experiment Nos. P-103, P-89 [14])

# EFFECT OF FLOW AT 30 MA/CM<sup>2</sup>



100 RPM



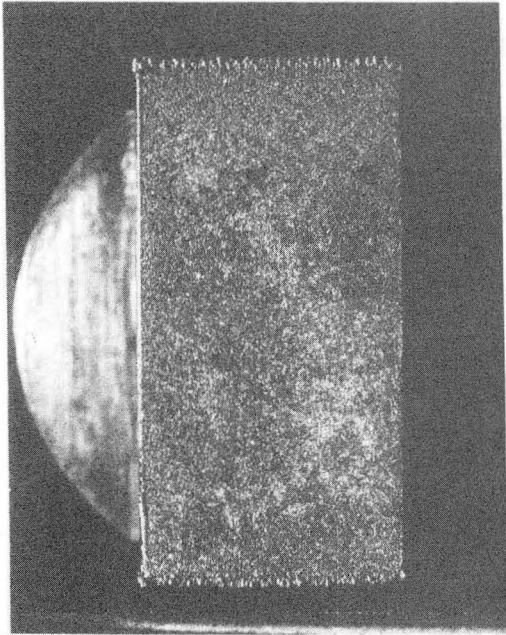
1600 RPM

XBB 784-11240A

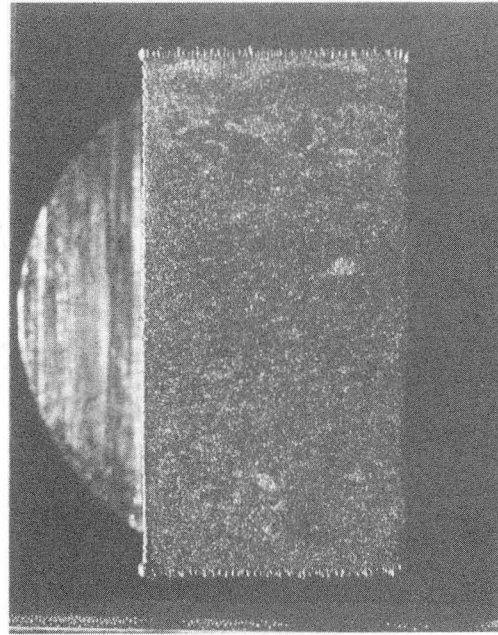
1 M ZNCL<sub>2</sub>, PH 2.4, 30 MA/CM<sup>2</sup> X 1 HOUR

Figure 4.5 (M. Jaksic with J. Faltemier, Experiment Nos. RDE-97, RDE-239 [14])

# EFFECT OF FLOW AT 100 MA/CM<sup>2</sup>



RE 850

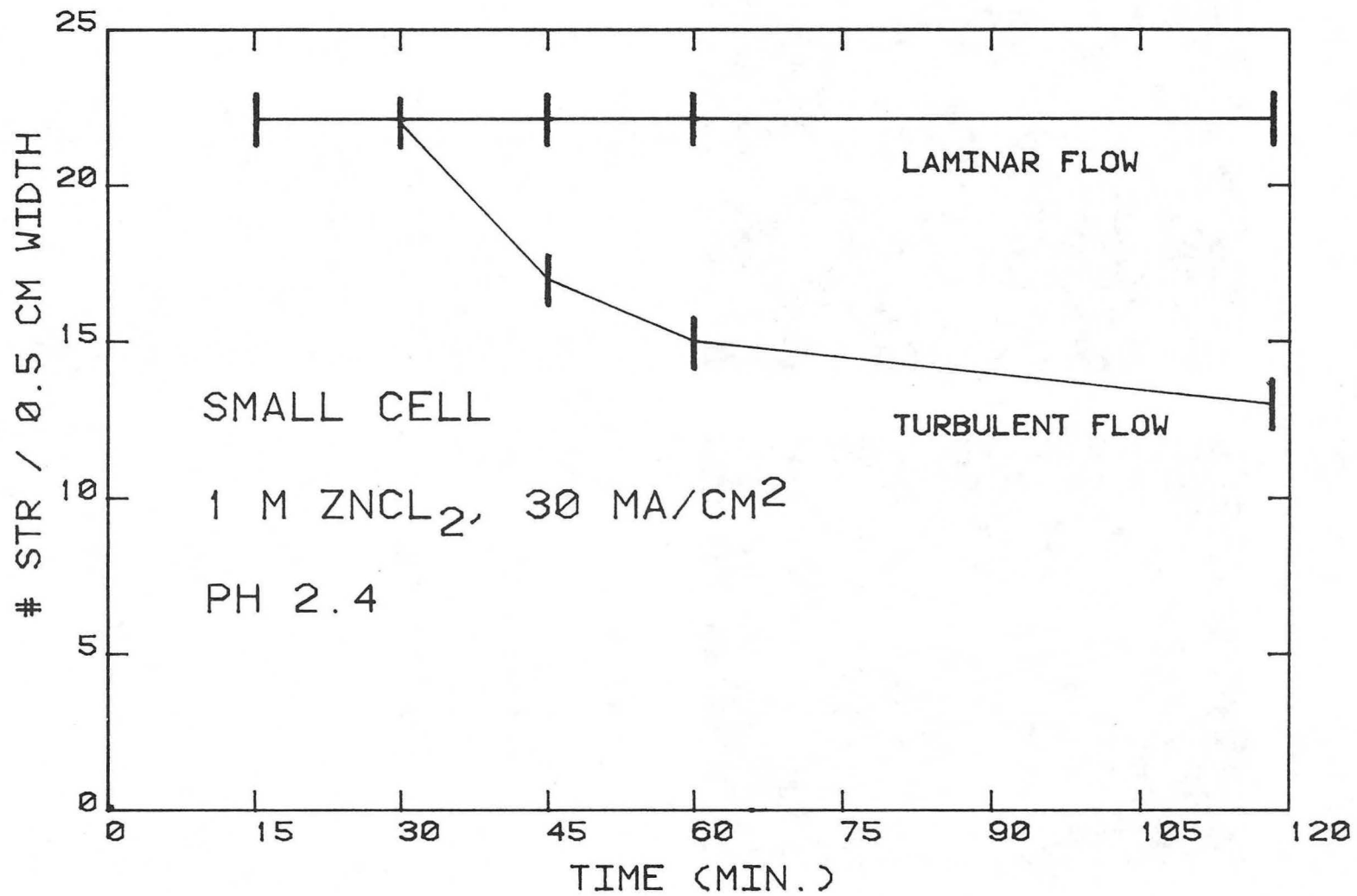


XBB 784-11723A

RE 5300

1 M ZNCL<sub>2</sub>, PH 2.4, 15 MIN

Figure 4.6 (M. Jaksic with J. Faltemier, Experiment Nos. P-119, P-127 [14])



-69-

XBL 837-10749

Figure 4.7 Approximate Number of Striations Across the Small Cell Cathode

already during the initial stages of deposition, when the first crystallites become visible on the surface under 5-10X magnification. Discussion of the initial stages of deposition is presented later in this chapter.

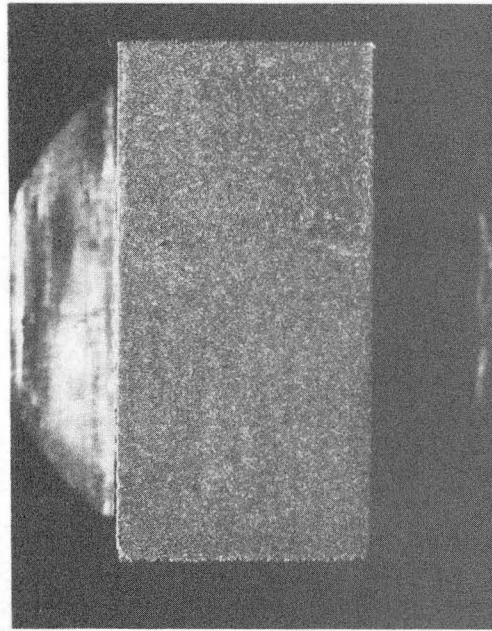
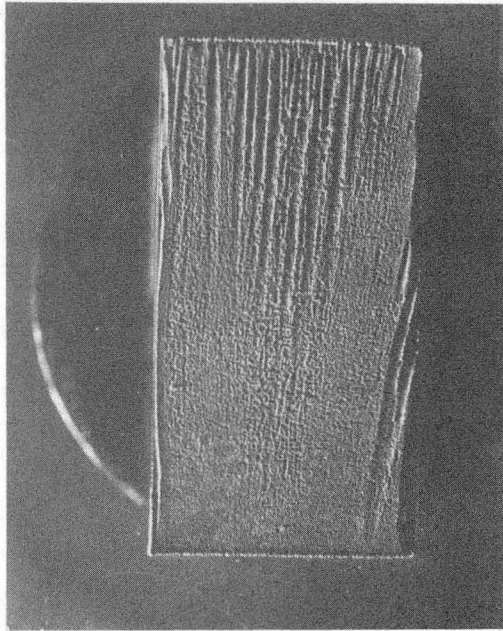
The number density of striations increases with current density, and above the upper current density limit listed before, macroscopically smooth deposits are always obtained. At  $10 \text{ mA/cm}^2$ , approximately 15 - 20 developed striations can be observed, while at  $30 \text{ mA/cm}^2$ , this number increases to approximately 22 striations across a  $1/2 \text{ cm}$  wide electrode in  $1 \text{ M ZnCl}_2$  solutions. The low current density limits at which striations occur are most likely associated with the critical overpotential needed for nucleation of crystals, but these could not be determined with this experimental setup. Even at current densities as low as  $1-2 \text{ mA/cm}^2$ , striations appear after approximately the same number of coulombs have passed. Fig. 4.8\* shows examples of how dissimilar zinc surfaces can be after approximately the same number of coulombs have been deposited in both cases.

The effect of current density in the RDE system is identical to the channel flow cells. Above the upper limits for striation appearance, the surface remains macroscopically smooth. Below this limit, spiral shaped deposits develop on the surface. Fig. 4.9\* shows two different current density cases under the same flow conditions, after an equal amount of zinc has been deposited. The higher current density case shows a smooth deposit that has formed, while the lower current density case shows the development of striated deposit over the entire surface.

---

\*from work done in collaboration with Milan Jaksic

# EFFECT OF C. D. AT RE 5300



XBB 784-11726A

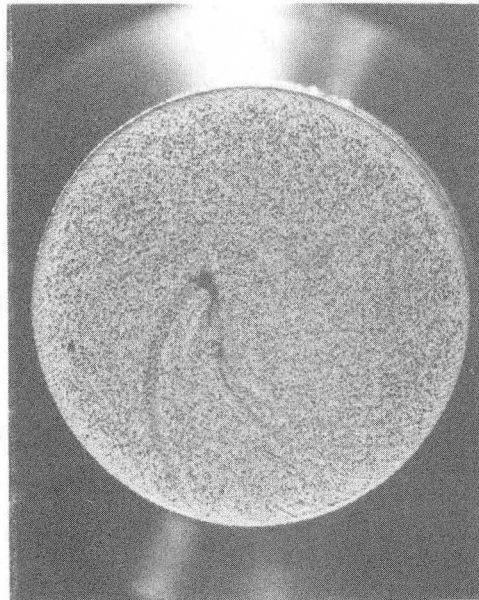
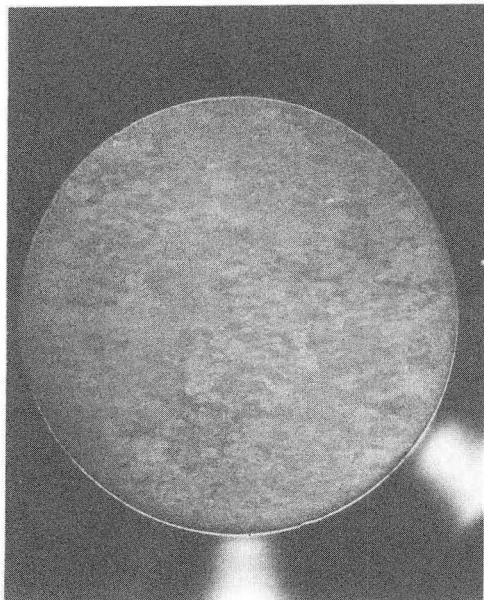
30 MA/CM<sup>2</sup>, 15 MIN

100 MA/CM<sup>2</sup>, 5 MIN

1 M ZNCL<sub>2</sub>, PH 2.4

Figure 4.8 (M. Jaksic with J. Faltemier, Experiment Nos. P-89, P-122 [14])

EFFECT OF C. D. AT 1600 RPM



XBB 784-11195A

100 MA/CM<sup>2</sup> X 3 MIN

10 MA/CM<sup>2</sup> X 30 MIN

1 M ZNCL<sub>2</sub>, PH 2.4

Figure 4.9 (M. Jaksic with J. Faltemier, Experiment Nos. RDE-194, RDE-244 [14])



Current density appears to be the key to the appearance of striations in the deposits. This idea of the importance of current density has been considered earlier by others, including Jaksic and Tobias [15,16] and Tsuda [10] in this laboratory, as well as Carlson [11] in copper deposition. Budevski [75] explains that the nucleation and crystal growth rates both play a major role in determining the morphological properties of the metal deposit. With an increase in current density (effectively, an overpotential increase to be applied either to nucleating or to growing crystals on the surface), the morphology of the deposit changes drastically from one in which crystal growth controls to one in which the rate of crystal nucleation controls. If nucleation is occurring massively over the entire electrode, crystal growth is not dominating, and the resulting deposit will not be as rough and granular.

#### 4.2.3 Variable Current Techniques

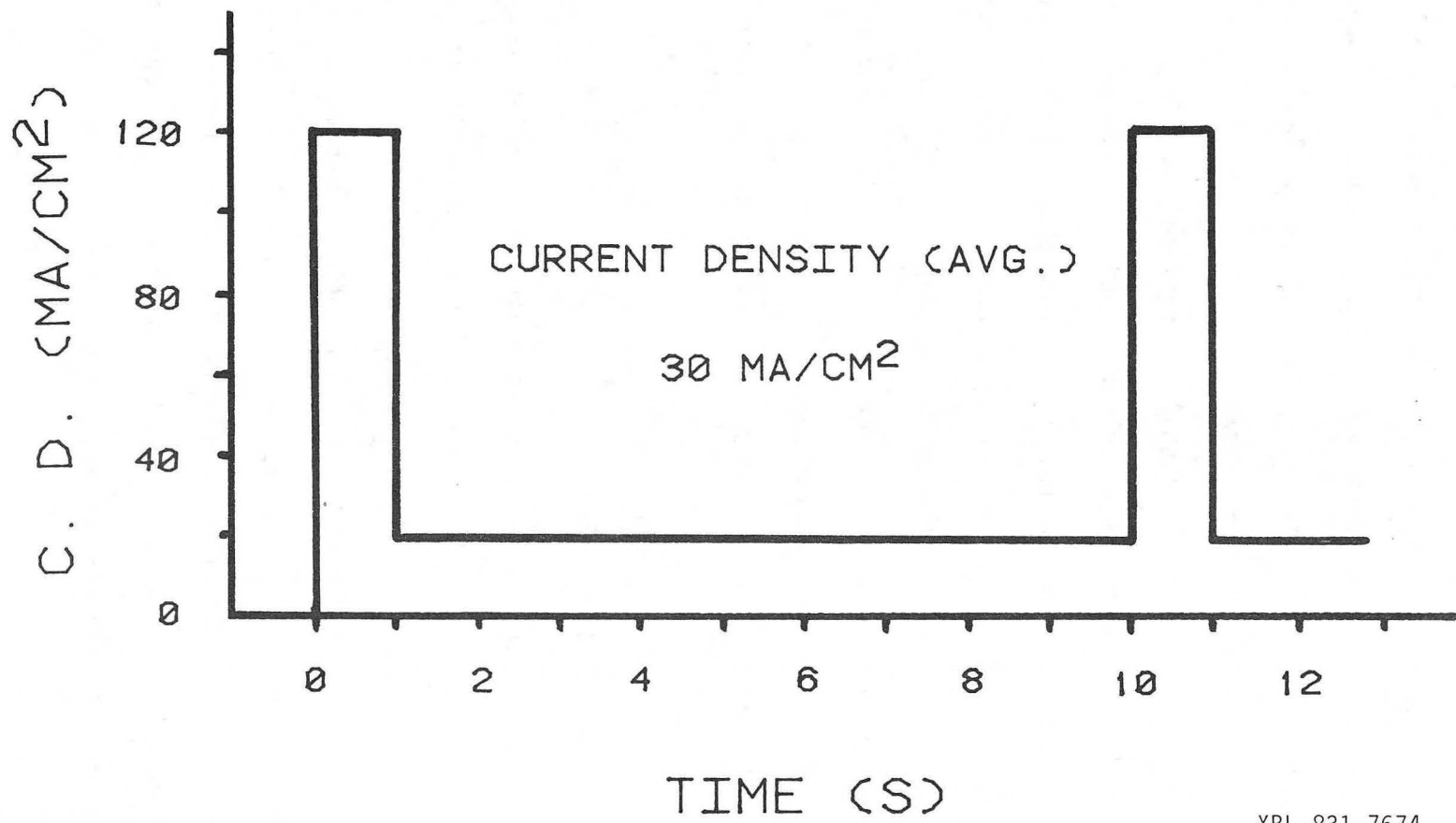
Variable cathodic current, pulse, and periodically reversed current techniques are widely recognized as effective means of producing smooth and level deposits. General mechanisms associated with this improved deposition process involve high nucleation rates at the potential or current peaks and the periodic relaxation of the solution concentration near the electrode. Many other investigators, including Ibl [76] and Cheh [77], have considered the experimental and theoretical aspects of pulsing. McBreen [26] found that in charging zinc electrodes in alkaline solutions, superimposing an alternating voltage on the cell greatly improved the zinc deposit morphology.

Variable current step experiments, performed independently by Tsuda [10], and by Kommenic and Faltemier, resulted in macroscopically smooth

deposits, very similar to the higher current density region reported before. The variable current step technique involves a cathodic current pulse of high intensity and short duration superimposed periodically on a small cathodic background current. The steady background current is within the striation formation range, while the pulse has a current level above the upper current density limit for striation formation. Fig. 4.10 gives the current profile that was employed in this investigation. A  $120 \text{ mA/cm}^2$  step pulse was superimposed for 1 second over a  $20 \text{ mA/cm}^2$  base current every 10 seconds, giving an average current density of  $30 \text{ mA/cm}^2$ . In the  $30 \text{ mA/cm}^2$  constant current density experiments, striations always appeared within 5-10 minutes of deposition. The resulting deposit after using this variable current technique is shown in Fig. 4.11. The deposits remained striation-free and were macroscopically smooth, even after 1 hour of deposition at an average current density of  $30 \text{ mA/cm}^2$ .

#### 4.2.4 Effect of Zinc Concentration

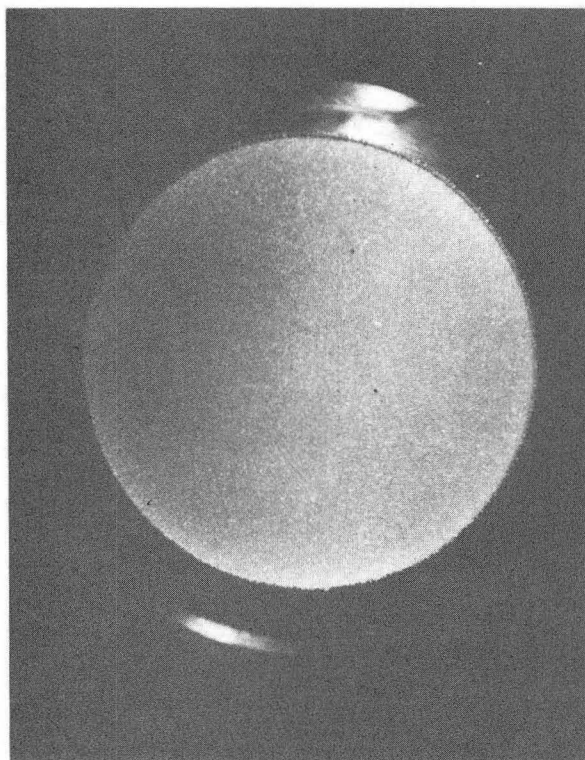
In the range studied, the bulk concentration of zinc ions does not play any major role on the striated deposit morphology. Generally, at the lower concentration of  $0.5 \text{ M ZnCl}_2$  slightly fewer and more widely spaced striations are obtained. From experiments conducted in conjunction with Jaksic,  $4 \text{ M ZnCl}_2$  solutions gave approximately the same number of striations with similar appearance. Experiments were conducted primarily in  $1 \text{ M}$  zinc solutions, however. An approximate, average number of developed striations across the width of the Small Cell electrode



XBL 831-7674

Figure 4.10 Current vs. Time Profile in Pulsed Deposition

## VARIABLE CURRENT DEPOSITION



XBB 835-4531

1 M  $\text{ZnCl}_2$ , PH 2.4

400 RPM, 1 HOUR

30 MA/ $\text{CM}^2$  (AVG.)

120 MA/ $\text{CM}^2$ , 1 SECOND

20 MA/ $\text{CM}^2$ , 9 SECONDS

Figure 4.11

(0.5 cm) for various zinc solutions is shown in Table 4.1. A relatively consistent number of striations across the electrode was observed.

Table 4.1

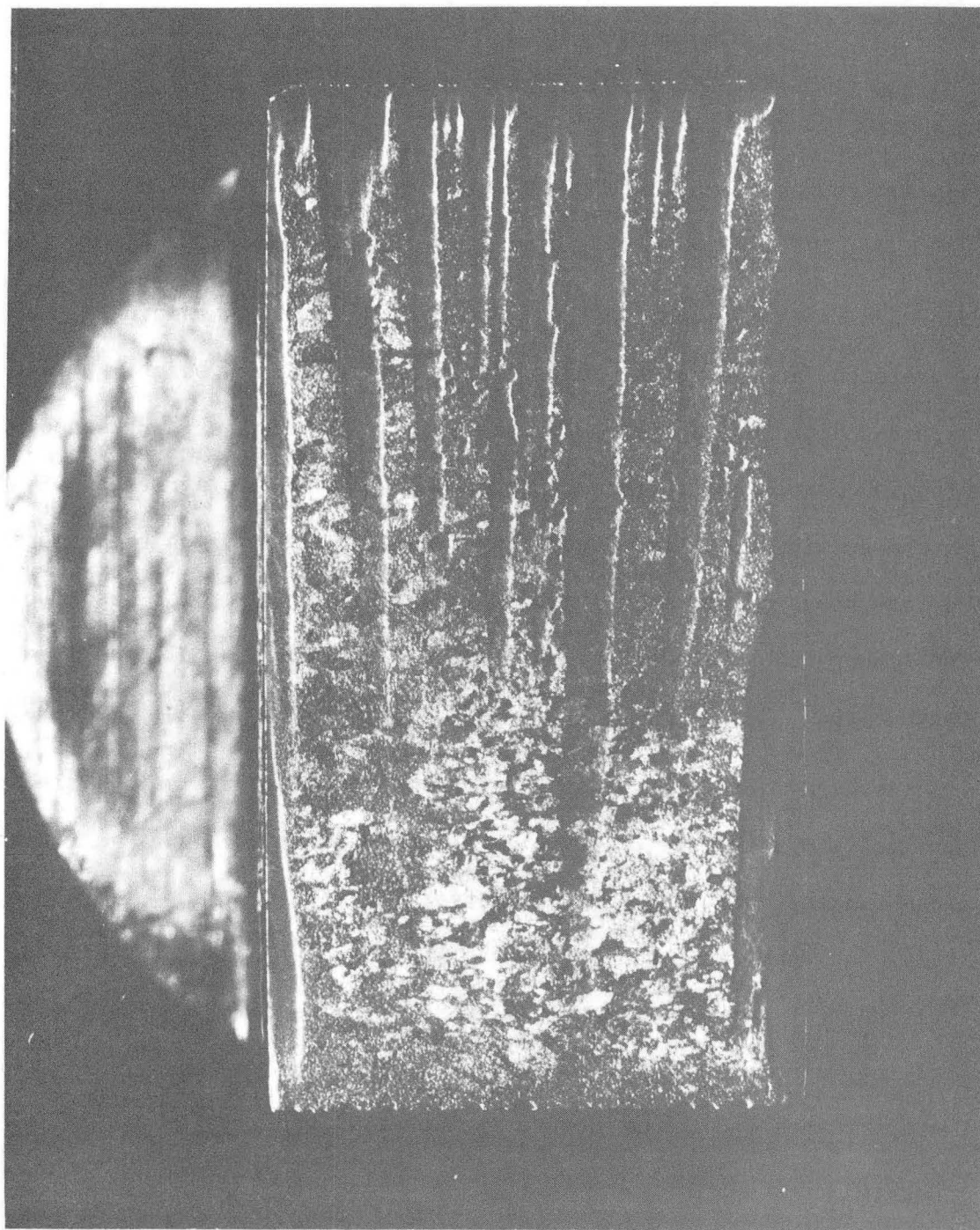
Approximate Number of Striations Across Small Cell Electrode

Solutions	# of Striations Across the 0.5 cm Electrode Width at 30 mA/cm <sup>2</sup> , 30 min.
1 M ZnCl <sub>2</sub>	22 ± 3
0.5 M ZnCl <sub>2</sub>	20 ± 3
1 M ZnCl <sub>2</sub> + 5 M LiCl	22 ± 3 (in collaboration with Jaksic)
4 M ZnCl <sub>2</sub>	26 ± 3 (in collaboration with Jaksic)
4 M ZnCl <sub>2</sub> + 0.1 % Zonyl FSB	22 ± 3 (Jaksic data)
1 M ZnBr <sub>2</sub>	3 ± 3 (Jaksic data)
1 M ZnCl <sub>2</sub> (from Large Cell, per 0.5 cm width)	25 ± 3

Some supported electrolytes with low zinc concentrations also gave striated zinc deposits but the deposit appearance was different. Jaksic used 0.1 M ZnCl<sub>2</sub> + 1 M LiCl solutions in the Small Cell, and obtained striated deposits with large, wide channels parallel to the flow direction. An example of this is shown in Fig. 4.12.

#### 4.2.5 Effect of Substrates

Several different substrate materials were used in this research. Platinum received the most usage as a substrate because of its dimensionally stable characteristics and because of the ease of cleaning and reproducing clean, polished surfaces. The other materials used as substrates included both single crystal and polycrystalline zinc, copper,



XBB 837-6196

Figure 4.12  $0.1 \text{ M ZnCl}_2 + 1 \text{ M LiCl}$ , pH 2.4,  $10 \text{ mA/cm}^2$ , 30 Min.  
RE 4700, (M. Jaksic, Experiment No. P-134 [14])

and pyrolytic carbon. The chemical nature of the substrate material was not the only substrate property considered in this study. Substrate roughness, using both mechanical and electrochemical techniques, was also varied in order to identify any possible influence that initial surface roughness may have on the zinc morphology.

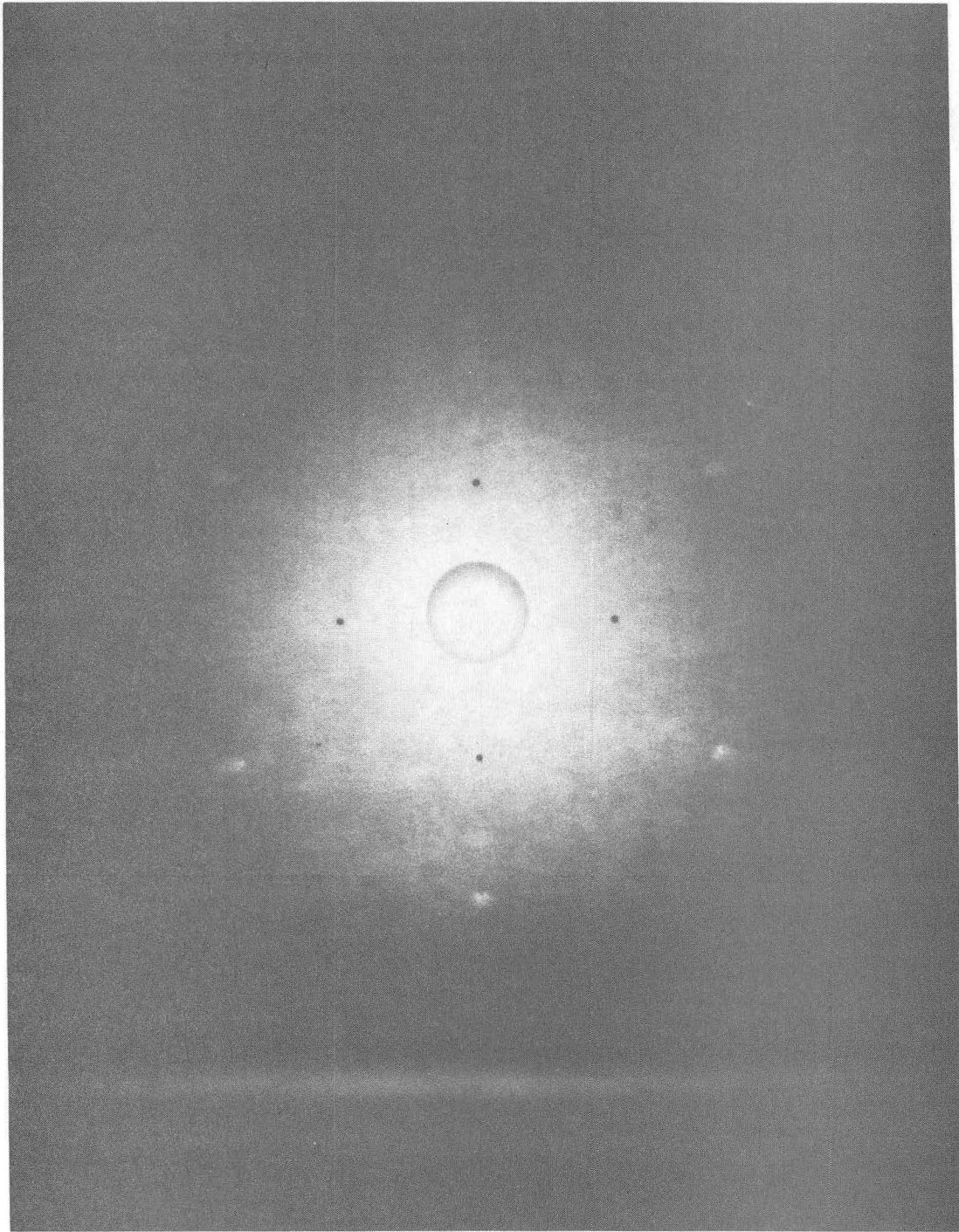
When the platinum substrates were only carbide-sanded and not polished with 1  $\mu\text{m}$  diamond paste, providing surfaces containing 15  $\mu\text{m}$  size depressions and scratch marks, the average time before striations appeared on the surface decreased to 2-5 minutes, instead of 3-15 minutes on polished surfaces. This observation is in agreement with the interpretation that less depositing time is needed to get the same ample surface roughness on a surface, if the initial surface is less smooth. The other substrate materials were all utilized in only the 1  $\mu\text{m}$  polished state.

An X-ray diffraction pattern for the single crystal zinc electrode surface is shown in Fig. 4.13. Zinc crystal structure is hexagonally close-packed (hcp), and the substrate surface that was used in this study was the basal plane (0001) of the crystal [78]. The single crystal substrate gave the same type of striated deposit as the polycrystalline zinc and the other substrate materials, as shown in Fig. 4.14. The appearance and the structure the striated surfaces is basically not dependent on the crystallographic orientation of the surface.

#### 4.2.6 Effect of pH

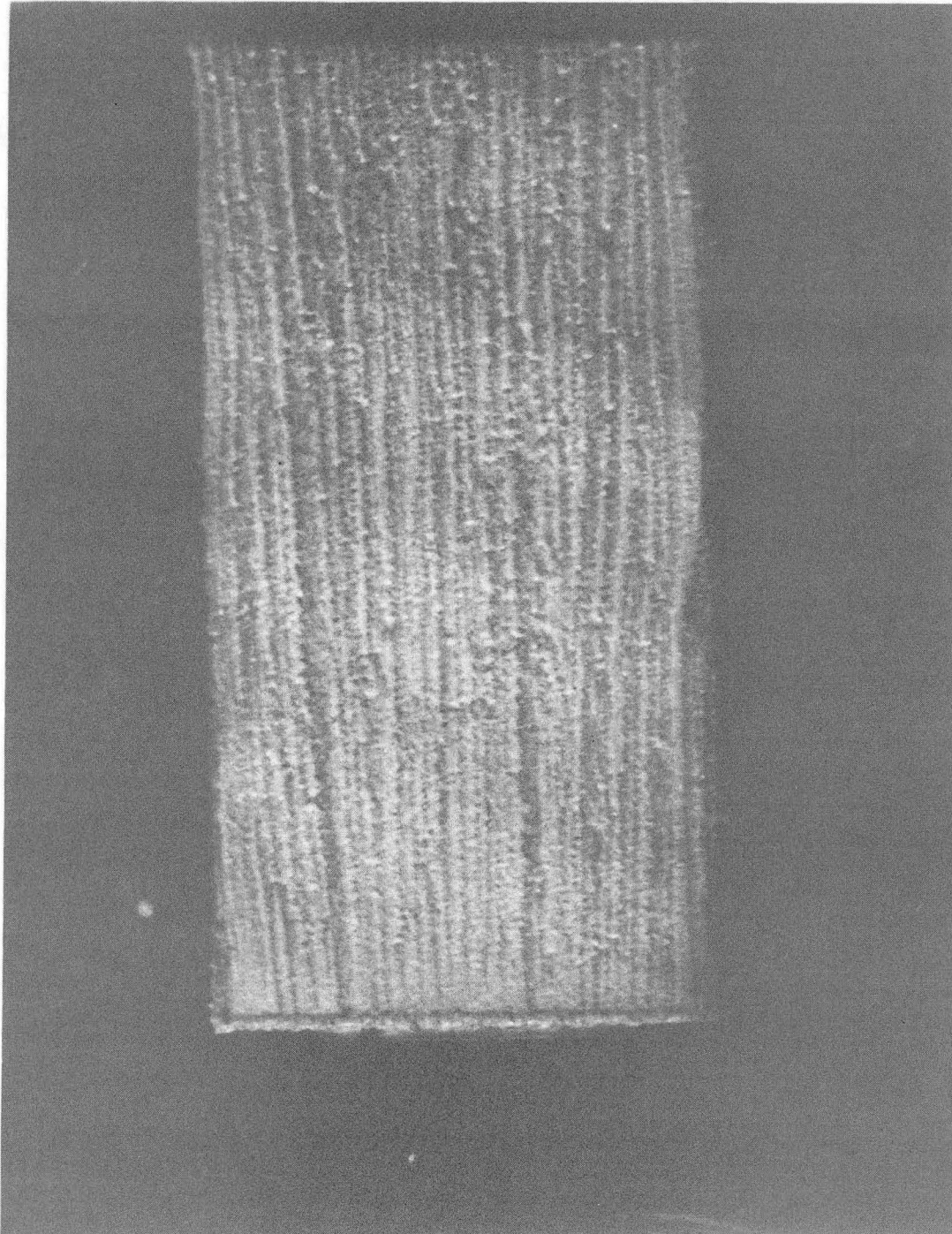
In the pH range of 2-5 in  $\text{ZnCl}_2$ ,  $\text{ZnBr}_2$ , and  $\text{ZnSO}_4$  solutions, no significant differences in number, shape, and speed of formation of the





XBB 835-4530

Figure 4.13 Laue X-Ray Diffraction Pattern of Basal (0001) Plane of Single Crystal Zinc



XBB 838-7160

Figure 4.14 Zinc Deposit on Zinc Single Crystal Substrate,  
1 M  $\text{ZnCl}_2$ , pH 2.1,  $30 \text{ mA/cm}^2$ , 30 Min., RE 5300

striated deposits were observed. Above this pH range, the colloidal solution of the zinc-chloro-hydroxides begins to form [93].

Hydrogen bubbles were not evident in most of the runs involving the RDE and in the channel flowcells. However, the motion pictures taken in the In Situ cell reveal bubbles near the free electrode edges. Hydrogen bubbles could also be detected indirectly through crater-shaped patterns left behind in some zinc deposits. These patterns were formed by zinc depositing around a hydrogen bubble adhering to the surface. The tendency for hydrogen evolution increased with decreasing pH, as expected. Below approximately pH 1.5, the corrosion of zinc by the acidic solution was clearly noticeable in the time scale of these experiments.

The standard potential (in volts) of the hydrogen electrode at equilibrium in a solution with a certain pH is approximately equal to  $0.059 \times \text{pH}$  [34]. In the ranges studied, the approximate difference in hydrogen overvoltage that is available in solutions of pH 2 and pH 5 is 0.180 volts. Yet, no large differences in the zinc deposit caused by hydrogen evolution, nor large change in the number of hydrogen bubbles have been observed.

#### 4.2.7 Effect of Impurities, Surfactants, and Electrolyte Purity

The effect of metallic cation impurities in the solutions has been addressed independently by Jaksic [15,16] and Tsuda [10]. Jaksic studied the morphological effect of addition of 10 - 100 ppm metallic cation ( $\text{Fe}^{+2}$ ,  $\text{Co}^{+2}$ ,  $\text{Cu}^{+2}$ , and  $\text{Ru}^{+3}$ ) impurities to 1 M  $\text{ZnCl}_2$  solutions. He found that these additions generally led to characteristic zinc spongy deposits and hydrogen evolution.

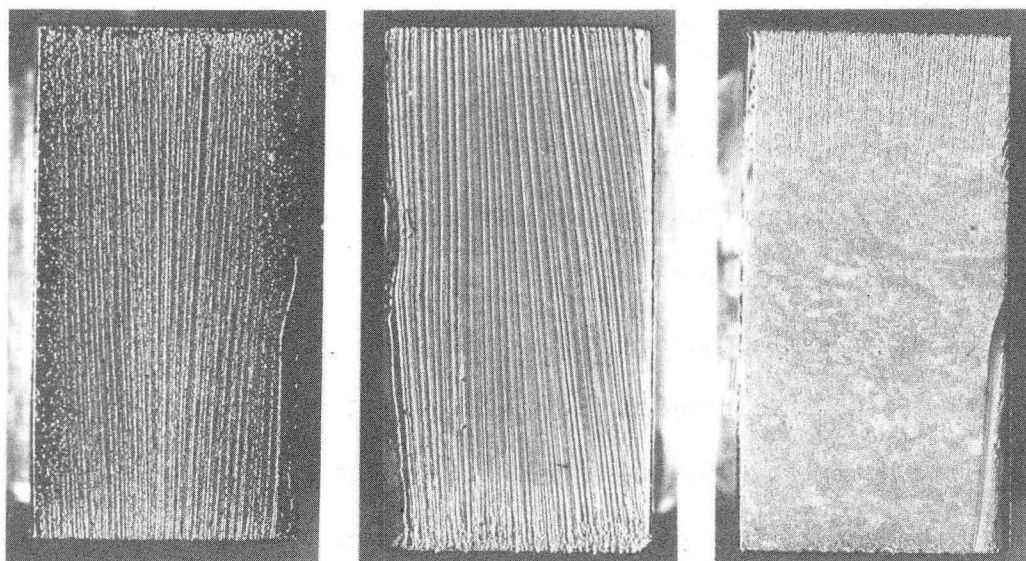
Tsuda studied how the developed spiral formation times changed with increasing Pb concentrations in the ppm range. He also observed spiral formation times in ultrapure zinc solutions with ultrapure electrodes. The major influence of Pb ions was to amplify the surface roughness through coalescence and preferred growth of initial protrusions. Although, the spiral formation time decreased as the lead concentration increased, the number density and shape of the spirals did not vary. He also conducted a few experiments with trace amounts of Cd, Sn, Co, Hg, and Th. Spiral formation times increased in ultrapure zinc solutions, but the resulting striation appearance had very similar characteristics.

The effect of addition of a fluorosubstituted surfactant (Zonyl-FSB, duPont) to the zinc solutions on the development of striations has been studied by Jaksic [16]. He found that this surface active agent inhibits rapid outward growth, resulting in almost instantaneous appearance, an increase in number density, and a decrease in amplitude, of striations on the surface. Fig. 4.15 shows zinc deposits with and without the addition of this surfactant.

Detailed chemical analysis performed on the 1 M  $ZnCl_2$  solutions provided very few surprises. The results of these analyses are shown in Appendix C. The largest contaminant in the solutions is cadmium, which is found naturally in the same minerals along with zinc. It was present in widely different amounts in different batch lot supplies, yielding from 0.002  $\mu g/cc$  to 0.7  $\mu g/cc$  in 1 M  $ZnCl_2$ . Lead and manganese were the other significant contaminants, both below concentration levels of 0.1  $\mu g/cc$ . Ultrapure electrolytes and lead-contaminated solutions were used



# EFFECT OF FLUOROSUBSTITUTED SURFACTANT



2 MIN

5 MIN

5 MIN  
WITHOUT ZONYL

0.1 % ZONYL FSB

4 M  $ZnCl_2$ , PH 2.1

30 MA/CM<sup>2</sup>, RE 3400

XBB 831-373

Figure 4.15 (M. Jaksic, Experiment Nos. P-231, P-232, P-218 [14])

in experiments by Tsuda [10]; chemical analysis data are also included in Appendix C for his solutions.

#### 4.2.8 Effect of Anions

Zinc has been deposited from chloride, bromide, and sulfate solutions. All of these solutions show grooved, striated profiles parallel to the direction of flow, in certain current density ranges. The deposits from all these solutions are very similar in appearance and structure. The differences between the halides and the sulfate solutions involve the current density range where striated deposits are formed, and correspondingly, the time needed before striations appeared in the deposit. This large difference in the ranges of current density where striated deposits develop is related to the choice of anion in the solution, but the full consequences of the anion behavior are not understood. The sulfate ion is much larger than the halide ions, and also, it does not form complexes in solution [79]. The halide ions form several complexes, which, even in dilute solutions, become the major zinc ion carriers upon electrodeposition [34,66].

#### 4.2.9 Effect of Electrode Size

The question of whether the striation phenomena persist over long electrodes was addressed in a special "Large Cell" constructed for this purpose. (See Section 3.1 and Appendix B for details.) Zinc deposits on 30 cm long platinum electrodes showed essentially the same striation patterns as on small electrodes. This behavior, observed in numerous runs, points to the fact that discontinuities on the leading edges of electrodes are not likely to be the original or sole causes for the

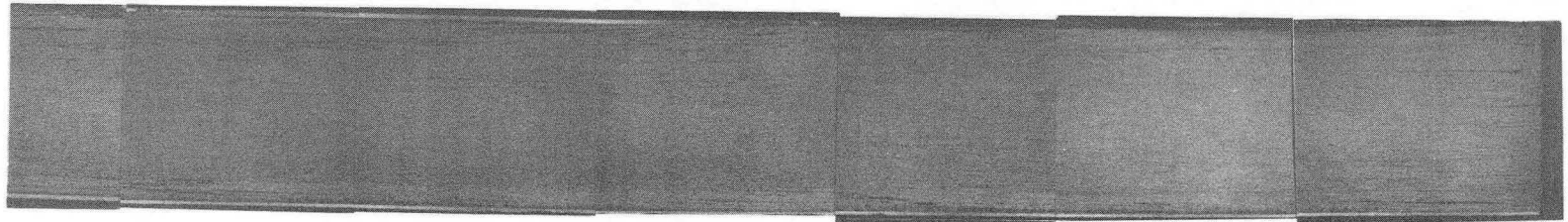
development of striated deposits. In fact, the rate at which striated deposits appeared over the entire Large Cell electrode demonstrates that this phenomenon is occurring over the entire surface and not just at the leading edge.

The Large Cell gave morphological results very similar to the Small Cell and the RDE. Above a certain current density, macroscopically smooth deposits were obtained. Fig. 4.16 shows results of three different experimental runs, with the same number of coulombs deposited in each case, on the Large Cell's platinum electrode. The leading edge is on the right, and the fluid flow is from right to left. The striations develop near the front edge and propagate down the entire length of cell. The striations have the same structure and are spaced the same approximate width apart in the Large Cell system as in the Small and In situ Cells. The number of striations that initially appear is approximately 20 - 25 per 1/2 cm electrode width. Fig. 4.17 shows a magnified view of the leading edge area of each of these three experimental deposits.

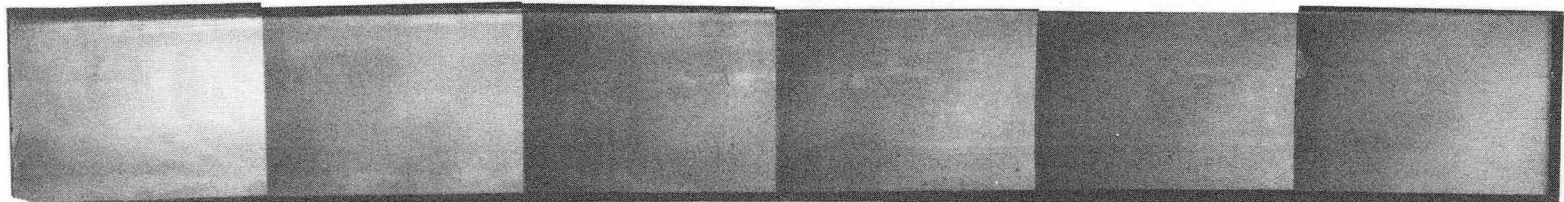
The Large Cell gave smooth, nonstriated deposits under the higher current density condition of  $100 \text{ mA/cm}^2$ , very similar to the Small Cell. These deposits show a thicker deposit directly along the front edge, and also, contain small crater marks where hydrogen bubbles have not been displaced along the side edges by the flow. Dendrites that point outward and upstream are noticeable at the front edge and rear edge after longer deposition times (e.g.,  $30 \text{ mA/cm}^2$ , 60 minutes).



1 M  $\text{ZnCl}_2$ , PH 4.6, RE 2300

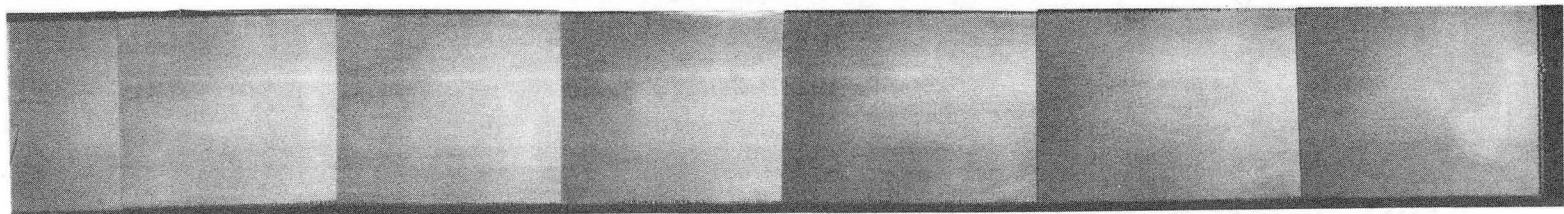


10 MA/CM<sup>2</sup> X 90 MIN



-78-

30 MA/CM<sup>2</sup> X 30 MIN

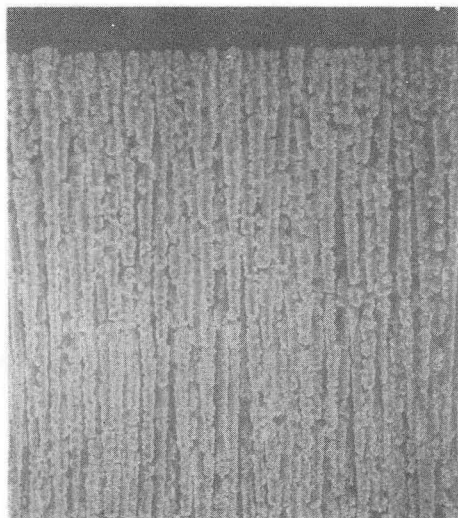


XBB 831-379

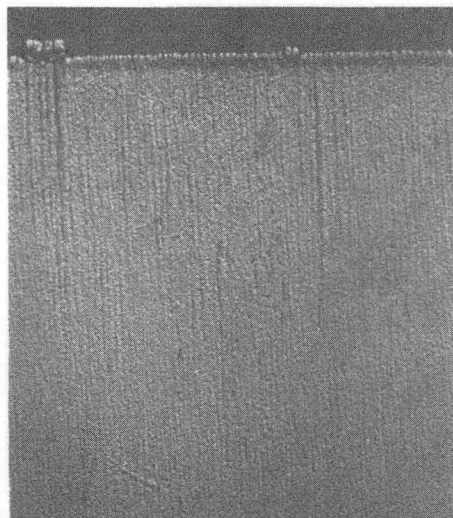
100 MA/CM<sup>2</sup> X 9 MIN

Figure 4.16 Large Cell Zinc Deposits

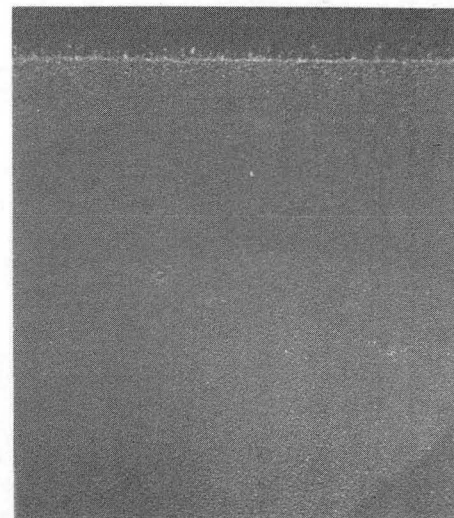
# LEADING EDGE



10 MA/CM<sup>2</sup> X 90 MIN



30 MA/CM<sup>2</sup> X 30 MIN



100 MA/CM<sup>2</sup> X 9 MIN

XBB 831-378

1 M ZNCL<sub>2</sub> , PH 4.6, RE 2300

1 CM

Figure 4.17 Enlarged View of Leading Edge Area of Large Cell Deposits Shown in Fig. 4.15

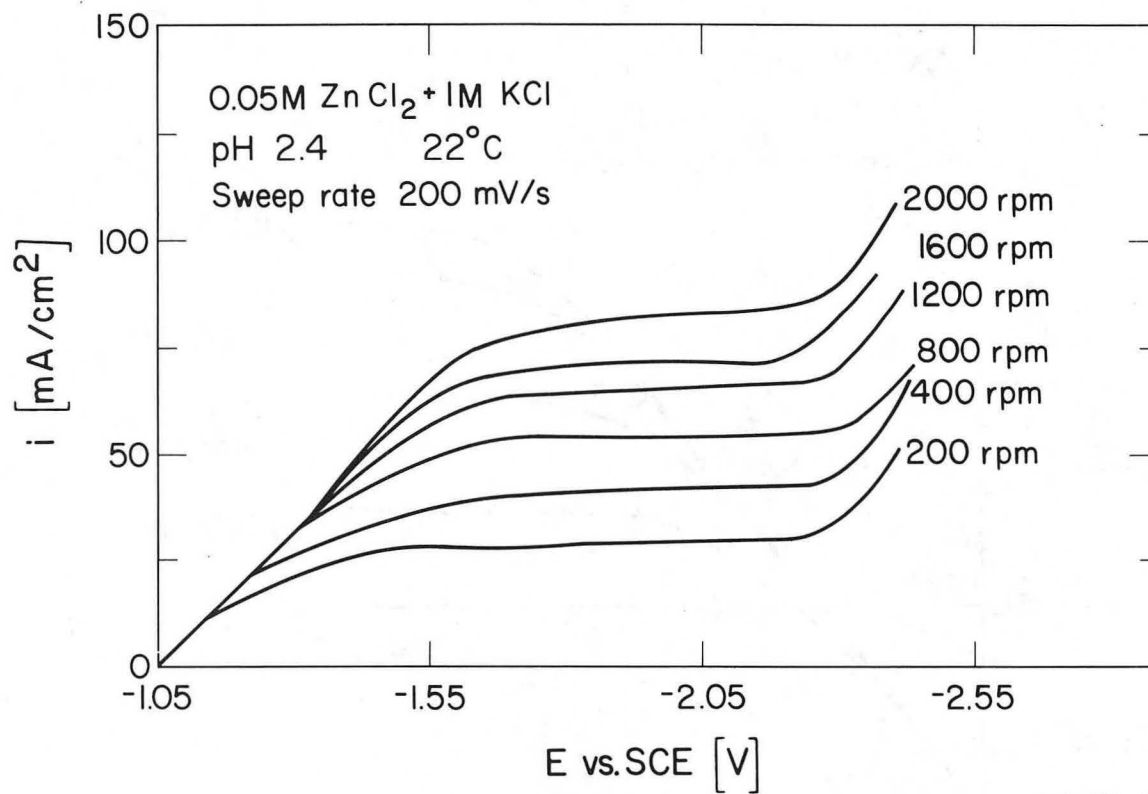
#### 4.3 Limiting Current Studies

Zinc forms striated deposits well below the limiting current. The current density ranges used in this study are small fractions of the zinc limiting current. The influence of mass transport is still very important, even though it is not limiting the actual average rate of the deposition process. Limiting current experiments were performed to determine just what transport conditions exist near the electrode surface.

This portion of research, carried out in collaboration with Darko Rajhenbah, has been reported in LBL Report LBL-15338 [47]. Cathodic polarization curves were obtained by potential scans at various rotational speeds of a zinc disk electrode in both  $\text{ZnCl}_2$  and  $\text{ZnSO}_4$  supported electrolytes. As shown in Figs. 4.18 and 4.19, at high scan rates, distinct limiting plateaus were obtained in KCl supported  $\text{ZnCl}_2$  solutions. Using data from these plateaus and the Levich equation [61] for limiting current on a RDE, limiting currents for 1 M zinc solutions used in this study were estimated to be always above  $300 \text{ mA/cm}^2$ , even for the low rotation speed of 100 rpm. This estimated value is indeed far above the current densities used in this study, and therefore, the experiments conducted in this study were not limited by average rate of mass transport of zinc to the cathode.

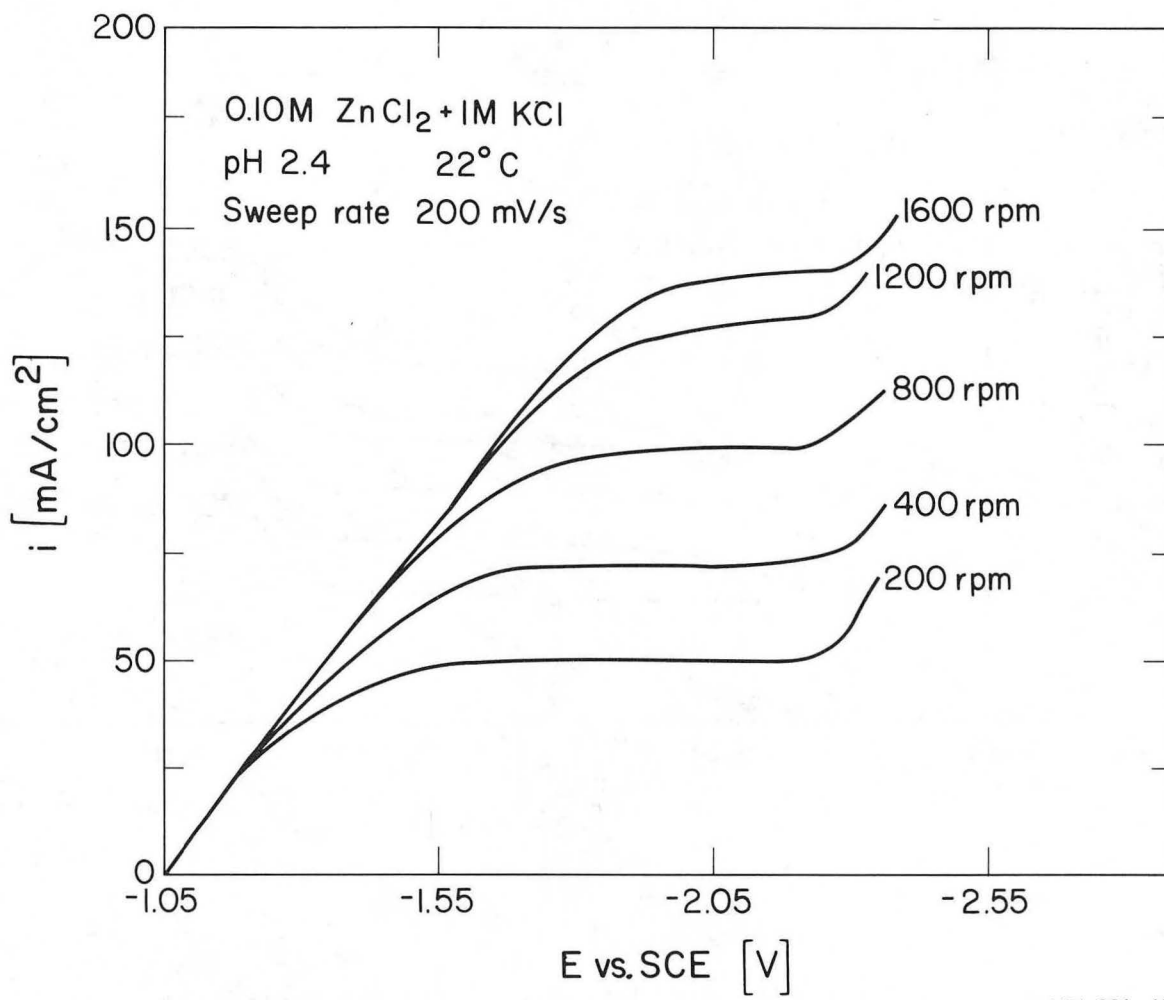
#### 4.4 In situ Time-Lapse Photographic Studies

The aim of the studies conducted in the In situ Cell was to permit further analysis of the sequence of morphological events occurring in



XBL 831 - 15

Figure 4.18 Limiting Current Plateaus for the Deposition of Zinc from 0.05 M ZnCl<sub>2</sub> + 1 M KCl



XBL 831 - 16

Figure 4.19 Limiting Current Plateaus for the Deposition of Zinc from 0.10 M  $ZnCl_2$  + 1 M KCl

the zinc deposition process. Time-lapse motion photography made possible observation of the completion of the deposition process, from initial substrate surface to the initial development of the striations, and finally, to fully developed striated deposits. The effects of current density and hydrodynamic flow were investigated using this procedure in 1 M  $\text{ZnCl}_2$  solutions at pH values in the range 1.9 - 4.6. The results essentially substantiate all the evidence compiled in earlier experiments in the Small Cell and Large Cell. The motion picture sequence summarizing this study is detailed in Appendix D. The movie allowed observation of the development of striations without the disturbances of removing and replacing the deposit in the cell during the experiment for the sole purpose of preparing photographs of the surface morphology. Considerable doubt exists as to what happens when a deposit is removed from a cell environment and externally analyzed, and then, returned to the cell, and the deposition process continued.

The motion picture has advanced our understanding of the deposition process because the events transpiring on the surface could be photographed without interrupting the deposition. The events that led to fully developed striations, as shown by motion pictures, occurred in the following sequence:

- a) Zinc deposits smoothly on the substrate surface, covering it completely (under 5X magnification) in less than 2 seconds at a current density of  $30 \text{ mA/cm}^2$ .
- b) The deposit retains this smooth texture, which is highly reflective in the camera, for approximately 2 minutes at  $30 \text{ mA/cm}^2$ .

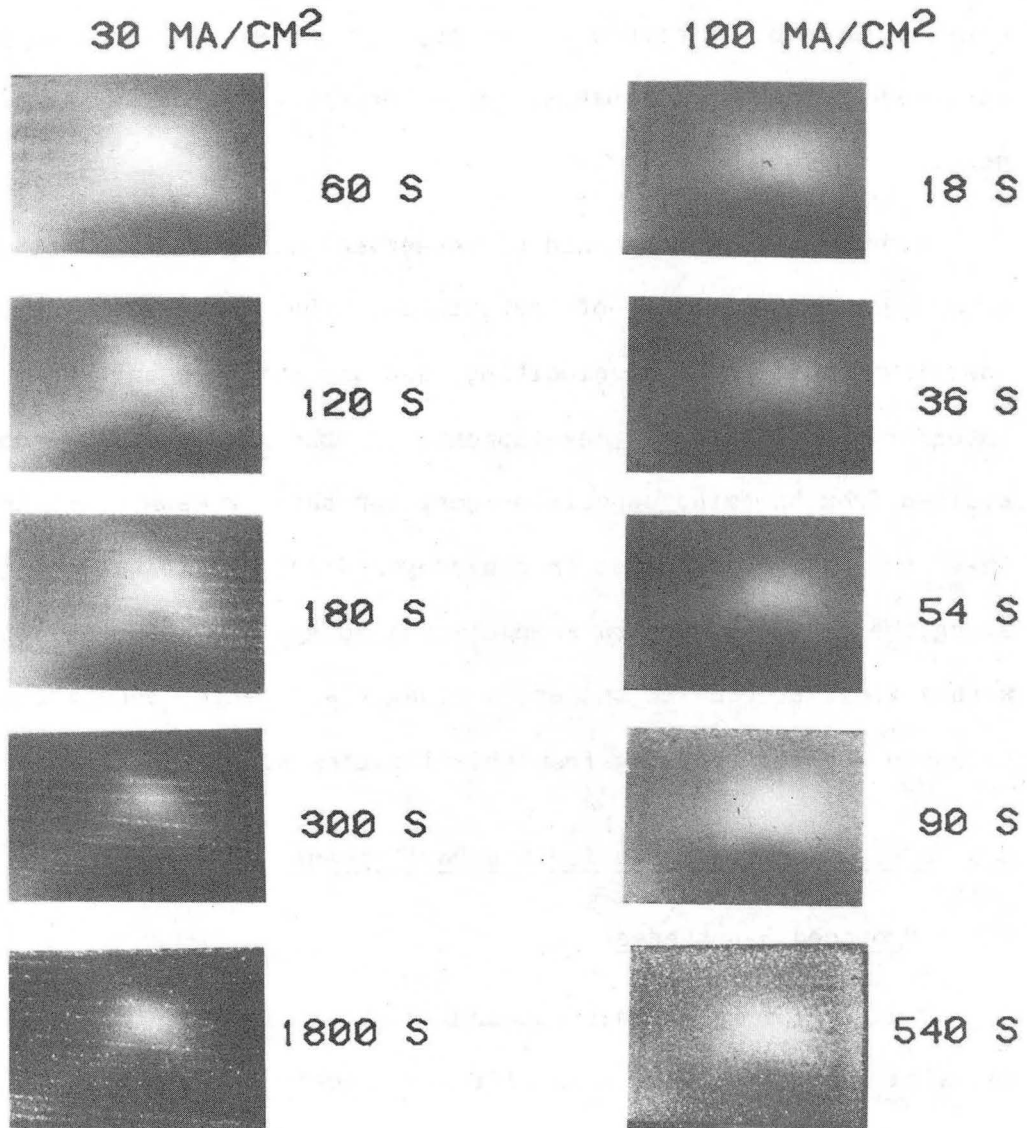
- c) Randomly scattered protrusions develop to a large enough size to be visible on the surface; these continue to grow in size.
- d) At this point, the larger protrusions tend to grow laterally in the low direction into elongated shapes. They grow extremely rapidly in the downstream direction, and much slower in the upstream direction, and in width.
- e) This complex phenomenon completely changes the area near the leading edge into striations in just another 2 - 4 minutes. During this time interval, the propagation of these striations in the flow direction occurs rapidly. In turbulent flow, the striations are more sharply delineated in the flow direction, while in laminar flow, the striations have a more wavy appearance in the flow direction.

The mechanisms involved in turning a surface with elongated protrusions into a deposit with parallel, well defined striations is not fully understood. This film does not provide sufficient clues as to how this complex event happens. It is evident, however, that this development from isolated crystallites to grooves occurs very rapidly, and it starts near the upstream area of the electrode.

Under the flow conditions studied in the In situ Cell, the propagation rate was extremely fast. Actual propagation rates were very similar to those shown in Fig. 4.3 with the highest flow rate resulting in the highest propagation rate of the striations. Fig. 4.20 shows sequences of zinc deposits in the In situ Cell at 30 and 100 mA/cm<sup>2</sup> in 1 M ZnCl<sub>2</sub>, pH 4.6 and Re 9000.



ZINC DEPOSITS FROM IN SITU CELL  
1 M  $ZnCl_2$ , PH 4.6, RE 9000  
FLOW RIGHT TO LEFT  
ELECTRODE WIDTH 0.5 CM



XBB 838-6779

Figure 4.20

At  $100 \text{ mA/cm}^2$ , the deposit immediately covered the substrate, but no large protrusions appeared, and striations did not develop at all. Instead, the depositing surface was very smooth, except for all the edges, which showed dendrites growing both outward from the surface and upstream (better mass transport and field effects). These dendrites did not appear to interfere with any of the smooth area; no striations appeared in the deposit behind large dendrites growing at the front edge.

Hydrogen evolution could be observed along the electrode edges after several minutes of deposition. The bubbles were swiftly swept downstream at high flow velocities, and did not show any marks or other interference with the development of the zinc deposit. No hydrogen evolved from the zinc deposit proper; for this reason, it is assumed that the gas originated from hydrogen discharge in the small fissures along the platinum substrate-insulating epoxy. One of the electrodes, with a visible crack in the epoxy along a side edge, consistently showed hydrogen bubbles evolving from this location along the side edge.

#### 4.5 Discussion of Causes for the Development of Striated Deposits

##### 4.5.1 Proposed Hypotheses

A number of hypotheses concerning the existence of the striated deposits have evolved from different facets of this project. Each of these hypotheses has been examined in light of the experimental facts provided by myself and former associates. Certain hypotheses can be partially substantiated, while others conclusively discarded.

Early ideas by Milan Jaksic and Charles W. Tobias [15] centered around possible Taylor-Goertler vortices which are caused by instabilities and secondary flow in the fluid near the surface. Taylor vortices have been observed in flow between two concentric, rotating cylinders and Goertler vortices in boundary layer flow along a concave wall [56,80]. When a certain Reynolds number is exceeded, Taylor vortices appear in the flow with axes located along the circumference and they rotate in alternately opposite directions. The flow remains well-ordered and laminar with these vortices present. Turbulent flow develops only at much higher Reynolds numbers. Evidence in this study clearly demonstrates that the striated appearance of zinc deposits occurs in both the laminar and highly turbulent flow regions, and not just in the transition region between the two flow regions. Striations propagate downstream at a rate which is directly related to the Reynolds number. Since the vortices only occur near the stability limit of laminar flow, and the striations appear even at low Re numbers, this vortex hypothesis requires more detailed development before its merits can be judged.

Another hypothesis [27] concerning the appearance of striations in zinc electrodeposition involved hydrogen co-evolving with the deposition of zinc. Thermodynamically, the  $Zn(+2)$  half-cell reaction is almost 770 mV more negative than the hydrogen half-cell reaction, so hydrogen should always evolve before zinc. That such is not the case is due to the high overpotential of hydrogen evolution on pure zinc. Hydrogen bubbles that stick to the surface may cause wakes in the zinc deposit downstream. However, experimental observations do not support such a

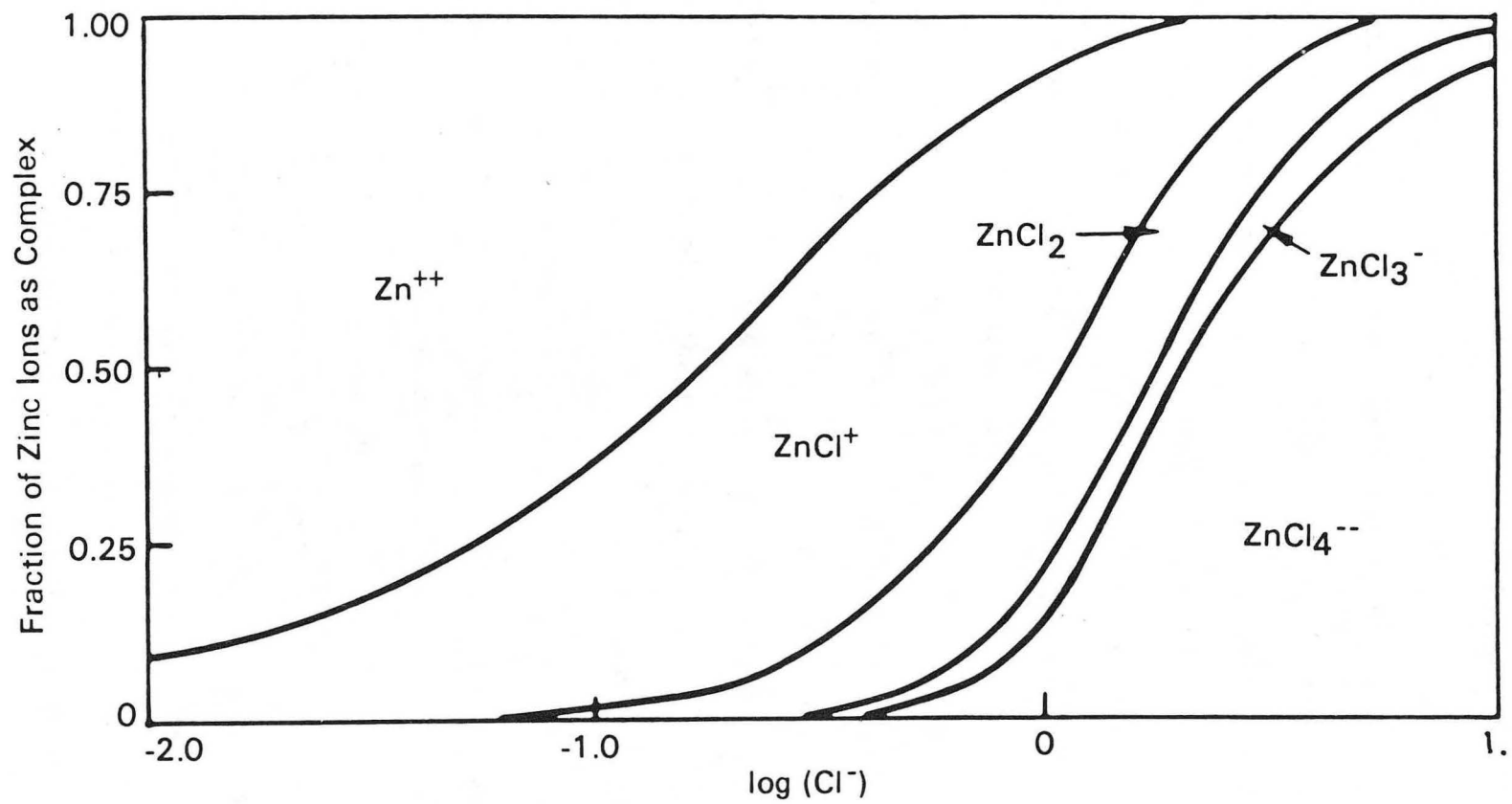
hypothesis. Two pieces of evidence deserve consideration: first, wakes caused by hydrogen bubbles on the surface have been observed at various times, but the appearance of the resulting striated deposit is totally different than the deposits obtained in the absence of hydrogen evolution. Hydrogen bubble wakes always originate from a site that is not covered with zinc. Secondly, no major differences in the appearance of striations has been observed with change in the 2 - 5 pH range. Within this range, the rate of evolution of hydrogen increases with a decrease in pH, but this increase causes no additional striations to develop on the surface.

Impurities codepositing with zinc may be catalyzing isolated sites to grow at accelerated rates. As Tsuda [10] established in his zinc deposition studies with contaminants, lead enhanced the preferential growth of specific sites (protrusions) on the surface. He also found that identical striations appeared on the zinc deposits when ultrapure solutions were used. The only difference between striated surfaces deposited from lead-contaminated solution and ultrapure solutions is the time that was necessary before spiral patterns became discernable under small magnification. Deposits from solutions containing lead exhibited spirals after 0 - 10 minutes, while deposits from ultrapure zinc solutions showed spiral patterns after 10 - 20 minutes.

Another hypothesis considered that zinc was actually being mass transport limited in these concentrated solutions because of the complexing tendency of halides in acidic media. In the concentration range of zinc chloride solutions used in this study, zinc is found to be principally in the following forms (shown without the hydrate):  $ZnCl_4^{2-}$ ,

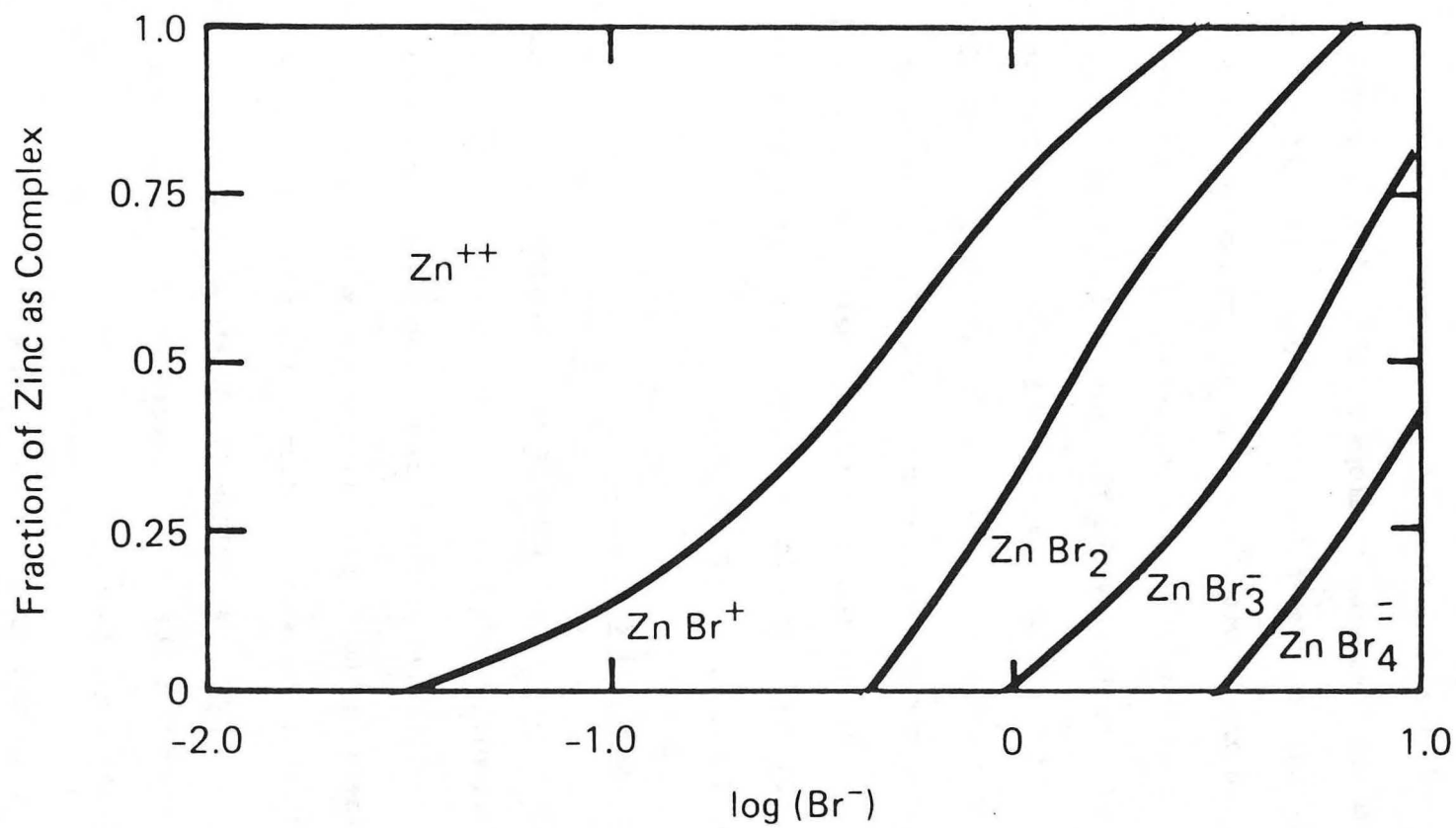
$\text{ZnCl}_3^-$ ,  $\text{ZnCl}_2$ , and  $\text{ZnCl}^+$  [66]. By using thermodynamic data found in Sillen [79] and a simple conservation balance, the fraction of zinc ions existing as each complex can be computed for different overall concentrations of halide ion in solution, and the results are shown for zinc chloride and zinc bromide solutions in Figs. 4.21 and 4.22, respectively. These Figures show that even for chloride ion concentrations as low as 0.1 M (or, bromide concentrations of 0.2 M), at least two complexes are thermodynamically stable in solution in nontrivial amounts. Moreover, for chloride concentrations below 0.01 M, zinc is still partially complexed as  $\text{ZnCl}^+$ . In zinc sulfate solutions, zinc does not form complexes with sulfate ions [79], yet striated deposits appear and are very similar to deposits from halide solutions. In addition, limiting current studies were conducted on both sulfate and chloride solutions of zinc, and results from these experiments [47] reveal that the zinc deposition is not mass transport limited at the current density levels used in this study.

Microscopic irregularities on the substrate, including roughness of the front edge of the channel electrodes were thought to be responsible for the appearance of protrusions and developing striations. The fact that similarly structured striations (spirals) appear on rotating disk electrodes negates the effect of disturbances in the flow patterns caused by discontinuities being directly or primarily at fault. As discussed before, different degrees of substrate smoothness led to striated deposits with the same structure characteristics and appearance; the only difference was in the time of appearance.



XBL 838-11146

Figure 4.21 Distribution Diagram of ZnCl<sub>2</sub> System



XBL 838-11145

Figure 4.22 Distribution Diagram of ZnBr<sub>2</sub> System



Jaksic and Tobias [15,16,17], and later, Tsuda and Tobias [10] hypothesized that the cause of striations could be reasonably explained by a mechanism involving development of surface roughness and a disturbance of the concentration field near the surface. Crystals would nucleate and grow, with preferential growth of larger protrusions. These large protrusions cause local eddy mixing, and because of the high exchange current density and fast kinetics of zinc, slight differences in zinc concentration locally along wakes on the surface may result in substantially enhanced nucleation in the well mixed locations. In highly reversible systems characterized by large exchange current densities, such as in the case of zinc, a small increase in the cathodic overpotential (or current density) can cause a large increase in the frequency of nucleation [75,94,95].

#### 4.5.2 Development of Striations

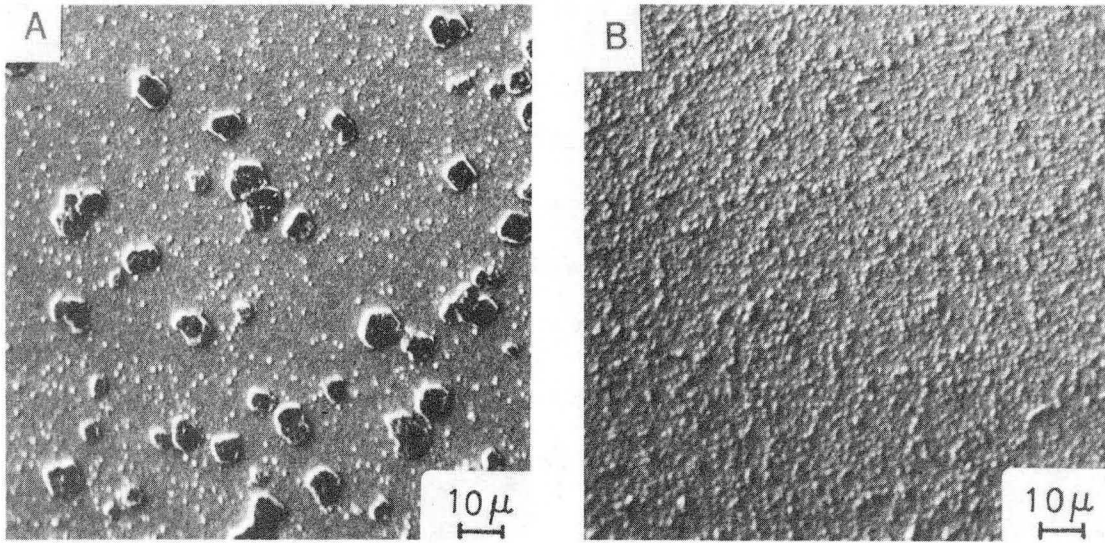
On the basis of work done in this laboratory by Tobias, Jaksic, Tsuda, Kommenic, Rajhenbah, and Faltemier over the last 7 years, the following qualitative picture emerges about the development of striations. These authors have each uniquely contributed to better understanding of this phenomenon. Some of the ideas in this study are not original, in that as scientific progress in this laboratory is made, more or different evidence is gathered which further substantiates or refutes previous hypotheses.

The development of the striated deposits occurs continuously during electrodeposition of zinc under the conditions discussed previously. The striations are evident to the naked eye after approximately 5 - 10 minutes in the current density range studied. This is especially

evident in the motion picture sequences from the In situ Cell. They develop into complete, connected grooves, continue to grow in size, and eventually, diminish in number across the surface due to melding. Zinc protrusions of different sizes first appear on the surface, and then, through a still poorly understood mechanism, evolve into striations in the flow direction. Both Jaksic [16] and Tsuda [10] reported observations of protrusions evolving into fully developed striations, but in situ observations of the developing surface, and "Large Cell" electrode size deposition studies were not yet completed.

Experimental data gathered by Jaksic, Tsuda, and in this study uncovered the fact that the events leading to fully-developed striations occur in two general steps: an initiation and growth step, in which the electrochemical mechanisms of nucleation, crystal growth, and coalescence of zinc crystallites occur on the surface with no apparent hydrodynamic effect, and a propagation step, in which the influence of hydrodynamic flow starts to control the surface profile.

In the initiation step, zinc covers the substrate surface within 2 seconds, so no substrate effect is observed in the macromorphological structure. In the first minutes, the zinc surface appears smooth under 10X magnification. However, under higher magnification, the microscopic picture is quite different for the lower current density range considered in this study. Fig. 4.23, taken from Tsuda's thesis [10], shows examples of the early stages of deposition under a scanning electron microscope. The crystals are randomly distributed on the surface for all the current density cases. The variation in crystal sizes on the surface is much larger at the lower current densities. At higher



XBB 831-242

EFFECT OF CURRENT DENSITY ON THE SIZE  
AND NUMBER OF INITIAL PROTRUSIONS  
1 M  $ZNCL_2$  , 800 RPM  
A. 10 MA/CM<sup>2</sup> X 90 S    B. 30 MA/CM<sup>2</sup> X 30 S

Figure 4.23 (T. Tsuda, [10])

current densities, the surface consists of crystals which are smaller and which vary less in size, due to higher nucleation rates and lower crystal growth rates associated with higher current densities (or overpotentials). At even higher current densities, the size of crystals is still smaller and the number density of crystals is much larger after the same number of coulombs have been passed. This larger variation in size of crystals at the lower range of current densities, as also noted by Tsuda [10], is considered by the present author as the dominant cause of the second general step, the propagation downstream.

Landau, Cahan, and Selman's work [29] on characterizing the morphology of zinc deposition agrees to a large extent with the early stages of deposition in this study. They observed a certain "initiation" time period during which the zinc surface was roughening, but the evolution of specific protrusions could not be discerned. They also noted that the number density of these "dendritic" sites increased with both concentration and overpotential, due to the increased nucleation rate with these parameters.

At some critical time, the hydrodynamic flow begins to influence the surface events. The largest protrusions cause the largest disturbance in the hydrodynamic flow because they protrude the farthest into the hydrodynamic boundary layer. Wakes form in conjunction with these protrusions, causing better electrolyte mixing downstream. This mixing enhances the local current density in the areas behind the protrusions and causes deposition rates there to increase. As these protrusions grow laterally in the flow direction into other protrusions downstream,

striations begin appearing on the surface. Eventually, the grooves will extend along the length of the entire electrode.

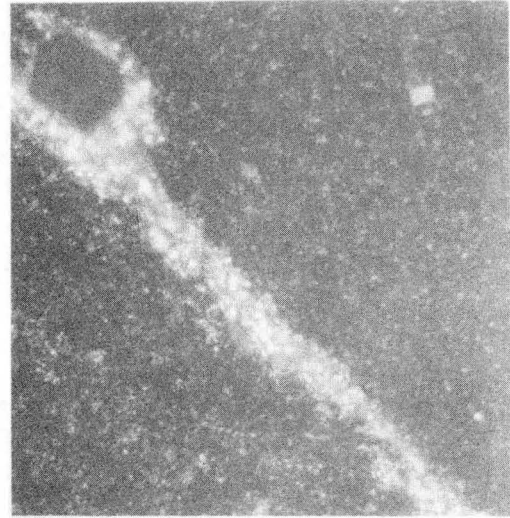
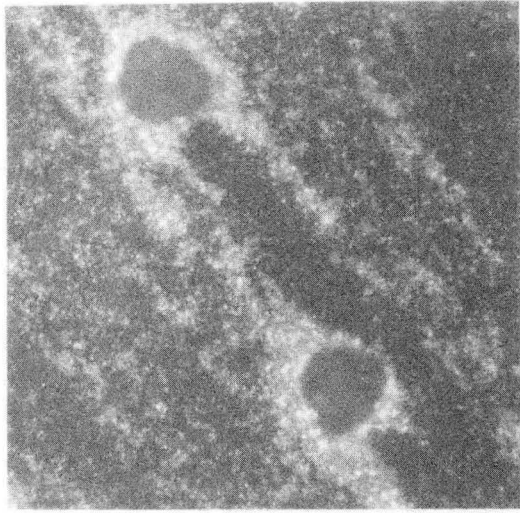
Many investigators have studied wake formation and shapes behind obstructions in the flow direction [61,80]. Carlson [11] studied the deposition of copper around small protrusions on a planar surface. His deposits showed distinctive wake regions associated with these protrusions. He inferred that the hydrodynamic changes produced by the protrusion thinned the boundary layer in the wake, and this resulted in an enhanced rate of deposition inside the wake region. Figs. 2.3 and 2.4 show examples of copper deposits formed behind cylindrical obstructions.

Fig. 4.24\* shows an example of wakes formed behind large protrusions in zinc deposition. These deposits in the wakes will continue to grow outward from the surface and propagate downstream, eventually connecting together to form a striation in the flow direction. After additional deposition time, these large protrusions are no longer symmetrical in shape, but are elongated downstream in the flow direction. Fig. 4.25\* shows examples of the initial phase of spiral striations on a rotating disk electrode. These elongated protrusions eventually will join together to form striations that cover the entire electrode.

The morphology changes of the deposit become noticeable as large protrusions form striations in the flow direction and these striations develop further with time. These changes with the time of deposition, as shown in Figs. 4.26 and 4.27, fully substantiate the explanation of propagation as discussed above. Each of these Figures shows a single RDE deposit photographed after three different times elapsed after start

---

\*from work done in collaboration with Vladimir Kommenic



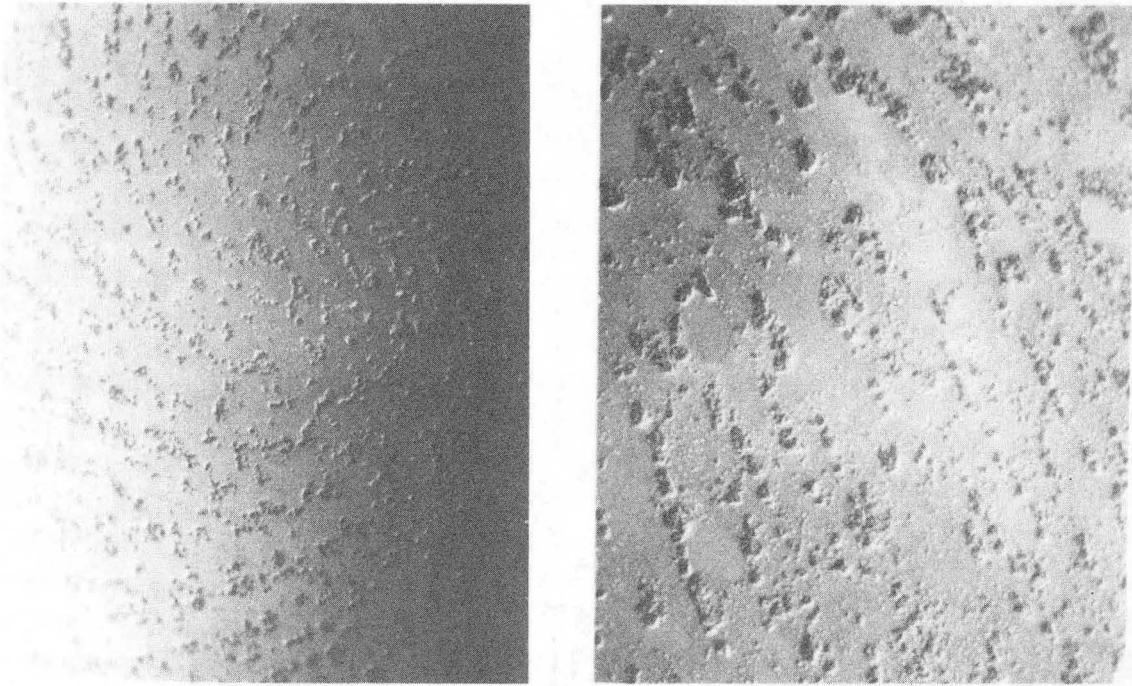
XBB 831-371




25 MICRON


1 M  $ZNSO_4$ , PH 4.6, 400 RPM  
5 MA/ $CM^2$  X 25 MIN

Figure 4.24 Zinc Deposit Patterned in Wake Formation Around Protrusions



XBB 831-372

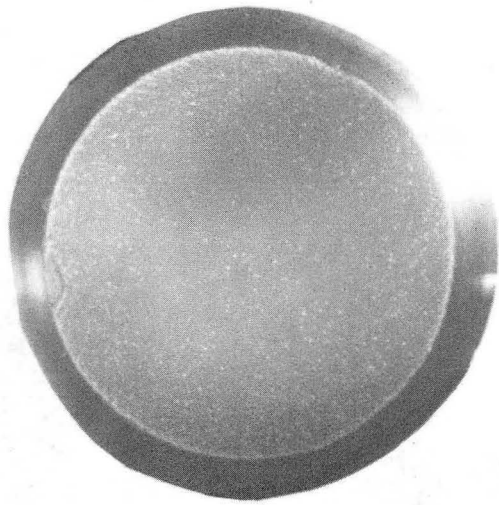
  
0.05 CM

  
0.05 CM

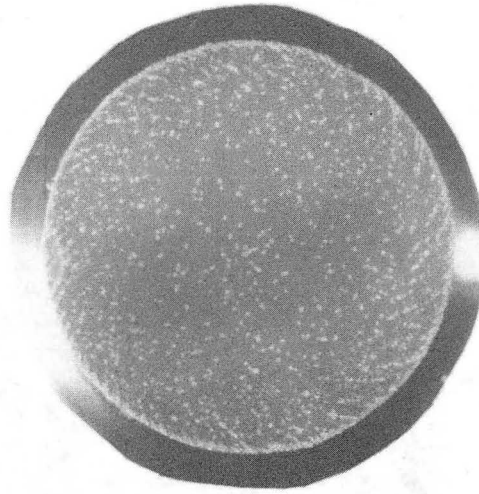
1 M  $\text{ZnCl}_2$ , PH 4.6, 800 RPM  
10 MA/ $\text{CM}^2$  X 9 MIN

Figure 4.25 Spiral, Elongated Protrusions in Zinc RDE Deposit

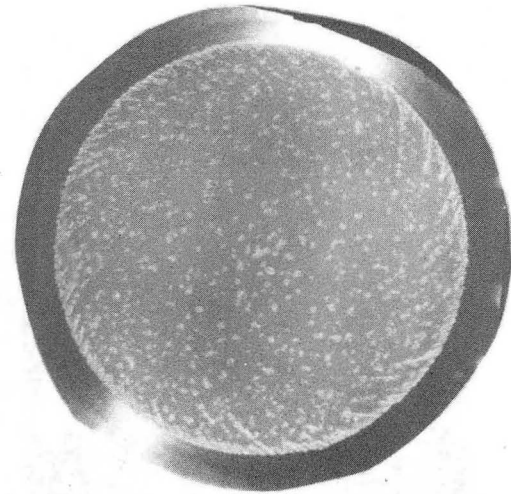




50 MIN



90 MIN

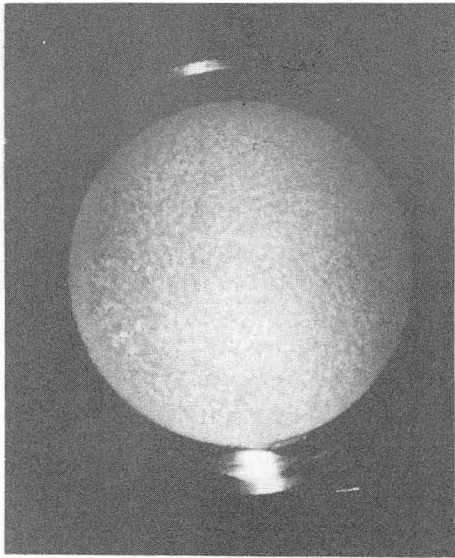


120 MIN

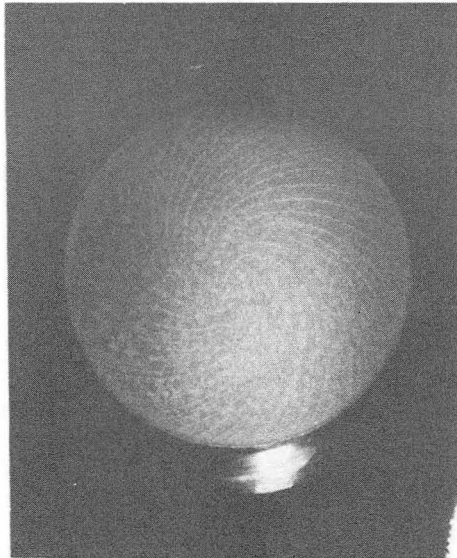
XBB 831-376

1 M  $ZNSO_4$ , PH 4.6, 400 RPM, 2 MA/CM<sup>2</sup>

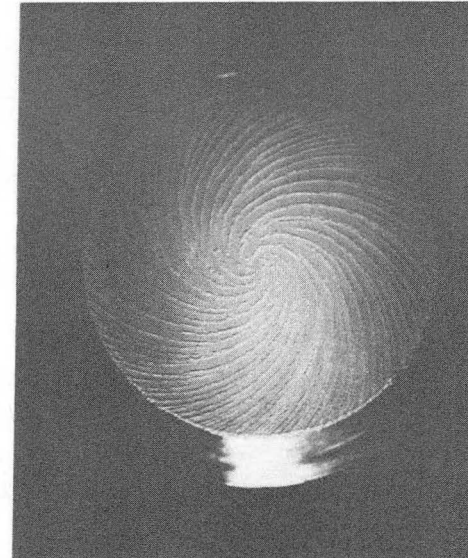
Figure 4.26



5 MIN



10 MIN



XBB 831-377

30 MIN

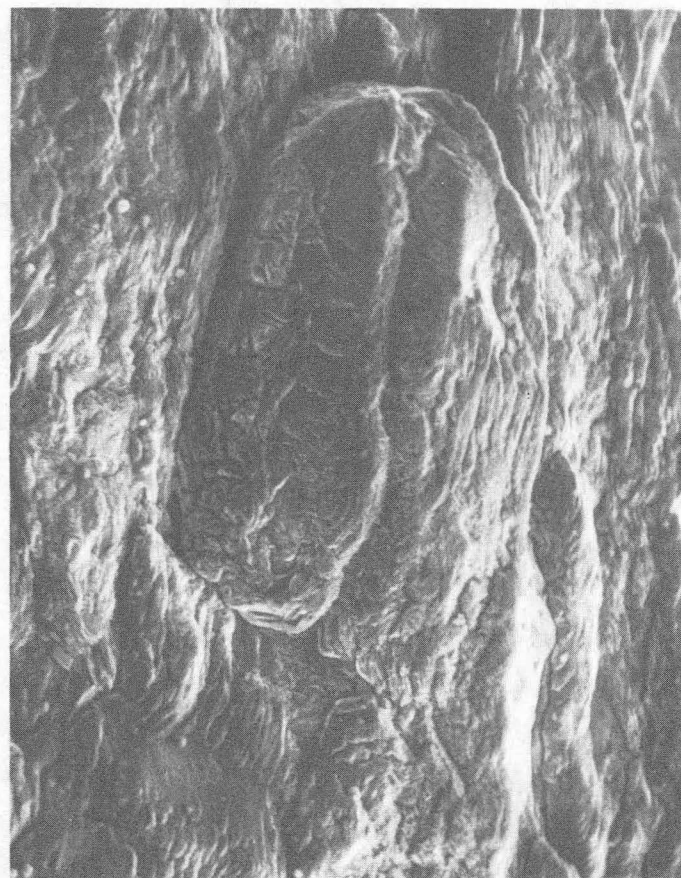
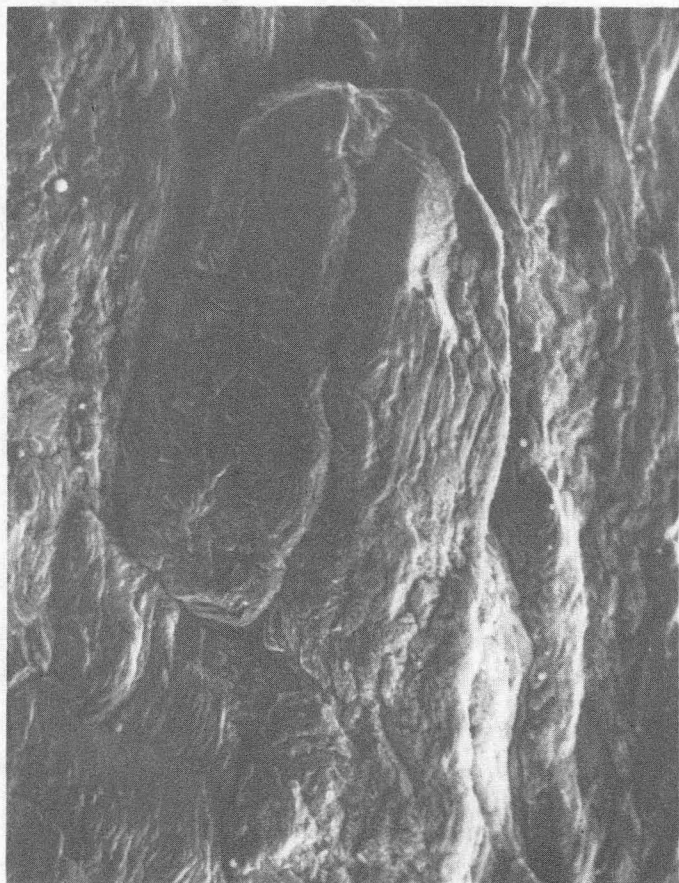
1 M  $\text{ZnCl}_2$ , PH 2.4, 800 RPM, 30 MA/CM<sup>2</sup>

Figure 4.27

of electrolysis. The growth of the largest protrusions on the surface into elongated-shaped protrusions is easily identified.

Stereo viewing of a fully developed striated surface offers further (interesting) evidence in support of protrusions growing laterally in the flow direction, eventually connecting together into developed striations. Two 3-D stereoscopic examples (four photos) of a large protrusion within a fully developed groove on a Small Cell electrode are shown in Figs. 4.28 and 4.29. The flow is from top to bottom in each of these figures. These stereo pairs offer a three-dimensional enhancement effect projecting the elongated protrusions toward the viewer. The compact layered growth of hexagonal zinc platelets with 120 degree angles is also noticeable.

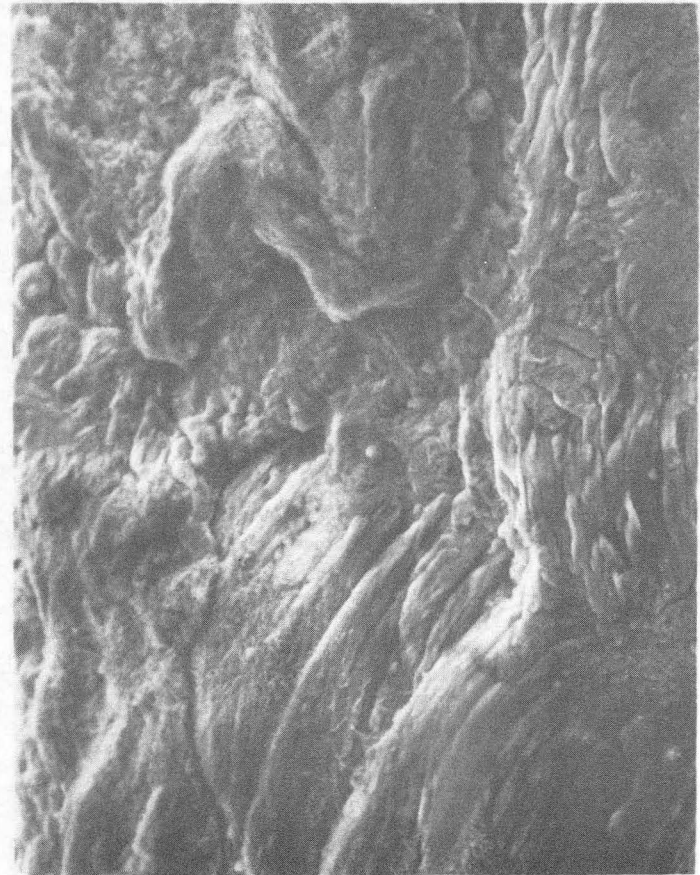
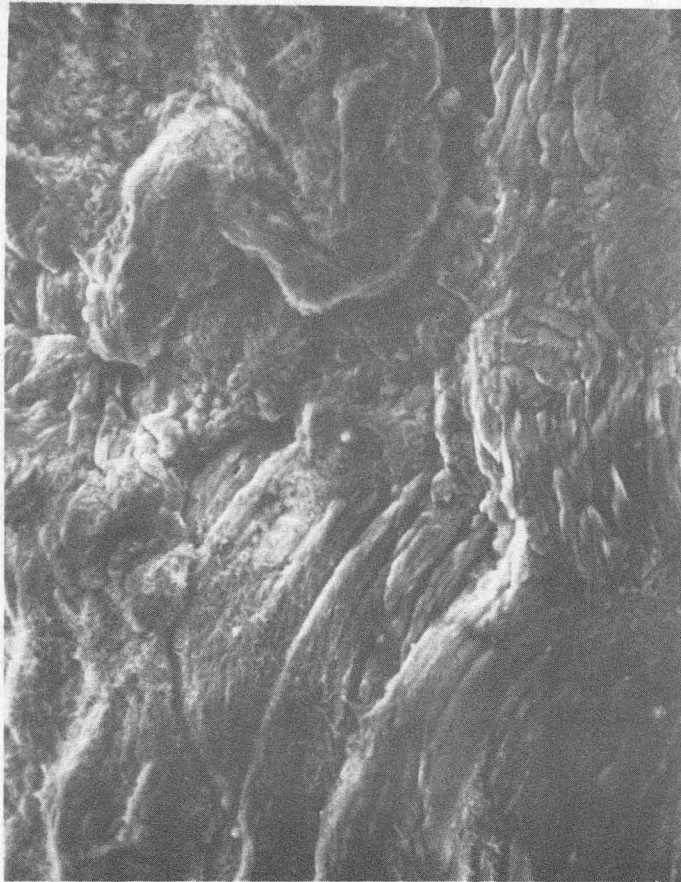
The development of these protrusions into evenly spaced and sized, striations is not as discernable as the lateral growth of protrusions. Tsuda [10] surmised that secondary flows occur around the large protrusions as connection of the protrusions proceeds and that greater mass transfer to the striation ridges rather than into the recesses causes the striations to grow and become more pronounced. Although this study also offers no definite, experimental evidence concerning this specific topic, Tsuda's hypothesis is very plausible. Secondary flows are indeed occurring around protrusions on the surface, as evidenced above in the deposition patterns in Fig. 4.24. Secondary flow patterns that are very similar to those found in this work also occurred around the developing striated copper deposits in Fenech's [33] and Hickman's [5,6] work. Their fully-developed striated deposits had very similar structure, in that their striations were also delineated in the flow direction,



XBB 837-6188A

Figure 4.28 Stereo Pair of Zinc Deposit  
1 M  $\text{ZnCl}_2$ , pH 2.1,  $30 \text{ mA/cm}^2$ , 2 Hours, RE 5000  
Flow Top to Bottom, 1 cm = 10 microns





XBB 837-6190A

Figure 4.29 Stereo Pair of Zinc Deposit  
1 M  $\text{ZnCl}_2$ , pH 2.1,  $30 \text{ mA/cm}^2$ , 2 Hours, RE 5000  
Flow Top to Bottom, 1 cm = 20 microns

developed in the same time frame, had very similar macromorphological appearances, and were also evenly spaced across the copper electrode. However, copper deposits are striated only very near the limiting current. Comparison of Carlson's [11] copper deposition patterns and deposits around protrusions in this study also provide definite evidence of similar types of interactions occurring between hydrodynamic flow and small obstructions on the deposit surface.

Solid evidence and explanations concerning the deposit developing from one which is seemingly occurring randomly on the surface to one in which evenly-spaced and sized, parallel striations exist is not available. Ideas in this study were discussed with and agree in general with those of Tsuda [10]. When individual protrusions grow to such a size to cause interferences with the laminar flow inside the diffusion layer next to the surface, the flow becomes chaotic in the sense that it is no longer 1-dimensional flow along a flat surface, but instead, a 3-dimensional flow interacting with protrusions of different sizes and heights. This interaction between the fluid and the largest protrusions on the surface results in continued downstream growth due to eddy mixing, and by some complex process, in the eventual patterning of fluid between large elongated protrusions. The important factors involved in this mechanism are still unknown, but must depend on both the zinc nucleation and crystal growth properties, as well as the physical characteristics of the fluid and the flowrate. Mass transfer is greater to the ridges than to the "recesses" between them causing the striations to grow wider and outward from the surface. As the deposition continues and the striations grow, they begin to overlap with each other because

of size, thus causing even more complex fluid-striation interactions and a melding effect of the striations.



## 5. SUMMARY AND CONCLUDING REMARKS

The aim of this research was to investigate the influences of hydrodynamic flow and other process variables on the morphology of electrodeposited zinc. Zinc forms striated deposits up to a moderately large current density ( $<80 \text{ mA/cm}$  in  $1 \text{ M ZnCl}_2$ ). Within this region, higher rate of flow causes the striations to develop more rapidly and to be more sharply contoured in the flow direction. Above this region of current density, macroscopically smooth zinc deposits were obtained in laminar and turbulent flow. Several other process variables were investigated; each having only minor, secondary effects on the macromorphology.

The experimental observations and results from this study can be summarized in the following manner:

- \* the striations always form parallel to the hydrodynamic flow direction; in channel flow cells this results in straight striations and in spiral-shaped striations in RDE systems
- \* the striations start at the highest current density portion of the electrode and progress toward lower current density regions
- \* the striations develop more rapidly with an increase in Reynolds number; the rate of propagation along an electrode also increases with Reynold's number
- \* striations appear only in certain current density regions; in  $1 \text{ M ZnCl}_2$  solutions, the upper limit for striations is approximately  $80 \pm 10 \text{ mA/cm}^2$ , whereas in  $1 \text{ M ZnSO}_4$  solutions, this

upper limit is  $15 \pm 2 \text{ mA/cm}^2$

- \* striation formation can be eliminated by sufficiently high current density or by pulsed current techniques; above the upper limits mentioned above, striation-free deposits are always obtained
- \* bulk zinc concentration has only minor influence on the deposit appearance in the range 0.5-4M  $\text{ZnCl}_2$ ; the average number of developed striations across a 1/2 cm electrode in a channel cell is approximately constant at 22 for various solutions
- \* pH variations (over the range 1.9 to 5) result in only minor differences in the deposit appearance; no major effect of hydrogen evolution or bubbles is observed
- \* striated deposits along large electrodes are very similar to deposits obtained in small cells; approximately the same number of striations across 1/2 cm of the cell appear, and smooth, nonstriated deposits are obtained above the upper current density limit for 1 M  $\text{ZnCl}_2$  mentioned above
- \* deposits of long continuous, regular striations from the Large Cell showed that any interference of the leading edge of the electrode with flow is not a major criterion
- \* a time-lapse motion picture reveals the deposition of zinc into striations without external transfer and manipulation of the deposit during the electrolysis
- \* a more detailed, continuous development of protrusions into striations is revealed in the In situ Cell motion picture

- \* secondary flows around protrusions is evidenced by deposition patterns of wakes around and behind protrusions
- \* the effects of substrate material and of polishing roughness are secondary; no differences in the striated deposit result with different metals or single-crystal zinc used as substrates; a less polished substrate results in striations appearing slightly earlier
- \* deposits in noncomplexing  $\text{ZnSO}_4$  are very similar to those in highly-complexing zinc halide solutions
- \* on the basis of mass-transfer limiting currents measured on the RDE in both chloride and sulfate supported electrolytes, the appearance of striations occurs far below the limiting current for zinc deposition.

Evidence concerning the development of striations in this study agrees with earlier conclusions of Jaksic's [15,16] and Tsuda's [10], according to which the striated deposits occur because of differences in crystal nucleation and crystal growth rates of zinc at different current densities (i.e., different overpotentials). As the current density (i.e., low overpotential) level is raised within this range, the nucleation of crystals becomes progressively more frequent on the surface at the expense of the growth of crystallites. At the low current density (i.e., low overpotential) levels, the nucleation of new crystallites is not favored, resulting in a surface with a much larger variation in crystallite sizes.

The results obtained in this study suggest possible directions for further exploration of the mechanism responsible for imprints of hydrodynamic flow in zinc deposits, including the following:

- \* studies of the initial stages of electrocrystalization concerning the nucleation and growth rates of crystallites
- \* better understanding of the role of zinc halide complexing and of impurities on this process.

REFERENCES

1. G. T. Wever, "Effect and Control of Impurities in the Electrowinning of Zinc", Journal of Metals, February 1959, pp. 130-134.
2. W. Bruce Darlington and Marino Y. C. Woo, "Report of the Electrolytic Industries - 1981", Industrial Electrolytic Division, The Electrochemical Society, May 12, 1982.
3. A. Lijoi, Program Manager, "Development of the Zinc-Chlorine Battery for Mobile Applications", Energy Development Associates, prepared for DOE under contract no. DE-AC0Z-76ET-20131, December 1981.
4. N. N. Kayander, Zhur. Russ. Fiz.-Khim. Obshch., 13, part 1, (1881).
5. C. W. Tobias and R. G. Hickman, "Ionic Mass Transport by Combined Free and Forced Convection", Z. Phys. Chem., 229 (1965), pp. 145-166.
6. R. G. Hickman, "The Effect of Buoyancy Forces on Forced Convection Ionic Mass Transfer at Horizontal Planar Electrodes", Ph. D. Thesis, University of California - Berkeley, December 1963.
7. G. T. Rogers and K. J. Taylor, "Effect of Small Protrusions on Mass Transport to a Rotating Disk Electrode", Nature, 200 (1963), pp. 1062-1064.
8. M. R. H. Hill, G. T. Rogers, and K. J. Taylor, "The Cause of Spirals on Electrodeposits formed on a Rotating Disc Electrode", J. Electroanal. Chem., 96 (1979), pp. 87-93.

9. R. White, C. M. Mohr, Jr. and J. Newman, "The Fluid Motion Due to a Rotating Disk", JES, 123 (1976), pp. 383-385.
10. Tetsuaki Tsuda, "The Influence of Lead Ions on the Macromorphology of Electrodeposited Zinc", M. S. Thesis, Lawrence Berkeley Laboratory, University of California - Berkeley, Report No. LBL-13057, September 1981.
11. E. J. Carlson, "Electrodeposition around Protruding Surface Imperfections in Turbulent Flow", M. S. Thesis, University of California - Berkeley, Lawrence Berkeley Laboratory, Report No. LBL-3175, January 1975.
12. U. Landau, "Diffusion and Migration in Electrochemical Systems", Ph. D. Thesis, University of California - Berkeley, Lawrence Berkeley Laboratory, Report No. LBL-2702, January, 1976.
13. A. Kindler, "The Morphology of Electrodeposited Copper", Ph. D. Thesis, University of California - Berkeley, Lawrence Berkeley Laboratory, Report No. LBL-12838, November, 1981.
14. J. L. Faltemier, M. Jaksic, T. Tsuda, and C. W. Tobias, "An Inventory of Photographs of Zinc Electrodeposited from Acid Electrolytes", Lawrence Berkeley Laboratory, Report No. LBL-16601, September 1983.
15. Lawrence Berkeley Laboratory, MMRD Annual Report 1976, Report No. LBL-6016, pp. 427-428.
16. Lawrence Berkeley Laboratory, MMRD Annual Report 1977, Report No. LBL-7355, pp. 509-510.

17. Lawrence Berkeley Laboratory, MMRD Annual Report 1978, Report No. LBL-8580, pp. 489-490.
18. M. Jaksic and C. W. Tobias, "Hydrodynamic Flow Visualization by an Electrochemical Method", presented September 9, 1980 in Bochum, Germany.
19. Lawrence Berkeley Laboratory, MMRD Annual Report 1980, Report No. LBL-12000, pp. 475, 486.
20. Lawrence Berkeley Laboratory, MMRD Annual Report 1981, Report No. LBL-13840, pp. 281-282.
21. Ya. V. Durbin and Z. V. Dukhnyakova, Sbornik, Statei po Obshchei Khim. Akad. Nauk. SSSR, [Collection of Articles on General Chemistry], 1 (1953), p. 157.
22. D. P. Gregory and A. C. Riddiford, "Dissolution of Copper in Sulfuric Acid Solutions", JES, 107 (1960), pp. 950-956.
23. G. R. Johnson and D. R. Turner, "The Effect of Addition Agents on the Kinetics of Copper Electrodeposition from a Sulfate Solution", JES, 109 (1962), pp. 918-922.
24. J. T. Kim and Jacob Jorne, "Mass Transfer of Dissolved Chlorine to a Rotating-Zinc Hemisphere in  $ZnCl_2$  Solution", JES, 125 (1978), pp. 89-93.
25. A. C. Riddiford, "The Rotating Disk System", in Advances in Electrochemistry and Electrochemical Engineering, Vol. 4, P. Delahay and C. W. Tobias, eds., Interscience, New York (1966).



26. McBreen, J., Principal Investigator, "Investigation of the Zinc Electrode Reaction", Annual Report, Brookhaven National Laboratory, October 1979 - September 1980, Report No. BNL-51370.
27. Jean Horkans, "Effect of Plating Parameters on Electrodeposited NiFe", JES, 128 (1981), pp. 45-49.
28. Y. Oren and U. Landau, "Growth of Zinc Dendrites in Acidic Zinc Chloride Solutions", Electrochimica Acta, 27 (1982), pp. 739-748.
29. U. Landau, Project Coordinator, "Zinc Electrodeposition and Dendritic Growth from Zinc Halide Electrolytes", Final Report, Electric Power Research Institute, May 1982, Report No. EPRI EM-2393.
30. F. Laghouiter, A. Laghouiter, D. Bodoit, and M. Daguinet, "Visualisation Electrochimique des lignes de mouvement parietales d'un fluide. Application a la mise en (oeuvre de la dimicroelectrode)", J. Chim. Phys. Phys. Biol., 72 (1975), No. 2, pp. 265-270.
31. J. S. Stanley, and J. A. Radley, Final Technical Report, U. S. Department of Army, Report No. FTR.1.JSS/RMR, 1959.
32. I. R. Krichevskii and Yu. V. Tsekhanskaya, Zh. Fiz. Khim., 33 (1959), p. 2331.
33. E. J. Fenech, "Ionic Mass Transport by Free Convection to Horizontal Electrodes", Ph. D. Thesis, University of California - Berkeley, Report No. UCRL-9079, April 1960.
34. Allen J. Bard, ed., Encyclopedia of Electrochemistry of the Elements, Vol. V, Chapter V-1, Marcel Dekker, Inc., New York (1976).

35. H. Frank Gibbard, "Physical Chemistry of the Zinc Bromine Battery, II. Transference Numbers of Aqueous Zinc Bromide", presented at Electrochemical Society meeting, Pittsburgh, PA., October 1978, Extended Abstract #13.
36. D. M. Egan and J. R. Partington, "Transport Numbers of Zinc Halides", J. Amer. Chem. Soc., 67 (1945), pp. 191-197.
37. E. P. Purser and R. H. Stokes, "Transference Numbers in Aqueous Solutions of Zinc Sulfate", J. Amer. Chem. Soc., 73 (1951), pp. 5650-5652.
38. G. M. Wolten and C. V. King, "Transference Numbers of Zinc and Cadmium Sulfates at 25° C, as Functions of the Concentration", J. Amer. Chem. Soc., 71 (1949), pp. 576-578.
39. A. C. Harris and H. N. Parton, "The Transport Numbers of Zinc Chloride from E.M.F. Measurements", Trans. Faraday Soc., 36 (1940), pp. 1139-1141.
40. H. N. Parton and J. W. Mitchell, "The Activity Coefficients and Transport Numbers of Zinc Bromide at 25° C from E.M.F. Measurements", Trans. Faraday Soc., 35 (1930), pp. 758-765.
41. R. H. Stokes and B. J. Levien, "Transference Numbers and Activity Coefficients in Zinc Iodide Solutions at 25° C", J. Amer. Chem. Soc., 68 (1946), pp. 1852-1854.
42. J. L. Dye, M. P. Faber, and D. J. Karl, "Transference Numbers and Conductances of Multivalent Salts in Aqueous Solution: Zinc Sulfate and Zinc Perchlorate", J. Amer. Chem. Soc., 82 (1960), pp. 314-318.

43. A. R. Despic and K. I. Popov, "The Effect of Pulsating Potential on the Morphology of Metal Deposits Obtained by Mass-Transport Controlled Electrodeposition", J. Applied Electrochemistry, 1 (1971), pp. 275-278.
44. J. R. Selman and C. W. Tobias, "Mass-Transfer Measurements by the Limiting-Current Technique", in Advances in Chemical Engineering, Vol. 10 (1978), pp. 211-318.
45. J. R. Selman and C. W. Tobias, "Unsteady-State Effects in Limiting Current Measurements", J. Electroanal. Chem., 65 (1975), pp. 67-85.
46. P. C. Andricacos and P. N. Ross, Jr., "Diffusion-Controlled Multisweep Cyclic Voltammetry - I. Reversible Deposition on a Rotating Disk Electrode", JES, 130 (1983), pp. 1340-1352.
47. D. Rajhenbah, J. Faltemier, and C. W. Tobias, "Mass Transfer Limiting Currents of Zinc Deposition in Acidic  $ZnCl_2$  and  $ZnSO_4$  Solutions", Lawrence Berkeley Laboratory, Report No. LBL-15338, January 1983.
48. J. T. Kim and J. Jorne, "The Kinetics and Mass Transfer of Zinc Electrode in Acidic Zinc-Chloride Solution", JES, 127 (1980), pp. 8-15.
49. D. Miller and J. Rard, "Transport in Aqueous Battery Systems", Lawrence Livermore National Laboratory, Contract Final Report, December 31, 1981.
50. J. Albright and D. Miller, "Mutual Diffusion Coefficients of Aqueous  $ZnSO_4$  at 25° C", J. Solution Chemistry, 4 (1975), pp. 809-816.

51. J. McBreen and E. Gannon, "Zinc Electrode Morphology in Acid Electrolytes" Annual Report on Subcontract P.O. #4516210, Lawrence Berkeley Laboratory, April 1983.
52. D. J. MacKinnon, J. M. Brannen, and R. C. Kerby, "The Effect of Lead on Zinc Deposit Structures Obtained from High Purity Synthetic and Industrial Acid Sulphate Electrolytes", J. Applied Electrochem., 9 (1979), pp. 55-70.
53. D. J. MacKinnon, J. M. Brannen, and R. C. Kerby, "The Effect of Cadmium on Zinc Deposit Structures Obtained from High Purity Industrial Acid Sulphate Electrolytes", J. Applied Electrochem., 9 (1979), pp. 71-79.
54. A. J. Gay and F. Bergsma, "The Influence of Nitrate Ion on the Morphology of Zinc Electrodeposits", Electrochimica Acta, 23 (1978), pp. 1067-1072.
55. B. K. Thomas and D. J. Fray, "The Effect of Additives on the Morphology of Zinc Electrodeposited from a Zinc Chloride Electrolyte at High Current Densities", J. Applied Electrochem., 11 (1981), pp. 677-683.
56. John Newman, Electrochemical Systems, Prentice-Hall, Englewood Cliffs, NJ (1973).
57. John Newman, "Engineering Design of Electrochemical Systems", Industrial and Engineering Chemistry, Vol. 60, No. 4, April 1968, pp. 12-27.
58. J. Newman, "Current Distribution on a Rotating Disk below the Limiting Current", JES, 113 (1966), pp. 1235-1241.

59. W. R. Parish and J. Newman, "Current Distributions on Plane, Parallel Electrodes in Channel Flow", JES, 117 (1970), pp. 43-48.
60. C. Wagner, "Contribution to the Theory of Cathodic Protection", JES, 99 (1952), pp. 1-12.
61. V. G. Levich, Physicochemical Hydrodynamics, Prentice-Hall, Englewood Cliffs, NJ (1962).
62. Yu. V. Pleskov and V. Yu. Filinovskii, The Rotating Disk Electrode, Consultants Bureau, New York (1976).
63. J. Newman, "Schmidt Number Correction for the Rotating Disk", J. Phys. Chem., 70 (1966), pp. 1327-1328.
64. W. H. Smyrl and J. Newman, "Limiting Current on a Rotating Disk with Radial Diffusion", JES, 118 (1971), pp. 1079-1081.
65. W. H. Smyrl and J. Newman, "Ring-Disk and Sectioned Disk Electrodes", JES, 119 (1972), pp. 212-219.
66. James McBreen and Elton J. Cairns, "The Zinc Electrode", in Advances in Electrochemistry and Electrochemical Engineering, Vol. 11, H. Gerischer and C. W. Tobias, eds., Interscience, New York (1977).
67. J. Jorne, J. T. Kim, and D. Kralik, "The Zinc-Chlorine Battery: Half-Cell Overpotential Measurements", J. Applied Electrochem., 9 (1979), pp. 573-579.
68. J. Jorne, "Flow Distribution in the Zinc-Chlorine Battery", JES, 129 (1982), pp. 2251-2253.

69. W. J. D. Escher and R. W. Foster, "An Assessment of the Status of Fuel Cell/Battery Vehicle Power Systems", Brookhaven National Laboratory, February 1980, Report No. BNL-51210.
70. R. A. Putt, "Development of Zinc-Bromine Batteries for Utility Energy Storage", Interim Report, Electric Power Research Institute, March 1981, Report No. EPRI EM-1717.
71. "Health and Environmental Effects Document for Batteries--1981: The Zinc/ Halogen Batteries", Argonne National Laboratory, November 1981, Report No. ANL/ES-119.
72. L. G. O'Connell, C. J. Anderson, E. Behrin, W. Cliff, R. Crisp, H. C. Forsberg, C. L. Hudson, J. S. Payne, R. Renner, M. D. Schrot, G. Strickland, M. Schwartz, and W. J. Walsh, "Energy Storage Systems for Automobile Propulsion: Final Report", Volume 1-5, Lawrence Livermore National Laboratory, December 15, 1980, Report No. UCRL-53053-80.
73. Ronald A. Putt, Alan J. Attia, Po-Yen Lu, and James H. Heyland, "Development of Zinc-Bromine Batteries for Utility Energy Storage", First Annual Report, US Department of Energy, May 1980, Report No. DOE/ET/29345-21.
74. Webster's Seventh New Collegiate Dictionary, G. & C. Merriam Co., Springfield, MA (1969).
75. E. B. Budevski, "Deposition and Dissolution of Metals and Alloys. Part A: Electrocrystallization", in Comprehensive Treatise on Electrochemistry, Vol. 7, B. E. Conway, et al., eds., Plenum Publishing Co., New York, to be published.

76. N. Ibl, "Some Theoretical Aspects of Pulse Electrolysis", Surface Technol., 10 (1980), pp. 81-104.
77. H. Y. Cheh, "Electrodeposition of Gold by Pulsed Current", JES, 118 (1971), pp. 551-557.
78. Eduard Preuss, Bernhard Krahl-Urban, and Rainer Butz, Laue Atlas, John Wiley & Sons, Inc., New York (1974).
79. L. Sillen, ed., Stability Constants of Metal Ion Complexes, The Chemical Society, London (1964).
80. Hermann Schlichting, Boundary-Layer Theory, McGraw-Hill Book Co., New York (1968).
81. G. A. Prentice, "Modeling of Changing Electrode Profiles", Ph. D. Thesis, University of California - Berkeley, Lawrence Berkeley Laboratory, Report No. LBL-11694, December, 1980.
82. Douglas A. Skoog and Donald M. West, Analytical Chemistry, Saunders College Publishing, Philadelphia (1980).
83. R. Byron Bird, Warren E. Stewart, and Edwin N. Lightfoot, Transport Phenomena, John Wiley & Sons, Inc., New York (1960).
84. N. A. Lange, ed., Handbook of Chemistry, 10th edition, McGraw-Hill Book Co., New York (1961).
85. International Critical Tables, 1st Edition, McGraw-Hill Book Co., New York (1929).
86. A. Agnew and R. Paterson, "Transport in Aqueous Solutions of Group IIB Metal Salts at 298.15 K (Part 6)", J. Chem. Soc. (Far. Trans. I), 74 (1978), pp. 2896-2906.



87. B. K. Thomas and D. J. Fray, "The Conductivity of Aqueous Zinc Chloride Solutions", J. Applied Electrochem., 12 (1982), pp. 1-5.
88. D. J. Robinson and T. J. O'Keefe, "On the Effects of Antimony and Glue on Zinc Electrocrystallization Behavior", J. Appl. Electrochem., 6 (1976), pp. 1-7.
89. D. J. MacKinnon and J. M. Brannen, "Zinc Deposit Structures obtained from High Purity Synthetic and Industrial Acid Sulphate Electrolytes with and without Antimony and Glue Additions", J. Appl. Electrochem., 7 (1977), pp. 451-459.
90. D. J. MacKinnon, J. M. Brannen, and V. I. Lakshmanan, "The Effects of Chloride Ions and Organic Extractants on Electrowon Zinc Deposits", J. Appl. Electrochem., 10 (1980), pp. 321-334.
91. T. Biegler and D. A. Swift, "Influence of Oxygen Reduction in the Electrowinning of Zinc", Hydrometallurgy, 6 (1981), pp. 299-309.
92. R. C. Kerby, H. E. Jackson, T. J. O'Keefe, and Yar-Ming Wang, "Evaluation of Organic Additives for Use in Zinc Electrowinning", Metallurgical Transactions B, 8B (1977), pp. 661-668.
93. F. A. Cotton and G. Wilkinson, Advanced Inorganic Chemistry, Interscience Publ., 3rd ed., New York (1972).
94. S. Fletcher, R. Deutscher, C. Harvey, R. Woods, E. J. Frazer, T. Lwin, G. Nelson, and D. Gates, "Zinc Battery Electrodes", Mineral Chemistry Communication, CSIRO Institute of Earth Resources (Australia), Report No. MCC-354, November 1981.

95. R. Lacmann and H.-J. Randig, "Electrolytic Nucleation of Copper and Brass on Platinum Single Crystal Spheres", J. Crystal Growth, 17 (1972), pp. 97-100.

ACKNOWLEDGMENTS

I wish to express the deepest appreciation and heartfelt thanks to everyone who has ever helped me to reach this milestone in my life. Many wonderful people have crossed my path, given me a full education, unknowingly challenged and swayed my thinking, and enriched my life. I have learned so much from all of you, and I thank you for being a part of my life. Ralph Waldo Emerson once wrote just what it means to succeed in one's life.

"To laugh often and much; to win the respect of intelligent people and the affection of children; to earn the appreciation of honest critics and endure the betrayal of false friends; to appreciate beauty; to find the best in others; to leave the world a bit better whether by a healthy child, a garden patch, or a redeemed social condition; to know even one life has breathed easier because you have lived. This is to have succeeded."

My parents, who never imagined that a son could wander for so many years in school, never lost faith and have always expressed their true love in many ways. I am blessed to have such a wonderful mother and late father, and such a close-knit and caring large tribe of brothers, sisters, and their families.

I give a most sincere thanks to Professor Charles W. Tobias; he has taught me so much about electrochemistry, science, philosophy, and life. His guiding efforts have helped to mold me into a competent engineer and scientist. I wish to also acknowledge Dr. Rolf Muller, a most able and intelligent scientist, who always took the time to solve any daily problems. I am indebted to my coworkers, Dr. Milan Jaksic, Tetsuaki Tsuda, Vladimir Kommenic, and Darko Rajhenbah, for their helpful assistance and ideas in this work and for always providing a stimulating environment in

the laboratory. My research group, with its constantly changing actors over the years, deserves a lot of gratitude for its infinite supply of ideas, unending patience, constructive criticisms, true friendships, and last but not least, excellent parties.

I am most fortunate to have met and to be able to share my life with Sharon Kong. She has made these years at Berkeley the best possible in my life. I thank her for all the good times, for her patient love, for her honest criticisms and listening abilities, for teaching me to backpack in the Sierra, and for just being herself.

I wish to thank Professor Elton Cairns and Professor James Evans for their comments and criticism, and for reading this manuscript. Many thanks to the Photo Lab staff for their professionalism and personal attention, and the TID staff for transcribing and printing this work. I wish to personally thank the following people for their special efforts and friendships: Don Bogard, Gay Brazil, J. Ronald Cain, Joe Farmer, Larry Galovich, Walter Giba, Sidney Harvey, Lee Johnson, Marianne Larsen, Herb Riebe, and Felix Schwager.

This work was supported by the Assistant Secretary for Conservation and Renewable Energy, Office of Energy Systems Research, Energy Storage Division of the U. S. Department of Energy under Contract No. DE-AC03-76SF00098.

APPENDIX A Remarks on the Background of this Investigation

A long-standing interest in this laboratory in problems related to the interaction of hydrodynamic flow and the morphological features of metals in electrodeposition formed a natural background for undertaking investigations on the electrodeposition of zinc. To a much larger degree than copper, which was the sole vehicle of earlier investigations [6,11,12,13,33] since the 1950's, zinc deposition in the absence of inhibitors presents a special problem because of the very strong tendency for the formation of protruding growths, so-called dendrites. It is very unlikely that rechargeable batteries involving zinc negatives can be successfully cycled in the presence of organic additives. The strong promise of  $Zn/Cl_2$  and  $Zn/Br_2$  rechargeable flow battery systems requires the development of understanding, and based on it, control, of the morphological features of zinc deposits. Research on electrocrystallization, including hydrodynamic effects in zinc deposition, has been continuously funded in this laboratory by the Department of Energy since 1976. Other projects under this sponsorship in the electrocrystallization area include studies on the macromorphology of copper in electrodeposition (Kindler [13]) and the modelling of advancing or receding profiles in electrodeposition under tertiary current distribution conditions (Prentice [81]).

The general aim of the zinc project in this laboratory is to understand, explain, and ultimately to control the curious phenomena responsible for imprints of hydrodynamic flow in zinc deposits, particularly in acid solutions. In other words, the purpose was to establish the mechanism for the genesis and propagation of surface textures in zinc

deposition, in the presence of hydrodynamic flow. The tools of this investigation included macro- and SEM photography, obtained under galvanostatic or potentiostatic control. Various substrates, concentrations, pH's, and impurity levels are used to detect their possible roles.

Dr. Milan Jaksic, a visiting scientist from Yugoslavia and a co-worker of Professor Tobias, initiated the original experimental work on this zinc project in 1976. Dr. Jaksic returned to Yugoslavia 6 months after I joined this project in October of 1978. I collaborated with Dr. Jaksic on some experiments performed in the Small Cell and in the RDE system during his last 4 months here. I also took data in these cells after he left until 2 new cells (Large Cell and In situ Cell) and new RDE electrodes were built according to my new specifications. In 1979, Vladimir Kommenic, a Yugoslavian IREX (International Research Exchange) scholar, and Tetsuaki Tsuda, a M. S. graduate student, both became associated with portions of this project. Mr. Tsuda investigated the development of macromorphology of zinc electrodeposits on rotating disk electrodes. He noted a strong dependence of crystallite formation (nucleation) frequency on current density, and found only relatively minor influence of small concentrations of lead ions in solution on the overall appearance and structure of striations (spirals). Tsuda's research was reported in a Lawrence Berkeley Laboratory report no. LBL-13057 [10]. During Mr. Kommenic's year-long residence, the morphology of zinc in sulfate solutions and the morphology of zinc under different pulsed and current step techniques was investigated. No independent report was filed on this work. Another Yugoslavian IREX scholar, Darko

Rajhenbah, joined this research effort in 1981 for a 10 month study. We collaborated on zinc limiting current studies on the rotating disk electrode system. This research, entitled "Mass Transfer Limiting Currents of Zinc Deposition in Acidic  $ZnCl_2$  and  $ZnSO_4$  Solutions", is reported in Lawrence Berkeley Laboratory report no. LBL-15338 [47]. The "In situ Cell" was machined by me and set up by Tsuda before he left in 1981; experiments were performed by me in this cell in 1982.

A comprehensive listing of experimental data and available photographic evidence produced by Dr. Milan Jaksic, James Faltemier, Tetsuaki Tsuda, Vladimir Kommenic, Darko Rajhenbah, or by collaboration of these investigators is reported in a Lawrence Berkeley Laboratory Report LBL-16601 [14]. The photograph negatives listed in this report are stored in and available from the Photographic Lab of the Lawrence Berkeley Laboratory, University of California, Berkeley, CA 94720.

The motion picture which is associated with this dissertation is available for loan from Professor Tobias or myself.

APPENDIX B Detailed Description of Experimental Systems

B.1 "Rotating Disk Electrode" System

Rotator	Disk Rotator Designed and Constructed at LBL Servo-Tek Products variable speed motor and controller  or  Analytical Rotator Pines Instruments Grove City, PA Model ASR2
Cell	Shortened 1 Liter Borosilicate Beaker Blown by LBL Glass Shop
Power	Elektronischer Potentiostat nach Wenking G. Bank Elektronik Co. West Germany  or  Potentiostat-Galvanostat Princeton Applied Research Princeton, NJ Model 371 with Model 178 Electrometer probe
Ammeter	Digital Multimeter Keithley Model 179 TRMS



XY Recorder      Hewlett-Packard XY Recorder  
Model 7001A

or

Gould XY Recorder  
Model 7056

Programmer      Universal Programmer  
Princeton Applied Research  
Princeton, NJ  
Model 175

B.2 "Small Cell" System

Pump              Little Giant Pump Company  
Oklahoma City, OK  
Model # 1-MD  
Polyethylene housing and impeller  
Magnetic drive pump

Flowmeter      Rotameter  
Gilmont Instruments, Inc.  
159 Great Neck Road  
Great Neck, NY 11021  
Model # F1500  
Special machining by L. Galovich

Tubing           3/8" polyethylene.  
LBL stock item

Unions           Teflon (3/8" Swagelock X 1/2" NP)

Machined by J. L. Faltemier

Valve

Nupro 3/8" Teflon

Oakland Valve & Supply Co.

2487 Estand Way

Pleasant Hill, CA 94523

Cell

Acrylic plastic

Outside Dimensions 5.7 cm x 5.4 cm x 62.2 cm

Flow Area Dimensions 0.5 cm x 0.5 cm with 1/2" NP  
threading at each end

Cathode Dimensions 0.5 cm x 0.95 cm

Anode Dimensions rectangular 0.5 cm x 0.95 cm  
circular 0.9 cm diameter

Size of Electrode Cavity 1.6 cm diameter

Brass Electrode Fasteners 5 cm x 5 cm x 0.65 cm

Machined by L. Galovich

Power

Constant Current Power Supply

Electronic Measurements

Eatontown, NJ

Model C618

Ammeter

Digital Multimeter

Keithley

Model 179TRMS

### B.3 "Large Cell" System

Pump

Gorman-Rupp Industries

Bellville, OH 44813

Model # 14110  
Magnetic drive pump, polypropylene housing,  
Ryton coated impeller and magnet

Flowmeter      Magnetic Flowmeter  
Controlotron Corporation  
111 Bell Street,  
West Babylon, L.I., NY 11704  
Model 241 Display Computer  
Model 240 Transducers

Pipe            Polypropylene Schedule 40 and Schedule 125  
LBL stock item

Tubing         Neoprene rubber hose  
LBL stock item

Valves,Fittings Polypropylene, 3/4" NP  
Sunnyvale Piping Supply Co.  
729 E. Evelyn Avenue  
Sunnyvale, CA 94086

Reservoir      Polyethylene 5 Gallon Container  
LBL stock item  
Special machining by H. Riebe and J. L. Faltemier

Cell            Polypropylene and Acrylic plastic parts (Figure 3.6)  
Outside Dimensions of Assembled Cell  
20.3 cm x 12.7 cm thick x 121.7 cm  
Flow Area Dimensions 0.5 cm x 3 cm  
Cathode Dimensions 3.0 cm x 30 cm

Anode Dimensions 3.0 cm x 30 cm

Polypropylene Electrode Holder Dimensions (approx.)

7.5 cm x 3.7 cm thick x 111.7 cm

Acrylic Plastic Covering Outside Dimensions

20.3 cm x 3.8 cm thick x 121.7 cm

with 3/8 inch Neoprene Rubber Hose

Aluminum Clamps

machined by LBL machinists in Bldg. 25, H. Riebe,

and J. L. Faltemier

Power Constant Current Power Supply

Sorenson Power Supply Co.

Model SRL 10-50

Ammeter Digital Multimeter

Keithley

Model 179TRMS

#### B.4 "In situ Cell" System

Pump Gorman-Rupp Industries

Bellville, OH 44813

Model # 14110

Magnetic drive pump, polypropylene housing,

Ryton coated impeller and magnet

Flowmeter Rotameter

Gilmont Instruments, Inc.

159 Great Neck Road

Great Neck, NY 11021

Model #1760A

Pipe 1/2" polypropylene  
LBL stock item

Tubing 5/8" Flexible Tygon  
LBL stock item

Valves,Fittings 1/2" Polypropylene  
Sunnyvale Piping Supply Co.  
729 E. Evelyn Avenue  
Sunnyvale, CA 94086

Reservoir Polyethylene 1 Gallon Container  
LBL stock item

Cell Polypropylene with Acrylic Plastic Covering and  
Aluminum Bracket  
Outside Dimensions 4.7 cm x 7.6 cm x 39.7 cm  
Flow Area Dimensions 0.6 cm x 1.0 cm with 1/2" NP  
threading at each end  
Cathode Dimensions 0.5 cm x 1.0 cm  
Anode Dimensions (2)-0.4 cm x 0.9 cm each  
1/8" Acrylic plastic covering  
1/4" Aluminum bracket  
machined by H. Riebe and J. L. Faltemier

Power Constant Current Power Supply  
Electronic Measurements  
Eatontown, NJ  
Model C618

Ammeter	Digital Multimeter Keithley Model 179 TRMS
Camera	Paillard-Bolex 16 mm Reflex Camera Switzerland Model H16 Rex
Camera	Control Samenco Movie Control Sample Engineering Co. Danville, IL Model MC-5E50
Illumination	Fiber-Lite High Intensity Fiber Optic Illuminator Dolan-Jenner Industries, Inc. Woburn, MA Model 180

APPENDIX C Chemical Analysis of Solutions

A chemical analysis was conducted on several solutions for this research project, and the results are shown in Table C.1. Some of the solutions that were tested were used in Tetsuaki Tsuda's thesis [10], and some in the present work. The analyses were completed by Tom Morrison in the Chemical Analysis Services Laboratory, College of Chemistry, University of California on a Perkin-Elmer Atomic Absorption Spectrometer Model 360. He completed the Atomic Absorption spectra utilizing both flame and nonflame atomizers in the spectrophotometer. The nonflame atomizer, a graphite furnace, offers unusually high sensitivity and poorer relative precision compared to the acetylene flame atomizer [82].

Seven solution samples were analyzed for various cationic impurities; six of the samples were 1 M  $\text{ZnCl}_2$  solutions, and the other a sample of the distilled water supply. Solution samples #1 and #6 were from different containers of "Analytical Reagent" grade  $\text{ZnCl}_2$ . Sample #2, #3, #4, and #5 were all used as part of Tsuda's project. Spectra using the graphite furnace atomizer were generated twice for the largest impurities (Pb, Fe, Mn, Ni, Cd) in some of the solution samples. The units are micrograms per cubic centimeter ( $\mu\text{g}/\text{cc}$ ), which is approximately equivalent to parts per million (ppm). The "limit of detection" is approximately the smallest concentration detectable by either the flame or the graphite furnace method used in that test.

Table C.1

Chemical Analysis of Solutions

TEST		SOLUTIONS							Limit of Detection
		(1)	(2)	(3)	(4)	(5)	(6)	(7)	
		(µg/cc)							
Pb	gr fur	0.03	6.3	0.04	-	-	0.06	-	0.001
	gr fur	0.02	17.0	0.06	0.004	0.003	UND	-	0.001
	flame	0.70	8.6	0.8	UND	UND	-	UND	0.4
Fe	gr fur	-	0.16	0.088	-	-	-	-	0.001
	gr fur	UND	0.02	0.16	0.002	0.005	UND	-	0.001
	flame	UND	0.06	UND	UND	UND	-	UND	0.04
Mn	gr fur	0.03	0.01	0.008	0.036	0.72	0.040	-	0.001
	gr fur	0.019	0.008	0.007	0.023	0.021	0.023	-	0.001
	flame	0.07	0.05	0.04	0.10	0.08	-	UND	0.04
Ni	gr fur	0.005	-	-	-	-	0.014	-	0.005
	gr fur	0.006	0.047	0.028	0.038	0.008	0.015	-	0.005
	flame	UND	0.08	0.07	0.05	UND	-	UND	0.04
Cd	gr fur	0.26	0.012	0.006	0.002	0.003	0.002	-	0.0004
	gr fur	0.70	0.008	0.005	0.002	0.003	0.002	-	0.0004
	flame	0.47	0.10	0.05	0.05	0.04	-	UND	0.04
Sb	flame	UND	UND	UND	UND	UND	UND	UND	0.4
Co	flame	UND	UND	UND	UND	0.06	UND	UND	0.04
Mo	flame	UND	UND	UND	UND	UND	UND	UND	0.4

gr fur = graphite furnace method

flame = flame method

UND = Undetected

- = no test conducted



SOLUTION SAMPLES

- (1) = 1 M  $\text{ZnCl}_2$  "Analytical Reagent" solution
- (2) = 1 M  $\text{ZnCl}_2$  "Analytical Reagent" solution with 10 mg/l Pb added
- (3) = 1 M  $\text{ZnCl}_2$  "Analytical Reagent" solution with 1 mg/l Pb added
- (4) = 1 M  $\text{ZnCl}_2$  "Analytical Reagent" solution, zinc-dust treated
- (5) = 1 M  $\text{ZnCl}_2$  "ultrapure" solution
- (6) = 1 M  $\text{ZnCl}_2$  "Analytical Reagent" solution
- (7) = distilled water

APPENDIX D Motion Pictures in In situ Cell

Time-lapse motion picture photography was used in the final portion of this research to gain further insight into and understanding of the electrodeposition process and to observe in accelerated time the events occurring on the surface. The movie camera was directed at the cathode surface through the acrylic cell covering in the In situ Cell; two fiberoptic light pipes, which were positioned above and below the camera lens, illuminated the cathode. An automatic timing device controlled the camera shutter at the specified intervals.

The experiments were photographed at 1 frame per second up to 10 minutes, and then for 1 frame per 4 seconds for the remaining experimental time. A block of approximately 5 dark frames was used to separate these two different filming rates. The fluid flow direction in the film is from right to left, and the front edge of the cathode is always perpendicular to the flow direction. Different surface magnifications were possible by simply changing the extension tube size between the movie camera and lens (Fig. 3.14). The two magnifications that were finally used gave frame sizes of 0.4 cm x 0.57 cm and 0.57 cm x 0.8 cm. The total deposit at the end of each experiment was the same, 54 Coulombs ( $108 \text{ C/cm}^2$ ), which corresponds to an average deposit thickness of 51 m. Appendix F lists the experimental conditions used in the In situ Cell.

As a component of this dissertation, a 270 foot motion picture has been prepared. This reel of film is composed of film segments photographed under various experimental conditions. Later, these filmclips were edited and spliced together with appropriate labels. The film shows deposition from 1 M  $\text{ZnCl}_2$  solution with pH 4.6 and 1.9 at

different flowrates (Re 9000, 3200, 1600) and different current densities (30 mA/cm<sup>2</sup>, 100 mA/cm<sup>2</sup>). The order in which these experimental observations are presented in the film and the projection time length of each segment are shown in Table D.1.

Table D.1

<u>Experimental Conditions and Projection Times of Segments in Film</u>				
<u>Experimental Conditions</u>			<u>Projection Times</u>	
pH	Re	Current (mA/cm <sup>2</sup> )	Max. Time (minutes)	(seconds)(at 24 frames/s)
4.6	9000	30	30	36
4.6	9000	100	9	23
4.6	3200	30	30	36
4.6	3200	100	9	23
4.6	1600	30	30	36
4.6	1600	100	9	23
1.9	9000	30	30	36
1.9	9000	100	9	23
1.9	3200	100	9	23
1.9	1600	30	30	36
1.9	1600	100	9	23

APPENDIX E Reynolds Number Calculations

The Reynolds number formulas for the channel flow cells and for the rotating disk electrode system are explained, and sample calculations are presented in this appendix. The Reynolds number for a rectangular channel has been calculated using the formula from Bird, Stewart, and Lightfoot [83], which states that the hydraulic diameter is four times the hydraulic radius, and that the hydraulic radius is the cross-sectional area of flow divided by the wetted perimeter. The experimental solution data for the examples in this appendix has been taken from Lange's Handbook of Chemistry [84]. The Reynolds number formula for the channel flow is

$$Re = \rho \times V \times D / \mu$$

where

$\rho$  = fluid density, gm/cc

V = fluid velocity, cm/s

D = hydraulic diameter, cm

$\mu$  = fluid viscosity, poise

Example

Small Channel Cell, 1 M ZnCl<sub>2</sub> at 25° C

Flow Area Dimensions      0.5 cm x 0.5 cm

Hydraulic Diameter      0.5 cm

Fluid Density      1.11 gm/cc

Fluid Viscosity      1.063 cP

Fluid Velocity      50 cm/s

Reynolds number                      2610

The Reynolds number formula for the rotating disk system [56] is

$$Re = r^2 \times \Omega \times \rho / \mu$$

where

$r$  = disk radius, cm

$\rho$  = fluid density, gm/cc

$\Omega$  = rotation speed, rad/s

$\mu$  = fluid viscosity, poise

Example

Rotating Disk Electrode system, 1 M  $ZnCl_2$  at 25° C

Disk Electrode Radius	0.5 cm
Rotation Speed	400 rpm
Fluid Density	1.11 gm/cc
Fluid Viscosity	1.063 cP
Reynolds number	1090

## APPENDIX F Experimental Conditions

Galvanostatic experiments were performed in various zinc solutions on the RDE system. Potentiostatic experiments were also conducted in supported zinc solutions on the RDE system in order to determine zinc mass transfer limiting currents. All the experimental conditions employed in the RDE system are listed in Table F.1.

Experiments in the Small Cell were performed under various flowrates, current densities, electrolytes, times, pH's, and substrates, as shown in Table F.2. A few experiments in copper sulfate solution were also conducted in the Small Cell.

Table F.3 shows the experimental conditions employed in studies in the Large Cell. A 1 M  $\text{ZnCl}_2$  solution of pH 4.6 was used for all the experiments.

The process conditions that were varied and their effects studied in the In situ Cell were flowrate, current density, substrate, and pH. All of the experiments were conducted in 1 M  $\text{ZnCl}_2$  solution. Table F.4 lists these conditions in the In situ Cell.

The experimental data are presented in Appendix H; a more detailed list of experimental data of several researchers in this laboratory, with LBL photograph numbers, is reported in LBL Report LBL-16601 [14]. The experiments on the RDE system and in the Small Cell that were completed in collaboration with Dr. Milan Jaksic are specially marked in this report.

Table F.1

Experimental Conditions in RDE System

Galvanostatic Experiments

Solutions	0.5 M, 1 M ZnCl <sub>2</sub> , 1 M ZnSO <sub>4</sub>
pH	2.0 - 5.0
C.d.	1 - 120 mA/cm <sup>2</sup> , pulsed 10-120 mA/cm <sup>2</sup>
Re	240 < 8100
Substrates	Pt, Zn, C
Time	variable, < 8 hours
Coul/cm <sup>2</sup>	variable
Temperature	25° C

Potentiostatic Experiments (Limiting Current Experiments)

Solutions	0.01 M - 0.5 M ZnCl <sub>2</sub> + 1 M KCl 0.01 M - 0.5 M ZnSO <sub>4</sub> + 1 M Na <sub>2</sub> SO <sub>4</sub>
pH	2.4-2.5
Rotation	200, 400, 800, 1200, 1600, 2000 rpm
Substrate	Zn
Scan rates	10, 100, 200 mV/s
Temperature	25° C

Table F.2

Experimental Conditions in Small Cell

Solutions	1 M ZnCl <sub>2</sub> , 1 M ZnSO <sub>4</sub> , 1 M ZnBr <sub>2</sub>
pH	2.0 - 5.0
C.d.	1 - 100 mA/cm <sup>2</sup>
Re	< 5300
Substrates	Pt, Cu, C, Zn, Zn(0001)
Times	variable, 8 hours maximum
Coul/cm <sup>2</sup>	variable,
Temperature	25° C

Table F.3

Experimental Conditions in Large Cell

Solution	1 M ZnCl <sub>2</sub>
pH	4.6
C.d.	10, 20, 30, 100 mA/cm <sup>2</sup>
Re	1600, 2300
Substrate	Pt, Zn
Time	variable, < 90 minutes
Coul/cm <sup>2</sup>	variable, 180 C/cm <sup>2</sup> maximum
Temperature	25° C

Table F.4

Experimental Conditions in In situ Cell

Solution	1 M ZnCl <sub>2</sub>
pH	1.9, 4.6
C.d.	10, 20, 30, 100 mA/cm <sup>2</sup>
Re	1600, 3200, 9000
Substrate	Pt, Zn, C, Cu
Time	variable, < 4 hours
Coul/cm <sup>2</sup>	variable, 108 C/cm <sup>2</sup> in filmclips
Temperature	25° C



APPENDIX G Physical Data on Zinc Electrolytes

The various physical and chemical data for the solutions used in this research have come from numerous literature sources. The density and viscosity data for the zinc salt solutions have been taken from the International Critical Tables [85] and Lange's Handbook of Chemistry [84] and are summarized in Table G.1. Transference number data are from Harris and Parton [39] and Purser and Stokes [37], and are listed in Table G.2. Rajhenbah, et. al. [47] and Landau, et. al. [29] report zinc diffusion coefficient data.

Table G.1

Density and Viscosity Data

Density (g/cc)		
ZnCl <sub>2</sub>	[85], 25° C	[84], 20° C
0.149 M	1.0154	1.0167
0.303 M	1.0335	1.0350
0.463 M	1.0515	1.0532
0.628 M	1.0696	1.0715
0.794 M	1.0878	1.0819
0.974 M	1.1063	1.1085
1.156 M	1.1251	1.1275
ZnSO <sub>4</sub>	[85], 25° C	[84], 20° C
0.122 M	1.0178	1.0190
0.239 M	1.0389	1.0403
0.350 M	1.0605	1.0620
0.458 M	1.0825	1.0842
0.560 M	1.1054	1.1071
0.840 M	1.1786	1.1806
1.004 M	1.2343	--

Viscosity (cP)

ZnCl <sub>2</sub>	[84], 25° C
0.125 M	0.9150
0.250 M	0.9407
0.500 M	0.9794
1.000 M	1.0626
ZnSO <sub>4</sub>	[84], 25° C
0.125 M	0.9257
0.250 M	0.9673
0.500 M	1.0480
1.000 M	1.2218

Table G.2

Cation Transference Number Data

Concentration (M)	ZnCl <sub>2</sub> [39], 25° C	ZnSO <sub>4</sub> [37], 25° C
0.10	- -	0.384
0.25	- -	0.331
0.50	0.331	0.294
0.70	0.249	- -
0.90	0.194	- -
1.00	0.171	0.255
1.5	- -	0.226
2.0	0.000	0.197
3.0	- 0.137	- -
4.0	- 0.256	- -
5.0	- 0.364	- -

Landau, et. al. [29] have assembled physical, transport, and kinetic properties of zinc halide solutions from various literature sources back to 1920 and correlated most of this data into polynomial expressions. The authors have also measured effective ionic diffusivities of zinc in KCl-supported solutions of ZnCl<sub>2</sub> and ZnBr<sub>2</sub>. Agnew and Patterson [86] have also correlated electrical conductivity,

diffusivity, and transference numbers of  $\text{ZnCl}_2$  solutions at  $25^\circ \text{C}$ . Thomas and Fray [87] report measurements of electrical conductivity of  $\text{ZnCl}_2$  solutions at  $25^\circ \text{C}$ .

APPENDIX H Experimental Data

This appendix lists the experiments, experimental conditions, and photograph numbers of those experiments completed by J. L. Faltemier, or J. L. Faltemier and V. Kommenic. The experiments, conducted in collaboration with Dr. M. Jaksic or with D. Rajhenbah, are listed in LBL Report LBL-16601 [14].

### H.1 Rotating Disk Electrode Experiments

photo#	soln	pH	rpm	c.d.	time	cath	spec
XBB 838-7360	1	2.0	400	30	10	Pt	
XBB 838-7361	1	2.0	800	30	30	Pt	
XBB 838-7362	1	2.0	800	30	5	Pt	
XBB 838-7363	1	2.0	800	30	10	Pt	
XBB 838-7364	1	2.0	1600	30	15	Pt	
XBB 838-7365	1	2.0	400	30	0.5	Zn	
XBB 838-7366	1	2.0	400	30	1.5*	Zn	
XBB 838-7367	1	2.0	400	30	2.5*	Zn	
XBB 838-7368	1	2.0	400	30	3.5*	Zn	
XBB 838-7369	1	2.0	400	30	0.5	Zn	
XBB 838-7370	1	2.0	400	30	1.5*	Zn	
XBB 838-7371	1	2.0	400	30	7*	Zn	
XBB 838-7372	1	2.4	800	30	5	Pt	
(also, see XBB 831-377)							
XBB 838-7373	1	2.4	800	30	10*	Pt	
(also, see XBB 831-377)							
XBB 838-7374	1	2.4	800	30	15*	Pt	
(also, see XBB 831-377)							
XBB 838-7375	1	2.4	400	30	10	Pt	
XBB 838-7376	1	2.4	400	30	20	Pt	
XBB 838-7377	1	2.4	400	30	30	Pt	
XBB 838-7378	1	2.4	400	30	60	Pt	
XBB 838-7379	1	2.4	600	30	20	Pt	
XBB 838-7380	1	2.4	600	30	30	Pt	
XBB 838-7381	1	2.4	600	30	45	Pt	
XBB 838-7382	1	2.4	600	30	60	Pt	
XBB 838-7383	2	4.6	400	5	10	Pt	
XBB 838-7384	2	4.6	1600	5	8.5	Pt	
XBB 838-7385	2	4.6	400	5	20	Pt	

XBB 838-7386	2	4.6	400	5	41	Pt	
XBB 838-7387	2	4.6	1600	5	20	Pt	
XBB 838-7388	2	4.6	400	5	40	Pt	
XBB 838-7389	2	4.6	1600	5	20	Pt	
XBB 838-7390	2	4.6	400	20	66	Pt	
XBB 838-7391	2	4.6	720	20	20	Pt	
XBB 838-7392	2	4.6	1600	20	20	Pt	
XBB 838-7393	2	4.6	400	50	20	Pt	
XBB 838-7394	2	4.6	1600	50	20	Pt	
XBB 838-7395	2	4.6	400	5	20	Pt	
XBB 838-7396	2	4.6	400	5	20	Pt	
XBB 838-7397	2	4.6	400	2	46	Pt	
XBB 838-7398	2	4.6	1600	2	50	Pt	
XBB 838-7399	2	4.6	400	2	50	Pt	
(also, see XBB 831-376)							
XBB 838-7400	2	4.6	400	2	90*	Pt	
(also, see XBB 831-376)							
XBB 838-7401	2	4.6	400	2	120*	Pt	
(also, see XBB 831-376)							
XBB 838-7402	2	4.6	400	5	40	Pt	
XBB 838-7403	2	4.6	400	5	10	Pt	
XBB 838-7404	2	4.6	1600	5	10	Pt	
XBB 838-7405	2	4.6	400	5	20	Pt	
(also, see XBB 808-9258)							
XBB 838-7406	2	4.6	400	5	8.5	Pt	
(also, see XBB 808-9260)							
XBB 838-7407	2	4.6	1600	5	8.5	Pt	
(also, see XBB 808-9260)							
XBB 838-7408	2	4.6	400	2	20	Pt	
XBB 838-7409	2	4.6	400	2	40	Pt	
XBB 838-7410	2	4.6	1600	5	10	Pt	200X
XBB 838-7411	2	4.6	400	5	10	Pt	200X
XBB 838-7412	2	4.6	0	5	10	Pt	200X

XBB 838-7413 (also, see XBB 831-371)	2	4.6	400	5	25	Pt	400X
XBB 838-7414 (also, see XBB 831-371)	2	4.6	400	5	25	Pt	400X
<hr/>							
Pulsed Deposition							
XBB 838-7415	1	4.6	400	30 avg	10	Pt	120 mA/cm <sup>2</sup> - 1 sec, 20 mA/cm <sup>2</sup> - 9 sec
XBB 838-7416	1	4.6	400	30 avg	30	Pt	120-1,20-9
XBB 835-4531	1	4.6	400	30 avg	60	Pt	120-1,20-9
XBB 838-7417	2	4.6	1600	5 avg	20	Pt	25-1,3-10
XBB 838-7418	2	4.6	400	5 avg	20	Pt	25-1,3-10
XBB 838-7419	2	4.6	1600	5 avg	30	Pt	25-1,3-10
<hr/>							
XBB 838-7420	2	2.5	400	5	10	Pt	
XBB 838-7421	2	2.5	1600	5	15	Pt	
XBB 838-7422	2	2.5	1600	5	20	Pt	
XBB 838-7423	1	4.6	800	30	10	Pt	
XBB 838-7424	1	4.6	800	100	10	Pt	
XBB 838-7425	1	4.6	800	100	90	Pt	
XBB 838-7426	1	4.6	800	20	1	Pt	250X
XBB 838-7427	1	4.6	800	20	1	Pt	300X
XBB 838-7428 (also, see XBB 831-372)	1	4.6	800	10	9	Pt	
XBB 838-7429 (also, see XBB 831-372)	1	4.6	80	10	9	Pt	
<hr/>							
XBB 838-7455	1	2.2	1600	18	28	Pt	
XBB 838-7456	1	2.2	1600	18	5	Pt	
XBB 838-7457	1	2.2	1600	18	2	Pt	
XBB 838-7458	1	2.2	1600	18	10	Pt	
XBB 838-7459	1	2.2	1600	18	75	Pt	

XBB 838-7460	1	2.2	200	18	10	Pt
XBB 838-7461	1	2.2	200	18	2	Pt
XBB 838-7462	1	2.2	200	18	30	Pt
XBB 838-7463	1	2.2	200	18	10	Pt
XBB 838-7464	1	2.2	200	18	30	Pt
XBB 838-7465	2	4.6	1600	18	2	Pt
XBB 838-7466	2	4.6	200	18	21	Pt
XBB 838-7467	2	4.6	200	18	30	Pt
XBB 838-7468	2	5.0	200	30	72 sec	Pt
XBB 838-7469	2	5.0	200	30	6	Pt
XBB 838-7470	2	5.0	200	30	18	Pt
XBB 838-7471	2	5.0	1600	30	18	Pt
XBB 838-7472	2	5.0	1600	30	6	Pt
XBB 838-7473	2	5.0	1600	30	72 sec	Pt
XBB 838-7474	2	5.0	200	10	3.5	Pt
XBB 838-7475	2	5.0	200	10	18	Pt
XBB 838-7476	2	5.0	200	10	18	Pt
XBB 838-7477	2	5.0	200	10	54	Pt
XBB 838-7478	2	5.0	200	10	18	Pt
XBB 838-7479	2	5.0	1600	10	3.5	Pt
XBB 838-7480	2	5.0	1600	10	54	Pt
XBB 838-7481	2	5.0	200	5	7.25	Pt
XBB 838-7482	2	5.0	200	5	36	Pt
XBB 838-7483	2	5.0	200	5	108	Pt
XBB 838-7484	2	5.0	1600	5	36	Pt
XBB 838-7485	2	5.0	1600	5	7.25	Pt
XBB 838-7486	2	5.0	1600	5	108	Pt

---



photo# = LBL Photograph number  
soln = solution (1=1 M ZnCl<sub>2</sub>, 2=1 M ZnSO<sub>4</sub>)  
c.d. = current density (mA/cm<sup>2</sup>)  
time = total deposition time (minutes, unless stated otherwise)  
\* = continuation from experiment above  
cath = cathode

H.2 Small Cell Experiments

photo#	soln	pH	flow	c.d.	time	subs
XBB 838-7338	1	4.8	90	30	15	Pt
XBB 838-7339	1	4.8	90	30	15	Pt
XBB 838-7340	1	4.8	90	30	1	Pt
XBB 838-7341	1	4.8	90	30	2	Pt
XBB 838-7342	1	4.8	90	30	5*	Pt
XBB 838-7343	1	1.9	90	30	10	Pt
XBB 838-7344	1	1.9	90	30	5	Pt
XBB 838-7345	1	1.9	50	30	10	Pt
XBB 838-7346	1	1.9	50	30	5	Pt
XBB 838-7347	1	1.9	20	30	10	Pt
XBB 838-7348	zinc anode after Experiment (XBB 838-7347)					
XBB 838-349	1	1.9	20	30	5	Pt
XBB 838-7350	1	2.2	70	20	18	Zn
XBB 838-7351	1	2.2	70	100	1	Zn
XBB 838-7352	1	2.2	70	2	50	Zn

3-Dimensional (Stereo Pair) Photos

	1	2.1	85	30	120	Pt
XBB 837-6184	100X - Left					
XBB 837-6187	100X - Right					
XBB 837-6185	500X - Left (also, see XBB-837-6188A)					
XBB 837-6188	500X - Right (also, see XBB-837-6188A)					
XBB 837-6186	2000X - Left					
XBB 837-6189	2000X - Right					
XBB 837-6195	1000X - Left (also, see XBB-837-6190A)					
XBB 837-6190	1000X - Right (also, see XBB-837-6190A)					
XBB 837-6193	2000X - Left					
XBB 837-6191	2000X - Right					
XBB 837-6194	5000X - Left					
XBB 837-6192	5000X - Right					

XBB 838-7353	1	2.1	90	30	45	Zn-SC
XBB 838-7160	1	2.1	90	30	30	Zn-SC
XBB 838-7354	1	2.1	50	30	45	Zn-SC
XBB 838-7355	1	2.1	50	30	60	Zn-SC
XBB 838-7356	1	2.1	80	100	20	Zn-SC
XBB 838-7357	1	2.1	80	20	5	Zn-SC
XBB 838-7358	1	2.1	80	100	5	Zn-SC
XBB 838-7359	1	2.1	70	40	40	Zn-SC

photo# = LBL Photograph number

soln = solution (1=1 M  $\text{ZnCl}_2$ , 2=1 M  $\text{ZnSO}_4$ )

flow = Rotameter setting

    flow 90 = 1550 ml/min

    flow 80 = 1400 ml/min

    flow 75 = 1300 ml/min

    flow 50 = 800 ml/min

    flow 20 = 250 ml/min

    flow 10 = 100 ml/min

\* = continuation from experiment above

c.d. = current density ( $\text{mA/cm}^2$ )

time = time (minutes)

cath = cathode material

    Zn-SC = single crystal zinc

    Zn = polycrystalline zinc

    Pt = platinum

### H.3 Large Cell Experiments

1 M ZnCl<sub>2</sub>, "AR" grade, pH 4.6, 25° C

expt#	photo#	flow	I	time	cath	loc
1	XBB 838-7260	1600	1.8	30	Zn	l.e.
1	XBB 838-7261	1600	1.8	30	Zn	...
1	XBB 838-7262	1600	1.8	30	Zn	...
1	XBB 838-7263	1600	1.8	32	Zn	...
1	XBB 838-7264	1600	1.8	32	Zn	...
1	XBB 838-7265	1600	1.8	32	Zn	...
1	XBB 838-7266	1600	1.8	32	Zn	...
1	XBB 838-7267	1600	1.8	32	Zn	r.e.edge
1	XBB 838-7268	1600	1.8	32	Zn	l.e. - 10X
1	XBB 838-7269	1600	1.8	32	Zn	l.e. - 25X
2	XBB 838-7270	1600	2.7	60	Zn	l.e.
2	XBB 838-7271	1600	2.7	60	Zn	...
2	XBB 838-7272	1600	2.7	60	Zn	...
2	XBB 838-7273	1600	2.7	60	Zn	...
2	XBB 838-7274	1600	2.7	60	Zn	near l.e. - 10X
2	XBB 838-7275	1600	2.7	60	Zn	...
2	XBB 838-7276	1600	2.7	60	Zn	near l.e. - 25X
2	XBB 838-7277	1600	2.7	60	Zn	near mid. - 25X
3	XBB 838-7278	1600	2.7	30	Pt	l.e.
3	XBB 838-7279	1600	2.7	30	Pt	...
3	XBB 838-7280	1600	2.7	30	Pt	l.e. - 10X
3	XBB 838-7281	1600	2.7	30	Pt	...

4	XBB 838-7282	2300	2.7	30	Pt	l.e.
	(also, see XBB 831-379)					
4	XBB 838-7283	2300	2.7	30	Pt	...
4	XBB 838-7284	2300	2.7	30	Pt	...
4	XBB 838-7285	2300	2.7	30	Pt	...
4	XBB 838-7286	2300	2.7	30	Pt	...
4	XBB 838-7287	2300	2.7	30	Pt	r.e.
4	XBB 838-7288	2300	2.7	30	Pt	l.e. - 10X
	(also, see XBB 831-378)					
4	XBB 838-7289	2300	2.7	30	Pt	...
4	XBB 838-7290	2300	2.7	30	Pt	near mid. - 10X
5	XBB 838-7291	2300	2.7	60	Pt	l.e.
5	XBB 838-7292	2300	2.7	60	Pt	...
5	XBB 838-7293	2300	2.7	60	Pt	l.e. - 10X
5	XBB 838-7294	2300	2.7	60	Pt	...
6	XBB 838-7295	2300	0.9	30	Pt	l.e.
6	XBB 838-7296	2300	0.9	30	Pt	...
6	XBB 838-7297	2300	0.9	30	Pt	...
6	XBB 838-7298	2300	0.9	30	Pt	...
6	XBB 838-7299	2300	0.9	30	Pt	...
6	XBB 838-7300	2300	0.9	30	Pt	...
6	XBB 838-7301	2300	0.9	30	Pt	r.e.
6	XBB 838-7302	2300	0.9	30	Pt	l.e. - 10X
6	XBB 838-7303	2300	0.9	30	Pt	...
7	XBB 838-7304	2300	0.9	60	Pt	l.e.
7	XBB 838-7305	2300	0.9	60	Pt	...
7	XBB 838-7306	2300	0.9	60	Pt	...
7	XBB 838-7307	2300	0.9	60	Pt	...

7	XBB 838-7308	2300	0.9	60	Pt	...
7	XBB 838-7309	2300	0.9	60	Pt	...
7	XBB 838-7310	2300	0.9	60	Pt	r.e.
7	XBB 838-7311	2300	0.9	60	Pt	l.e. - 10X
7	XBB 838-7312	2300	0.9	60	Pt	...
8	XBB 838-7313	2300	9.0	30	Pt	l.e.
	(also, see XBB 831-379)					
8	XBB 838-7314	2300	9.0	30	Pt	...
8	XBB 838-7315	2300	9.0	30	Pt	...
8	XBB 838-7316	2300	9.0	30	Pt	...
8	XBB 838-7317	2300	9.0	30	Pt	...
8	XBB 838-7318	2300	9.0	30	Pt	...
8	XBB 838-7319	2300	9.0	30	Pt	r.e.
8	XBB 838-7320	2300	9.0	30	Pt	l.e. - 10X
	(also, see XBB 831-378)					
8	XBB 838-7321	2300	9.0	30	Pt	...
9	XBB 838-7322	1600	9.0	6	Pt	l.e.
9	XBB 838-7323	1600	9.0	6	Pt	...
9	XBB 838-7324	1600	9.0	6	Pt	l.e. - 10X
10	XBB 838-7325	2300	9.0	3	Pt	l.e.
10	XBB 838-7326	2300	9.0	3	Pt	...
10	XBB 838-7327	2300	9.0	3	Pt	l.e. - 10X
11	XBB 838-7328	1600	2.7	20	Pt	l.e.
11	XBB 838-7329	1600	2.7	20	Pt	l.e. - 10X

12	XBB 838-7330	2300	0.9	90	Pt	l.e.
	(also, see XBB 831-379)					
12	XBB 838-7331	2300	0.9	90	Pt	...
12	XBB 838-7332	2300	0.9	90	Pt	...
12	XBB 838-7333	2300	0.9	90	Pt	...
12	XBB 838-7334	2300	0.9	90	Pt	...
12	XBB 838-7335	2300	0.9	90	Pt	r.e.
12	XBB 838-7336	2300	0.9	90	Pt	l.e. - 10X
	(also, see XBB 831-378)					
12	XBB 838-7337	2300	0.9	90	Pt	...

---

expt# = Experiment #  
 photo# = LBL Photograph Number  
 flow = Flowrate (ml/min)  
 I = Current (amps)  
 time = Total deposition time (minutes)  
 cath = Cathode material (zinc or platinum)  
 loc = Photo location on electrode  
 l.e. = leading edge  
 ... = continuation from preceding photo  
 mid. = middle of electrode  
 r.e = rear edge

#### H.4 In situ Cell Experiments

1 M ZnCl<sub>2</sub>, "AR" grade, 25° C

flm#	pH	flow	c.d.	e.t.	fstp	fr/s	fr.	time
1	4.6	65	30	sm	11	1	200	3.3
1	4.6	65	10	sm	11	1	349	5.8
1	4.6	65	30	sm	11	1	1200	20
1	4.6	65	30	med	5.6	1	814	13.6
2	4.6	65	30	sm	11	1+4	1350	
2	4.6	65	30	sm+med	8	1+4	1575	
2	4.6	65	30	lrg	4	1+4	1025	
3	4.6	65	10	sm	11	1+4	1125	45
3	4.6	65	10	med	8	1+4	1125	45
3	4.6	65	10	lrg	4	1+4	1125	45
3	4.6	65	10	med	5.6	1	555	22 (s.c. zinc)
4	4.6	65	100	sm	8	1	360	6
4	4.6	65	100	med	5.6	1+4	580	20
4	4.6	65	100	lrg	2.8	1	360	6 (s.c. zinc)
testing of F-STOP								
5	4.6	65	30	sm	11	1	1200	20 (carbon)
5	4.6	65	30	med	8	1	1200	20
5	4.6	65	30	lrg	4	1	1200	20
5	4.6	65	100	lrg	4	1	300	5
6	4.6	65	10	med	8	1+4	1350	60
6	4.6	65	10	lrg	4	1+4	1350	60
6	4.6	0	100	med	8	1	360	6
6	4.6	65	100	med	8	1	615	10
7	4.6	65	10	med	16	1	1200	20
7	4.6	65	30	med	11	1+4	1825	60
7	4.6	65	10	med	11	1+4	905	30



8	4.6	65	30	lrg	5.6	1+4	1800	60
8	4.6	65	30	lrg	8	1+12	1800	250
9	4.6	25	100	med	8	1	1080	18
9	4.6	25	30	med	8	1+4	1600	45
9	4.6	25	100	med	8	1	1200	20
10	4.6	25	30	med	8	1	600	10
10	4.6	5	30	med	8	1	600	10
10	4.6	5	100	med	8	1	1200	20
10	4.6	5	30	med	8	1+4	1355	60
11	4.6	65	20	med	8	1	900	15
11	4.6	65	30	med	8	1+4	1125	45
11	4.6	65	10	med	8	1+4	1500	70
12	4.6	65	10	med	8	1+4	1220	51
12	4.6	65	30	lrg	4	1	1025	45
12	4.6	65	100	lrg	4	1+4	800	20
12	4.6	65	10	lrg	4	1+4	900	30
13	4.6	65	10	med	8	1+4	900	30
13	4.6	65	30	lrg	4	1+4	900	30
13	4.6	65	100	lrg	4	1	600	10
13	4.6	65	30	med	8	1+4	725	25 (zinc)
13	4.6	65	30	med	8	1	600	10 (copper)
14	4.6	25	30	med	8	1+4	900	30
14	4.6	25	30	med	8	1+4	900	30
14	4.6	25	10	med	8	1+4	1125	45
		filmed titles						
15	4.6	25	10	med	8	1+4	1125	45
15	4.6	25	100	med	8	1	660	11
15	4.6	25	100	sm	11	1	600	10
15	4.6	5	100	sm	11	1	600	10

16	4.6	65	10	med	5.6	1+4	1800	90
16	4.6	5	30	med	5.6	1+4	900	30
16	4.6	5	100	sm	8	1	600	10
16	4.6	5	100	med	4	1	600	10
17	1.9	65	100	sm	5.6	1	600	10
17	1.9	25	100	sm	8	1	600	10
17	1.9	5	100	sm	8	1	600	10
17	1.9	5	100	sm	8	1	600	10
17	1.9	65	30	sm	8	1+4	900	30
17	1.9	5	30	sm	8	1+4	900	30 (zinc)
18	1.9	25	30	sm	8	1+4	900	30
18	1.9	25	30	sm	11	1+4	900	30
18	1.9	5	30	sm	8	1+4	900	30
		filmed titles						
19	1.9	5	30	sm	8	1+4	900	30
19	1.9	25	100	sm	8	1	600	10
19	1.9	65	30	sm	8	1+4	900	30
19	1.9	65	100	sm	8	1	600	10
19	1.9	65	100	sm	8	1	600	10
20	1.9	5	100	sm	11	1	600	10
20	1.9	25	30	sm	8	1+4	900	30
20	1.9	65	10	sm	8	1+4	1125	45
20	1.9	25	30	sm	8	1+4	900	30 (zinc)
21		filmed titles						

flm# = Film #

flow = Rotameter setting

flow 65 = 4100 ml/min

flow 25 = 1500 ml/min

flow 5 = 700 ml/min

c.d. = Current density (mA/cm<sup>2</sup>)

e.t. = extension tube size

fstp = F-stop

fr/s = frames per second

fr/s 1 = only 1 frame per second used

fr/s 1+4 = a combination of 1 fr/sec and 1 fr/4 sec used

fr/s 1+12 = a combination of 1 fr/sec and 1 fr/12 sec used

fr. = total number of frames

time = time (minutes)

This report was done with support from the Department of Energy. Any conclusions or opinions expressed in this report represent solely those of the author(s) and not necessarily those of The Regents of the University of California, the Lawrence Berkeley Laboratory or the Department of Energy.

Reference to a company or product name does not imply approval or recommendation of the product by the University of California or the U.S. Department of Energy to the exclusion of others that may be suitable.

TECHNICAL INFORMATION DEPARTMENT  
LAWRENCE BERKELEY LABORATORY  
UNIVERSITY OF CALIFORNIA  
BERKELEY, CALIFORNIA 94720